Electric Vehicle Energy Management Considering Stakeholders' Interest in Smart Grids

Thesis submitted in accordance with the requirements of
the University of Liverpool for the degree of Doctor in Philosophy by

Bing Han

Department of Electrical Engineering & Electronics
School of Electrical Engineering, Electronics and Computer Science

November 2019

Abstract

With the electrification in transportation systems, Electric Vehicles (EVs) have developed rapidly in recent years. At the same time, with large-scale EV integration to power grids, the charging behaviours of EVs bring both challenges and opportunities to power grids operation. This thesis focuses on the EV energy management in smart grids, and the EV energy management problem is studied considering three stakeholders' interests, i.e. EV owner, aggregator and grid, respectively.

First, the economic relationship between EV owners and the aggregator is studied (EV owners' and aggregator's interest). Two multi-objective optimisation methods are applied to investigate the economic relationship between these two stakeholders and the aggregator–owner economic inconsistency issue is presented. To mediate this issue, a rebate factor is proposed in the model. The results show that a significant reduction in the EV owners' charging fee from self-scheduling can be achieved while the aggregator profit is maximised.

Second, the EV aggregator bidding strategy in the electricity market is studied (aggregator's interest). By jointly considering the reserve capacity in the day-ahead market and the uncertainty of reserve deployment requirements in the real-time market, a scenario-based stochastic programming method is used to maximise the expected aggregator profit. The risk of the deployed reserve shortage is addressed by introducing a penalty factor in the model. In addition, an owner–aggregator contract is designed to mitigate the economic inconsistency issue between EV owners and the aggregator. The results show that the expected aggregator profit is guaranteed by maximising reserve

deployment payments and mitigating the penalties and thus the uncertainty of the reserve market is well managed.

Third, the EV integration in a transmission system is studied (grid's interest) to achieve the coordination between generators and EVs. To tackle the challenge of large-scale EV integration problem, a bi-level scheduling strategy is proposed. The bi-level strategy clearly defines the responsibility of transmission system operator and the aggregator. An EV information grouping method is designed, which could efficiently tackle the optimisation complexity problem. In addition, a detailed EV battery charging model is built. The results show that the total cost of the systems is minimised and EVs could shave the peak and fill the valley loads.

This thesis discusses the EV energy management problem considering three stakeholders' interests, respectively. The proposed strategies in this thesis clearly evaluate and define the economic relationships and responsibility among EV owners, aggregator and the grid in managing EV charging and discharging behaviours. Based on three case studies conducted in this thesis, EV energy management could benefit the stakeholders as follows: (1) the EV owner charging fee is minimised while their driving requirements are satisfied; (2) the aggregator profit is maximised by participation in the electricity market; (3) the cost of the system is minimised by achieving the coordination between EVs and generators.

Acknowledgements

I would like to offer my deepest gratitude my primary supervisor, Dr. Shaofeng Lu for his tremendous encouragement, patience and supervision during my PhD. Without his support, my research would not be possible. I would also like to sincerely thank my secondary supervisors, Dr. Fei Xue and Dr. Lin Jiang for their excellent guidance and constructive comments.

I would like to thank my research group members, Mr. Chaoxian Wu and Dr. Xiaotong Xu, who shared experiences and ideas during my PhD study. Additionally, I would like to thank Dr. Liuying Li, who introduced me PhD life and inspired me in doing research during my undergraduate study.

I would also thank my colleagues and friends in EE511 office, Mr. Shufei Zhang, Dr. Haochuan Jiang, Mr. Jaehoon Cha, Dr. Xing Luo, Ms. Yujie Liu, Ms. Jingchen Wang and Ms. Zhenzhen Jiang. I felt honoured to work with them together and special thanks to them for our friendship.

I would like to express my most sincere to my parents and family, for their unconditional love, support throughout my life. Especially, I am deeply grateful to my girlfriend Ms. Jue Yuan, who support and encourage me over the past six years.

Finally, I would like to thank my closest friends and the people who I am not able to list.

Contents

List of Figures

List of Tables

List of Acronyms

AC	Alternating Current
BESS	Battery Energy Storage Systems
BEV	Battery Electric Vehicle
CAES	Compressed Air Energy Storage
CC-CV	Constant Current-Constant Voltage
CPP	Critical Peaking Pricing
DAM	Day-Ahead Market
DC	Direct Current
DG	Distributed Generation
DOD	Depth of Discharge
DR	Demand Response
DSO	Distribution System Operator
ESS	Energy Storage Systems
EV	Electric Vehicle
FES	Flywheel Energy Storage

GHG	Greenhouse Gases
HEV	Hybrid Electric Vehicle
ICE	Internal Combustion Engine
ISO	Independent Systems Operator
KCL	Kirchhoff's Current Law
LP	Linear Programming
MG	Micro Grid
MIQP	Mixed-Integer Quadratic Programming
MILP	Mixed-Integer Linear Programming
MOO	Multi-Objective Optimisation
MPC	Model Predictive Control
MSS	Mechanical Storage Systems
OPF	Optimal Power Flow
PHEV	Plug-in Hybrid Electric Vehicle
PHS	Pumped Hydroelectric Storage
PJM	Pennsylvania, New Jersey and Maryland
PV	Photovoltaic
RDR	Reserve Deployment Requirements
RES	Renewable Energy Source
RHO	Rolling-Horizon Optimisation
RO	Robust Optimisation

RTM	Real-Time Market
RTP	Real-Time Price
SOC	State of Charge
TGD	Truncated Gaussian Distribution
TOU	Time of Use
TSO	Transmission System Operator
V2G	Vehicle-to-Grid
WSM	Weighted Sum Method

List of Symbols

Parameters

n	Number of EVs from 1 to N
t	Time from 1 to M
m	Any time between 1 and M
ω	Number of scenarios from 1 to Ω
q	Number of days from 1 to Q
i, j	ID of bus of the transmission network
v	Number of EV group's ID
M	The total number of time intervals
N	The total number of EVs
Ω	The total number of scenarios
Q	Number of days for Monte Carlo simulation
V_ω	The number of days for scenario ω
π'_t	The hourly probability of reserve deployment at time t
π_ω	The probability of reserve deployment for scenario ω

ΔT	Duration of each time interval (1 h)
$\overline{P}_n^{\mathrm{ev}}$	The maximum charging and discharging power of EV n (kW)
$\overline{P}^{\mathrm{ess}}$	The maximum charging and discharging power of ESS (kW)
E_n^{ev}	Battery capacity of EV n (kWh)
E^{ess}	Battery capacity of ESS (kWh)
D^{ev}	The battery degradation parameter of EV ($/kWh)
D^{ess}	The battery degradation parameter of ESS ($/kWh)
SOC_n^a	The SOC of EV n at arrival time
$\mathrm{SOC}^{\mathrm{d}}$	The SOC at departure time of all EVs
$\mathrm{SOC}^{\mathrm{b}}, \mathrm{SOC}^{\mathrm{e}}$	The SOC at the beginning/ending time of ESS
$\underline{SOC}_{t,n}$	The minimum SOC of EV n at time t
$\underline{SOC}_t$	The minimum SOC of ESS at time t
$\underline{\mathrm{SOC}}$, $\overline{\mathrm{SOC}}$	The lower/upper battery SOC boundaries of EVs and ESS
t_n^a, t_n^d	The arrival/departure time of EV n
r_t^+, r_t^-	The charging/discharging real-time prices at time t ($/kWh)
r_t^{up}, r_t^{dw}	The reserve up/down capacity prices at time t ($/kWh)
$\widetilde{r}_t^u, \widetilde{r}_t^d$	Deployed up/down reserve price at time t ($/kWh)
γ^{up}, γ^{dw}	The penalty for reserve up/down deployment shortage ($/kWh)
λ^{up}, λ^{dw}	The amount of the reserve deployment requirements
$x_{t,q}^{up}, x_{t,q}^{dw}$	Reserve up/down deployment requirement at time t of day q

$\widetilde{x}^{up}_{t,\omega}, \widetilde{x}^{dw}_{t,\omega}$	Reserve up/down deployment requirements at time t of scenario ω
β	The charging fee discounted parameter
$\overline{P}_{i,n}$	The maximum charging/discharging power of EV n at bus i (kW)
$E_{i,n}$	The battery capacity of EV n at bus i (kWh)
$SOC^{a}_{i,n}$	The SOC of EV n at bus i at arrival time
$t^{a}_{i,n}$, $t^{d}_{i,n}$	The arrival/departure time of EV n at bus i

Sets

$\boldsymbol{G}$	Set of generator of the transmission network
$\boldsymbol{L}$	Set of load of the transmission network
$\boldsymbol{K_{i,v}}$	Set of the EVs in bus i and group v
$\boldsymbol{N_i}, \boldsymbol{N_j}$	Sets of the branch from bus i to bus j of the transmission network

Variables

$p^{+,e}_{n,t}$, $p^{-,e}_{n,t}$	The Charging and discharging power of EV n at time t under self-scheduling strategy (kW)
$p^{+,d}_{n,t}$, $p^{-,d}_{n,t}$	The base load plan variables for EV n at time t (kW)
$p^{+,d}_{t}$, $p^{-,d}_{t}$	The base load plan variables for ESS at time t (kW)
$p^{+}_{i,n,t}$, $p^{-}_{i,n,t}$	The charging/discharging power of EV n at bus i at time t (kW)
$p^{up}_{n,t}$, $p^{dw}_{n,t}$	The reserve up/down capacities plan of EV n at time t (kW)
p^{up}_{t}, p^{dw}_{t}	The reserve up/down capacities plan of ESS at time t (kW)
$\widetilde{p}^{up}_{n,t,\omega}$, $\widetilde{p}^{dw}_{n,t,\omega}$	The deployed up/down reserve of EV n at time t under scenario ω (kW)

$\widetilde{p}^{up}_{t,\omega}$, $\widetilde{p}^{dw}_{t,\omega}$	The deployed up/down reserve of ESS at time t under scenario ω (kW)
$\Delta p^{+}_{n,t,\omega}$, $\Delta p^{-}_{n,t,\omega}$	The power deviations of EV n at time t under scenario ω (kW)
$\Delta p^{+}_{t,\omega}$, $\Delta p^{-}_{t,\omega}$	The power deviations of ESS at time t under scenario ω (kW)
$s^{up}_{t,\omega}$, $s^{dw}_{t,\omega}$	Reserve up/down deployment shortage at t of scenario ω (kW)
$k_{i,v}$	The number of EV in group v at bus i
$P_{i,v}$	The average charging/discharging power of EVs in group v at bus i (kW)
$E_{i,v}$	The average battery capacity of EVs in group v at bus i (kWh)
$SOC^{a}_{i,v}$	The SOC of EV group v at bus i at arrival time
$t^{a}_{i,v}$, $t^{d}_{i,v}$	The arrival/departure time of EV group v at bus i
$p^{G}_{i,t}$	The output power of the generator at bus i at time t (MW)
$\theta_{i,t}$	The voltage angle of bus i at time t (rad)
$p^{\mathrm{ev}}_{i,t}$	The EV load at bus i at time t (MW)

Chapter 1

Introduction

1.1 Background

The energy crisis and environmental problems are becoming crucial issues for the whole world and urgently require humans to take action to save energy and reduce the Greenhouse Gases (GHG) emission. The emissions of GHG contribute to atmospheric pollution, climate change, and global warming problems. Faced with this situation, governments have made plans and policies to reduce GHG emissions. The EU is responsible for 10% global GHG emissions, and an objective was set in 2009 to reduce GHG emissions by 80–95% in 2050 [1]. In 2015, a historic announcement was made about the post-2020 climate targets for the U.S. and China. The U.S. government announced plans to reduce emission by 26-28% below 2005 levels by 2025 [2]. In the thirteenth "five-year plan of development" of China, it is targeted that by 2020, the carbon dioxide (CO_2) emission per unit of GDP decreased by 18% compared to that of 2015 [3].

It has been reported that over 60% of the global primary demand is from electricity generation and transportation (electricity generation accounts the majority of the coal demand and transportation accounts the majority of the oil demand), and a significant amount of the GHG and pollutant emissions are contributed by transportation [4, 5]. According to the United States Environmental Protection Agency, transportation

accounted for 20% of GHG emissions of the U.S. in 2017, where light-duty vehicles contributed 59% of emissions. Owing to high travelling demands, GHG emissions in the transportation sector increased faster than those in other sectors from 1990 to 2017 [6].

Electric Vehicle (EV) is regarded as a good candidate in reducing GHG emissions in the transportation sector [7]. Compared with traditional Internal Combustion Engine (ICE) vehicle, EV is eco-friendly because it has the advantage of less dependence on fossil fuels, lower noise levels and less GHG emissions. In addition, electricity is the main power source of EVs, which is originated from central power plants. With the integration of Renewable Energy Source (RES), EVs could be charged by using clean energy, such that the GHG emissions could be further reduced. Based on these advantages, EVs are developed all around the world nowadays.

1.1.1 Electric Vehicles

Typically, EV can be categorised into three types according to the electricity used as the vehicle energy source: Hybrid Electric Vehicle (HEV), Plug-in Hybrid Electric Vehicle (PHEV) and Battery Electric Vehicle (BEV).

- **HEVs** have both a small-size electric battery and an ICE, which is powered by both electricity and gasoline. Because HEVs have no external socket, the electric battery only can be charged by using the vehicle's (regenerative) braking systems and ICE.

- **PHEVs** have both a battery and an ICE. Compared with HEVs, PHEVs have an external socket (plug) and a larger size battery. The battery is charged both from the external electricity from the plug and the regenerative braking systems.

- **BEVs** have an electric battery and no ICE. The electric battery is charged only from the external socket.

The recent global development progress of EVs is summarised in Table 1.1, which shows the total number of EVs by country [8, 9]. It is noted that there are more than 5

Table 1.1: Total number of EVs by country from 2011-2018 (thousands) [8, 9]

	2011	2012	2013	2014	2015	2016	2017	2018
Australia	0.05	0.30	0.60	1.92	3.69	5.06	7.34	10.95
Brazil				0.06	0.15	0.32	0.68	1.11
Canada	0.52	2.54	5.66	10.73	17.69	29.27	45.95	90.10
Chile	0.01	0.01	0.02	0.03	0.07	0.10	0.25	0.41
China	6.98	16.88	32.22	105.39	312.77	648.77	1227.77	2306.3
Finland	0.06	0.24	0.47	0.93	1.59	3.29	6.34	12.05
France	3.03	9.29	18.91	31.54	54.49	84.00	118.77	165.48
Germany	1.89	5.26	12.19	24.93	48.12	72.73	109.56	177.07
India	1.33	2.76	2.95	3.35	4.35	4.80	6.80	10.30
Japan	16.14	40.58	69.46	101.74	126.40	151.25	205.35	255.10
Korea	0.34	0.85	1.45	2.76	5.95	11.21	25.92	59.60
Mexico		0.09	0.10	0.15	0.25	0.66	0.92	4.01
Netherlands	1.14	6.26	28.67	43.76	87.53	112.01	119.33	148.48
New Zealand	0.03	0.06	0.09	0.41	0.91	2.41	5.88	11.42
Norway	2.63	7.15	15.67	35.44	69.17	114.05	176.31	249.00
Portugal							1.78	17.03
South Africa			0.03	0.05	0.29	0.67	0.86	1.01
Sweden	0.18	1.11	2.66	7.32	15.91	29.33	49.67	78.63
Thailand	0.01	0.02	0.03	0.10	0.37	0.38	0.40	0.60
U.K.	2.89	5.59	9.34	24.08	48.51	86.42	133.67	184.03
U.S.	21.50	74.74	171.44	290.22	404.09	563.71	762.06	1123.37
Others	2.60	5.31	9.35	18.73	37.17	61.63	103.44	216.41
Total	61.33	179.03	381.30	703.65	1239.45	1982.04	3109.05	5122.46

million EVs in the world and 45% were from China; the U.S. and the EU each accounted for approximately 23% in 2018. It is estimated that there will be 200 million EVs in China by 2050 and two-thirds of light-duty vehicles in the U.S. will be EVs by 2040 [10, 11].

Although the growth in the number of EV remained rapid from 2011 to 2018, the number of vehicles per thousand people in China is still much lower than in developed countries. In 2020, the number of vehicles per thousand people in China is expected to be 176, which is far less than those in the U.S. (808) and west Europe (589) in 2012 [12]. Table 1.2 shows the estimated future development of EVs in China [13]. China has huge potential of EV development and as a new type of load, the impact of the charging behaviours of EVs on power grids should not be neglected.

Table 1.2: Estimation of EV development in China [13]

	2020	2030	2040	2050
Total vehicle number (million)	250	370	381	410
Vehicles/1000 people	176	255	270	291
EV number (million)	5	16.6	42	135
EV penetration rate	2.6%	4.5%	11%	33%

1.1.2 Smart Grids and Demand Response

In the 19^{th} century, the first Alternating Current (AC) power grid was built in the U.S., which was a centralised unidirectional system. The traditional power grids produces electricity at centralised power plants, and the electricity is delivered to end-users based on transmission and distribution networks.

The generated electricity from power plants, such as thermal plants and nuclear plants, is delivered through transmission lines at a high voltage level under the usage of step-up transformers. For the sake of loss minimisation, the high voltage reduces the current of the transmission systems, such that the power loss caused by the resistance is minimised. The Transmission System Operator (TSO) is responsible for the security of the systems, where the generated electrical energy should equal the total demand and

the transmission capacity should be ensured. When the demand exceeds the generation capacity, the TSO disconnects certain loads to maintain the balance. Distribution systems are connected with transmission systems through step-down transformers. By using step-down transformers, the high voltage level is transferred to a low voltage level and the electricity is distributed to end-users. The Distribution System Operator (DSO) is responsible for the operation of distribution systems, maintaining their resilience and security, and implementing necessary expansions of the distribution systems.

A smart grid is a modern electric grid, which utilises information and communication technologies to collect and monitor the electricity generation, transmission, and distribution status. Compared with tradition power grids, smart grids involve a variety of smart meters, smart appliances, and Distributed Generation (DG), etc. Figure 1.1 illustrates the general components of smart grids.

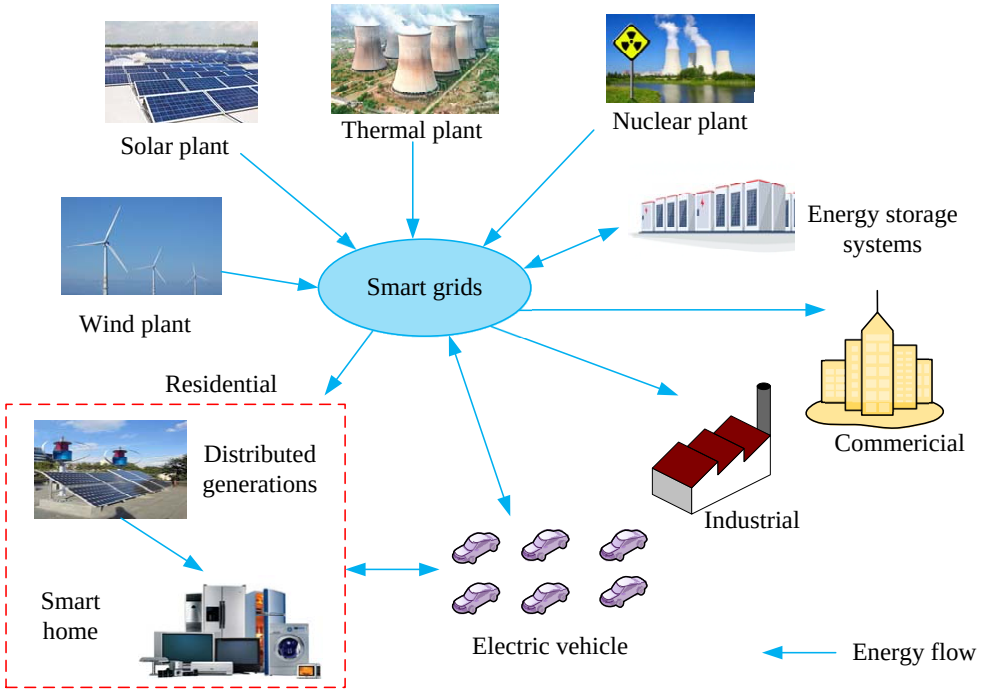

Figure 1.1: Components of smart grids

In smart grids, bidirectional power flow is enabled and the generation is decentralised, owing to the installation of DG. Based on advanced metering infrastructure, e.g. smart meter, the willingness of end-users' participation in power grid operation is enhanced. With the utilisation of smart meters in power grids, the power consumption, voltage, and frequency could be monitored in real time. The data collected from the smart meter provide an opportunity to the system operators to design different types of tariffs for end-users. End-users could respond based on the tariffs and their own energy consumption requirements.

Demand Response (DR) enables flexible load in power grids operation, by encouraging end-users to change their electricity usage patterns. The concept of DR is defined by the Federal Energy Regulatory Commission:
'Changes in electric usage by end-users from their normal consumption patterns in response to changes in the price of electricity over time, or to incentive payments designed to induce lower electricity use at times of high wholesale market prices or when system reliability is jeopardised.' [14]. DR programmes could be generally classified into two types:

- **Price-based DR** provides end-users with time-varying electricity prices, whereby the electricity price is high during peak hours. End-users are thus encouraged to use less electricity during these time. Price-based DR programmes include Real-Time Price (RTP), Time of Use (TOU), and Critical Peaking Pricing (CPP).

- **Incentive-based DR** requires end-users to reduce their electricity consumption during peak hours. End-users will be penalised if they fail or declare to reduce loads. Incentive DR programmes include direct load control, interruptible/curtailable service, and ancillary service, etc.

DR programmes provide opportunities of EV energy management in smart grids, where the charging and discharging behaviours of EVs could be scheduled based on RTP. With the utilisation of EV in smart homes and buildings, the flexibility of electric loads will be significantly improved, and a variety of strategies could be implemented. Based

on DR programmes and Vehicle-to-Grid (V2G) technology, the connection between EV owners and systems operators (TSO and DSO) can be made based on real-time information (price signals or incentive payments). Such DR programmes allow EV owners to potentially shift charging load based on real-time information, which generate economic benefits for EV owners.

1.1.3 Stakeholders in EV Energy Management

As discussed above, DR programmes and V2G technology enable EV energy management in smart grids. Typically, the EV energy management relates to three stakeholders, which are EV owners, EV aggregator and the grid. Three stakeholders are illustrated in Figure 1.2.

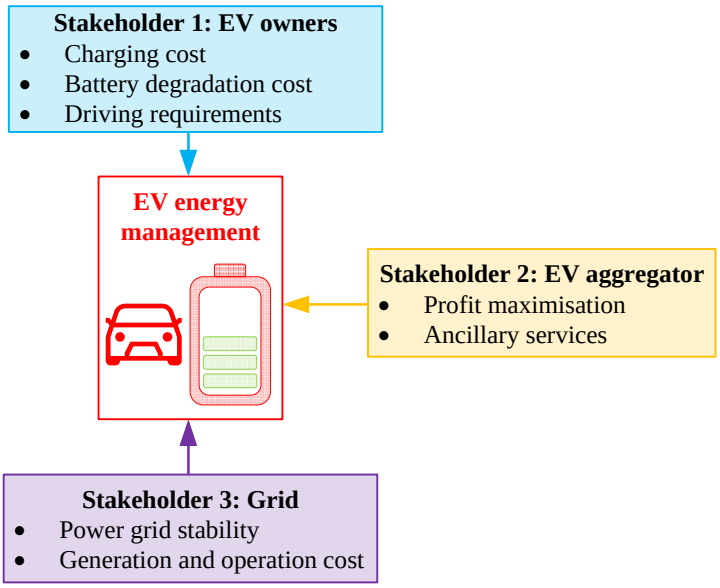

Figure 1.2: Stakeholders in EV energy management

EV owners are concerned with the EV energy management problem, since it relates to their economic benefits, including charging cost and battery degeneration cost. Based on different DR programmes and the charging flexibility of EV batteries, EV energy management provides an opportunity to minimise the charging fee for owners. In addition, it has been reported that the high charging and discharging power (e.g. fast

charging) could significantly increase the EV battery degradation. Thus, EV energy management to reduce charging cost and degradation cost is the major concern of owners.

EV aggregator represents the third party between EV and power grids, such as carpark operator or charging station. Typically, ancillary services in electricity markets are implemented on MW-basis generators, whereas single EVs could only provide limited power (10–20 kW). Under this circumstance and to achieve a large-scale power rating, the concept of the aggregator has been developed. This is a central entity and a good candidate to participate in DR programmes by coordinating the charging and discharging behaviours of an EV fleet. The aggregator could obtain profit in attending electricity markets.

Grid is a general concept in this thesis, which represents several supporting organisations in power grids operation from generation to distribution, such as generation wholesalers, Independent Systems Operator (ISO)—i.e., TSO and DSO—and reliability coordinators, etc [15]. Thus the interest of the grid includes operation cost, reliability etc. Based on DR programmes and V2G technology, the charging and discharging behaviours of EV will offer essential benefits to the grid.

1.2 Motivations

EV energy management is the first motivation of this research. With the rapid development of EVs and the electrification of transportation systems, the EV charging behaviours impose significant negative impacts on the operation of power grids, such as voltage drop, energy losses, and transformer overloading. Studies have shown that when the EV penetration level reaches 40% under uncoordinated charging, the distribution transformers need to be replaced [16]. However, the charging processes of EVs are flexible and can be scheduled, because EVs are parked for 96% of the time at homes or offices [17]. Consequently, EV energy management is necessary and EVs are not just electricity loads under management, but also can be regarded as dynamic Energy

Storage Systems (ESS). In this case, EV is not only a type of green transportation tool, but it can provide ancillary services to power grids (frequency regulation and spinning reserve). Furthermore, studies have showed that the coordinate charging of EVs received special attention from the grid and that with the utilisation of EVs, the stability of the power grids could be enhanced. Moreover, from the long-term planning and updating of the power grids viewpoint, the construction of the EV charging network, i.e. the sitting and sizing of charging stations, relates both to power and transportation network. Thus, the EV energy management is vital and it needs to be investigated.

The second motivation of this research is that the EV energy management relates to three stakeholders, as discussed in Section 1.1.3. It is challenging to develop a cooperative mechanism between the EV owners, aggregator and the grid. The EV energy management problem not only involves different stakeholders but also is complicated by several uncertainties, such as EV owners driving behaviours, price signals and power grids requirements, etc. Therefore, designing a set of strategies, which could take different stakeholders' interest into consideration, is important in EV energy management.

1.3 Objectives

This thesis aims to propose a set of EV energy management strategies considering stakeholders' interest. Three objectives relate to three stakeholders' interests in this thesis are listed as follow:

- The first objective of this thesis is to evaluate the economic relationship between two stakeholders. The issue is raised of an economic inconsistency between the aggregator profit maximisation and EV owners' charging fee minimisation.

  A Multi-Objective Optimisation (MOO) method, i.e. Weighted Sum Method (WSM), is used to incorporate two stakeholders' benefits into one optimisation problem. In addition, a rebate factor is introduced in the ε-constraint method, which is used to guarantee owners' benefits in aggregator scheduling.

- The second objective of this thesis is to explore an aggregator bidding strategy in Day-Ahead (DA) reserve and energy markets. The reserve deployment in Real-Time Market (RTM) and its impact on DA bidding is considered.

  A stochastic programming method is applied to handle the uncertainty of the reserve deployment, where the uncertainty is represented by several scenarios and probabilities. The risk of reserve deployment shortage is considered, where a penalty factor is introduced in the optimisation model.

- The third objective of this thesis is to investigate the coordination between EV (demand side) with the generators (generation side). The spatial information of the power grids is formulated based on Direct Current (DC)-Optimal Power Flow (OPF), which achieves coordination of aggregators at different locations with generators.

  A bi-level strategy is designed which clearly defines the relationship between and responsibilities of the grid and the aggregator. In addition, the proposed EV information method could effectively tackle the large-scale (complexity) optimisation problem.

1.4 Thesis Structure

This thesis consists of seven chapters which address the EV energy management problem considering three stakeholders' interest, and the relationships among the three stakeholders are investigated.

Chapter 1 introduces the background information of the state-of-the-art of smart grids and DR. With the development of EVs and the integration of EVs into the grids, the motivation for this thesis is presented. For the EV energy management problem in smart grids, three objectives are set in this thesis in terms of the different stakeholders' interest.

Chapter 2 provides a review of ESS and EVs. A general review of EVs is presented according to their categories and applications. The working principles of Pumped

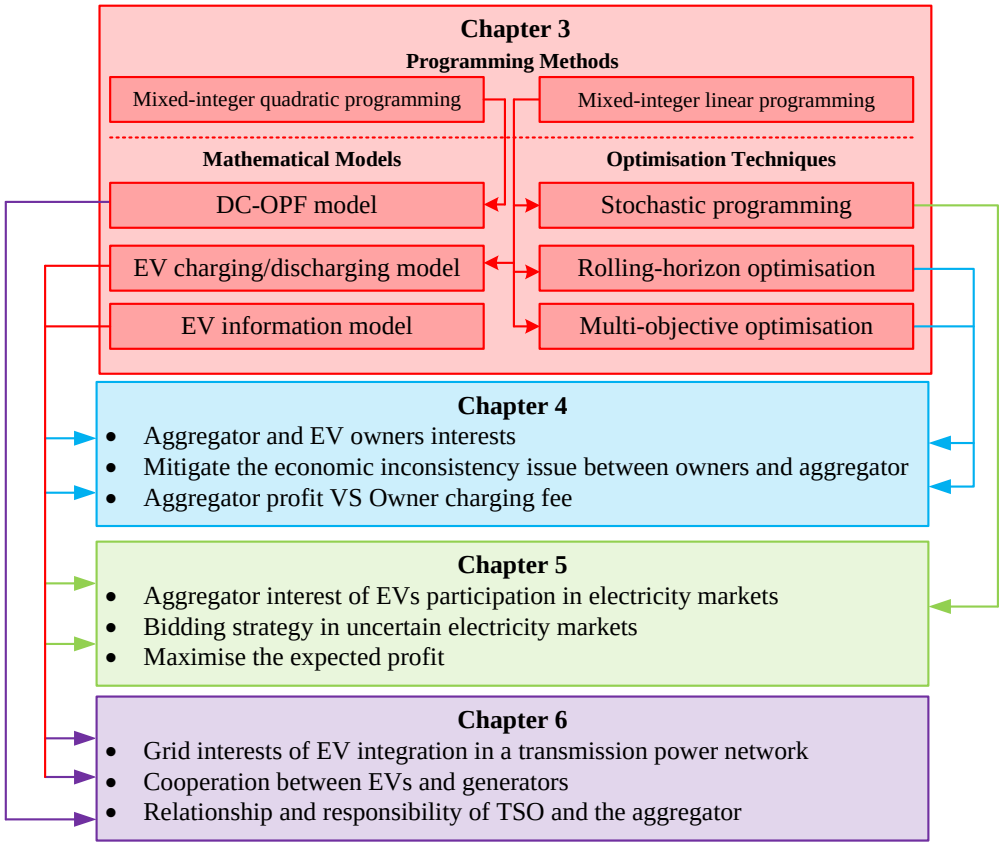

Figure 1.3: Structure of the thesis

Hydroelectric Storage (PHS), Flywheel Energy Storage (FES), supercapacitors, lead-acid batteries, and Li-ion batteries are discussed. After that, the application of EVs in power grids based on V2G technology is reviewed.

Chapter 3 presents the mathematical models used in the thesis, including the ESS model, EV charging and discharging model, EV information model, and DC-OPF model. Then, three optimisation methods are introduced, which are MOO, stochastic programming, and Rolling-Horizon Optimisation (RHO).

The general structure of this thesis is outlined in Figure 1.3. Three case studies are discussed in Chapter 4, 5, and 6 based on the mathematical models and optimisation techniques proposed in Chapter 3. The relationships and associations among the chapters are explained as follows:

Chapter 4 describes the economic inconsistency issue between the EV owners and the EV aggregator in the Day-Ahead Market (DAM). The EV information model as well as the EV charging and discharging model are involved in this chapter. A scenario of the EV aggregator participation in DA energy and reserve markets for profit maximisation is proposed and the economic inconsistency issue between aggregator profit and EV owners' charging fee is addressed. A rebate factor is introduced, which is used to guarantee the owners' benefits in participating in aggregator scheduling. MOO method is utilised to balance the aggregator profit and owners' charging fee. However, the RT reserve market is not considered in this chapter.

Chapter 5 introduces an EV aggregator DA bidding strategy in attending the DAM and RTM by considering reserve deployment. The economic inconsistency issue examined in Chapter 4 is mitigated by using an owner–aggregator contract. The uncertainty in the Reserve Deployment Requirements (RDR) announced by the grid is formulated by various scenarios and probabilities. A stochastic programming method is used in the model and achieves the maximisation of the expected aggregator profit.

Chapter 6 focuses on the cooperation between EV aggregators (demand side) and generators (generation side) considering the interest of the grid (TSO in this chapter); this is different from Chapter 5, which only discusses the bidding strategy only from the aggregator viewpoint In order to reduce the computation complexity, a bi-level strategy and an EV information grouping method are proposed in this chapter. The relationship between two stakeholders—i.e., grid and EV aggregator—is examined by clearly defining the responsibility of each stakeholder.

Chapter 7 draws the main conclusions of the thesis and discusses the potential future work.

1.5 Summary

In this chapter, the background information of smart grids and the state of the art of EVs is introduced. The challenges and motivations of this thesis are presented.

After that, the objectives and contributions of this thesis are summarised. Finally, the structure of the thesis and the relationships among the chapters are explained.

Chapter 2

Review of ESS and EV Energy Management in Power Grids

2.1 Introduction

ESS play a crucial role in modern power grids, owing to the integration of RESs. The utilisation of ESS has become a necessary component in the solution of power grid operation issues such as stability, power quality, and system balancing. In this chapter, various ESS technologies are discussed based on their intrinsic characteristics, including the working principle, application status, and future development prospects. Furthermore, the advantages and disadvantages of ESS are evaluated from the perspective of power grids. In particular, the integration of EVs in the power grid is reviewed. EV energy management strategies are examined with respect to several aspects, such as stakeholders, objectives, and optimisation methods. The effectiveness of EV energy management in terms of power quality, peak load shaving, system balancing, and frequency control is reviewed.

In recent years, faced by the growth in global electricity consumption, environmental problems, and fossil fuel limitations, the penetration of RESs in the power generation sector has been rapidly increasing, which has reduced the dependency on traditional

sources and thus decreased waste gas and CO_2 emissions. However, there are also some disadvantages of RESs. One of the significant drawbacks of renewable sources is intermittency. For example, solar and wind power are uncertain, varying, and environmentally dependent. With a high penetration of renewable sources, various economic and stability challenges of power grids may emerge, such as power generation and consumption imbalance, as well as power quality and congestion management problems.

Among solutions to solve a series of power grids problems, one of the effective and promising approaches is to use ESS. ESS perform as an energy bank, which can convert electrical energy from the power grid to a storable form of energy and convert the stored energy back to electrical energy for the power grid when needed [18]. Different types of ESS have different characteristics and thus perform differently to improve the performance of power grids [19]. The main functions of ESS include:

- Load levelling: peak shaving and valley filling;
- Power quality improvement;
- Voltage and frequency control;
- Transmission congestion management;

In this thesis, a general review of ESS is given in Section 2.2, where the characteristics of Battery Energy Storage Systems (BESS) is discussed. Then the application of EV integration in power grids is discussed in Section 2.3, the EV energy management strategies are reviewed in terms of different stakeholders' interests.

2.2 Review of Energy Storage Systems

Various types of ESS can be categorised by several criteria from different viewpoints. Generally, ESS can be grouped into three categories based on the discharge duration and storage capacity. Figure 2.1 shows the category of typical ESS [20].

It can be seen from the figure that Compressed Air Energy Storage (CAES) and PHS systems have the largest power and long discharging time, such that these two types of

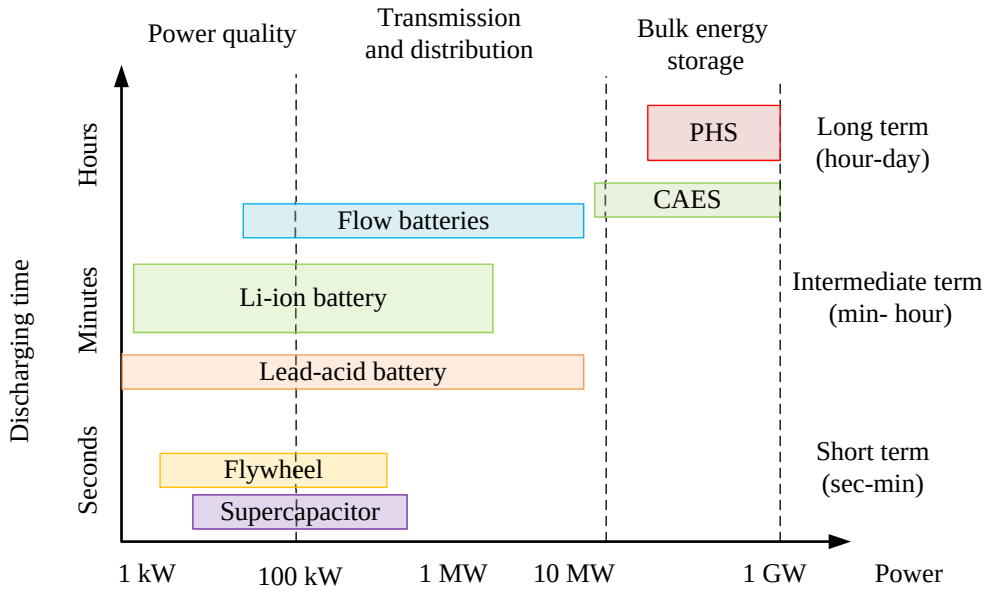

Figure 2.1: Discharging duration and capacity of energy storage systems [20]

ESS are suitable for bulk energy storage. BESS have relative shorter discharging time, which can be used to support the grid. FES and supercapacitors have short discharging time but very short response time, and thus they are suitable for improving power quality.

Normally, the form of energy stored is the most widely used metric for ESS classification, based on which ESS can be classified into six categories: (1) mechanical, (2) electrochemical, (3) chemical, (4) electrical, (5) thermal, and (6) hybrid. These categories are shown in Figure 2.2 [21].

2.2.1 Energy Storage Systems in Power Grids

In the 21st century, global electric power systems are facing a dramatic revolution, owing to the growth in load demand and the large integration of renewable sources. This situation raises challenges for the security and flexibility of power systems. One of the effective solutions of these issues is to use ESS, which can be utilised in each part of power grids. Figure 2.3 shows that ESS can be used in each part of power grids.

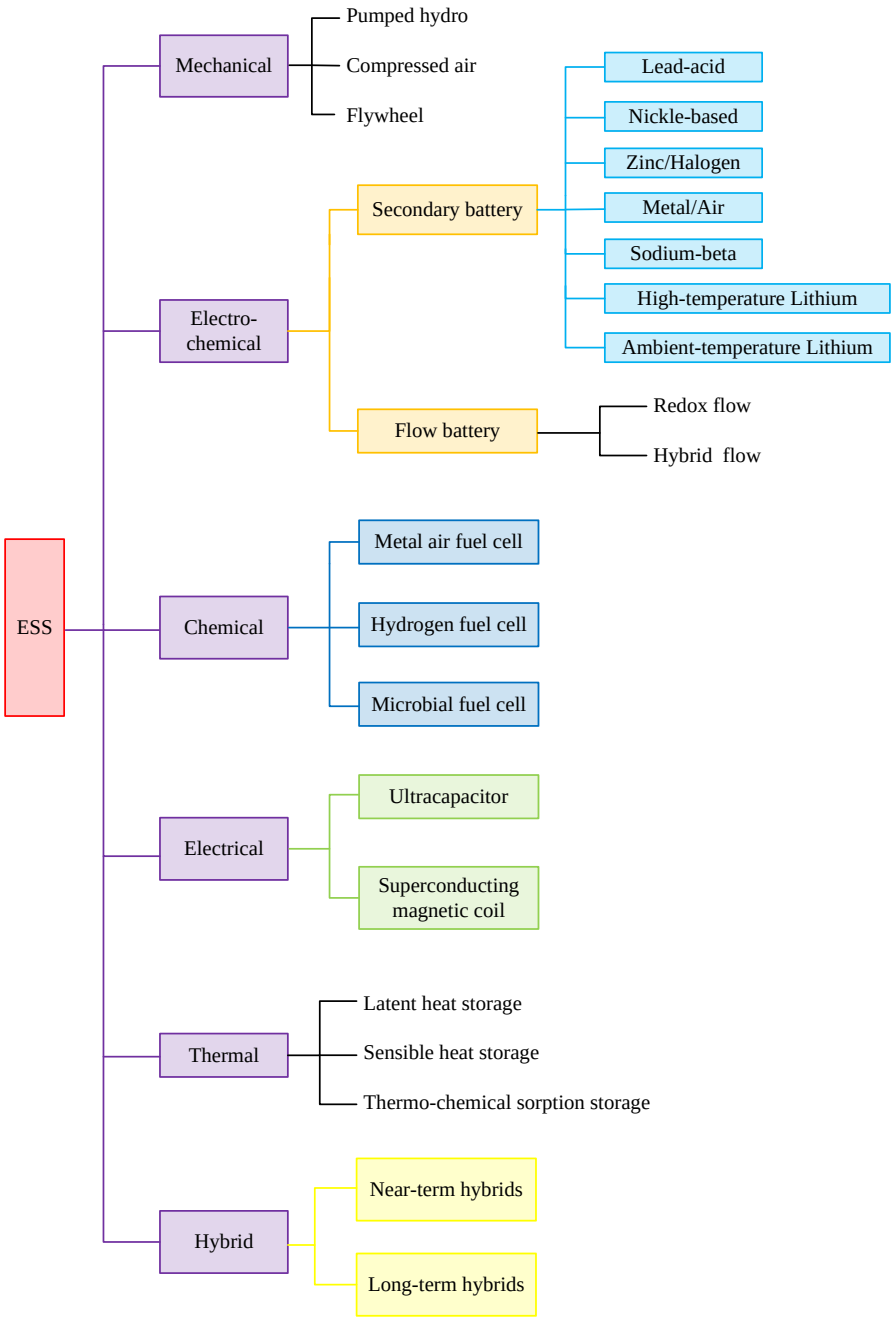

Figure 2.2: General categories of energy storage systems [21]

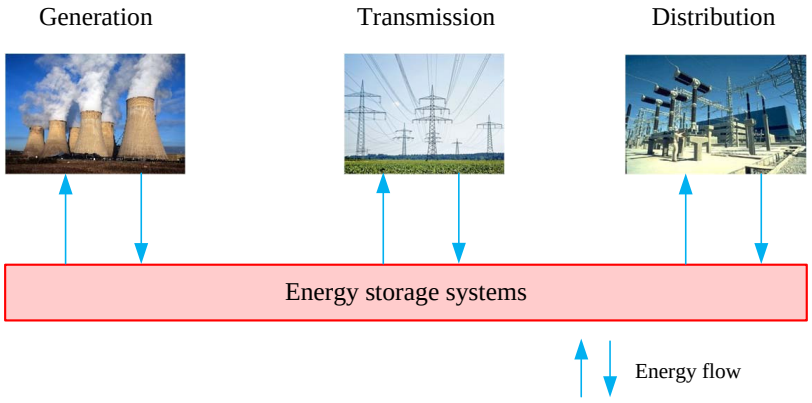

Figure 2.3: Energy storage systems in power grids

ESS in Power Generation

PHS and CAES units are referred to as bulk energy storage systems, which are particularly suitable for energy management on the power generation side of the system at a scale of over 100 MW. Because these two systems have long lifetimes and unlimited cycle stability. PHS and CAES have good performance in balancing demand and supply, load levelling, and spinning reserve, in cooperation with renewable energy sources [22]. In many countries, PHS is integrated with wind power generation systems to form hybrid ESS named wind hydro pumped storage systems.

Owing to the characteristics of large capacity, one of the drawbacks of PHS and CAES systems is their negative impact on the environment. The construction of PHS requires a large area of land. Moreover, PHS needs two large reservoirs and dams. Long construction time (more than 10 years) and high initial construction cost (hundreds to thousands of millions of dollars) are also two constraints on the wide application of PHS.

Similarly, CAES has geographic and environmental constraints on its wide application. In general cases, CAES is suitable for power plants near rock mines and salt caverns.

ESS in Power Transmission

Traditional transmission systems operate in a single direction, where the electrical power is delivered from power plants to customers. Owing to the penetration of DGs, the transmission systems have become bidirectional [23], which requires cooperation with ESS for the purpose of system stability. Supercapacitors, FES, and BESS are designed to be installed in transmission and distribution systems, as they have the characteristics of high power density and fast response speed.

Owing to the rapidly increasing load demand, transmission lines need to be upgraded urgently. Especially during peak hours, the load demand is beyond the maximum capacity of the transmission line. Long construction periods (normally 10 to 15 years) [24] and high cost are the two main constraints on transmission line upgrades. Another problem is that the peak demand lasts for a short time, such that during most of the time, the transmission line capacity is not fully used, leading to a certain waste. In light of these problems, ESS can be installed across the transmission line. ESS can be charged during off-peak hours, and during peak hours, energy is sent directly to the load, thus decreasing the transmission line congestion level [25].

ESS in Power Distribution

In distribution systems, BESS have the advantages of modularity, low space occupation, movability, and easy construction. Lead-acid batteries and sodium batteries have a large power rating and relatively long operation time. Such battery units in transmission and distribution systems can be used for load peak shaving.

Li-ion batteries with a high power density and short response time would be especially suitable for power system frequency regulation. BESS could control the real power and thus regulate the frequency. BESS could also help to reduce the absolute value of the area control error and improve the stability of the system [26]. Moreover, BESS could cooperate with supercapacitors and work as hybrid ESS, which could satisfy various system application requirements [27].

2.2.2 Battery Energy Storage Systems

The first battery was invented around the 1800s in Italy, which consisted of zinc and copper in a salt sink separated by cardboard. A battery stores electricity in the form of chemical energy. Chemical reactions occur inside the battery and generate a flow of electrons between two electrodes through the external circuit. If an external voltage is applied across the two electrodes, the reaction is reversed and the battery is charged.

There are various types of battery systems, such as lead–acid batteries, nickel–cadmium (NiCd) batteries, sodium–sulphur (NaS) batteries, sodium–nickel–chloride (ZEBRA) batteries, and lithium-ion (Li-ion) batteries. The Li-ion battery system is a new and developing technology which has huge potential in the future.

Lead-acid Battery

The lead-acid battery was invented by the French physicist Gaston Planté in 1859, and it has the longest history among the secondary/rechargeable batteries.

The positive and negative electrodes of the lead-acid battery are composed of PbO_2 and Pb, respectively, and the electrolyte solution is H_2SO_4. The redox reaction of the lead-acid battery is shown in (2.1)–(2.3)

$$Pb + PbO_2 + 4H^+ + 2SO_4^{2-} \rightleftharpoons 2PbSO_4 + 2H_2O \tag{2.1}$$

Oxidation at the anode (negative electrode):

$$Pb + SO_4^{2-} \rightleftharpoons PbSO_4 + 2e^- \tag{2.2}$$

Reduction at the cathode (positive electrode):

$$PbO_2 + SO_4^{2-} + 4H^+ + 2e^- \rightleftharpoons PbSO_4 + 2H_2O \tag{2.3}$$

As a widely used rechargeable battery with a long application history, the lead-acid battery is installed all around the world, owing to its advantages of small daily

self-discharge rate (<3%), fast response time, low cost, relatively high cycle efficiency (63–90%), technical maturity, abundant materials and large-scale manufacturing. It has been applied in the fields of communication, transportation, grid utility, renewable energy smoothing and backup power supply, etc. [28]. The largest lead-acid BESS is a 40-MWh system installed in Chino, California [18]. However, there are still some drawbacks of lead-acid batteries, which limit their installation as utility-scale ESS, such as low energy density (50–90 Wh/L), sensitivity to room temperature, relatively low recycling counts (up to approximately 2000), and employed toxic materials [29].

Currently, several advanced lead-acid batteries have been developed, which have fast response times close to those of FES and supercapacitors [30].

Lithium-ion Battery

The Li-ion battery was invented by Bell Labs in the 1960s and the first commercial product was produced by Sony company in the 1990s. The Li-ion battery is a good candidate for energy storage and EVs, as it has a short response time (approximately 20 ms), low dimensions (∼1500–10,000 W/L), and relatively high energy and power density (∼75–200 Wh/kg, ∼150–2000 W/kg). In addition, it has relatively high conversion efficiency of up to 97%. However, the Li-ion battery has the drawbacks of high cost (>$600/kWh) and the cycle Depth of Discharge (DOD) impacts the battery lifetime [18].

The structure of the Li-ion battery consists of a graphite carbon anode and lithiated metal oxide ($LiCoO_2$, $LiNiO_2$, $LiMn_2O_4$, and $LiFePO_4$) cathode. During the charging period, Li atoms in the cathode become ions and migrate to the carbon anode. The ions then combine with external electrons in the anode. During the discharging periods, this process is reversed, and a chemical reaction occurs at the two electrodes, which generates an electron flow in the external circuit. The electrochemical reaction inside the Li-ion battery during operation is represented by (2.4)–(2.6):

$$C + LiXXO_2 \rightleftharpoons Li_nC + Li_{1-n}XXO_2 \tag{2.4}$$

Oxidation at the anode (negative electrode):

$$\mathrm{LiXXO_2} \rightleftharpoons \mathrm{Li_{1-n}XXO_2} + \mathrm{nLi^+} + \mathrm{ne^-} \tag{2.5}$$

Reduction at the cathode (positive electrode):

$$\mathrm{C} + \mathrm{nLi^+} + \mathrm{ne^-} \rightleftharpoons \mathrm{Li_nC} \tag{2.6}$$

Li-ion batteries have the characteristics of high power density and energy density, and they are being widely developed for transportation and other small-scale applications.

Table 2.1 and Table 2.2 summarise the technical and economic characteristics of different ESS.

2.3 EV Integration in Power Grids

The previous section discusses the categorisation and generally applications of ESS, especially the working principle of BESS is introduced, i.e., lead-acid batteries and Li-ion batteries. As discussed in Section 1.2, the security of power grid operations is threatened by the large scale of EV integration. On the other hand, EV energy management strategies could enable EVs to work as dynamic BESS. Owing to the dynamic characteristics of EVs, the EV energy management is more challenging than BESS. The following parts of this section review the EV energy management problem in current research.

2.3.1 EV Types and Charging Levels

Three types of vehicles competed for market share at the beginning of the 20^{th} century, which are steam-powered engines, ICEs, and EVs [32]. Owing to the drawbacks of the EVs such as relatively short driving range and long charging periods, ICEs began to dominate the market. Nowadays, with the development of battery technology, EVs are becoming popular again. Certain types of EVs in the existing market are shown in

Table 2.1: Energy storage system characteristics [21, 30, 31]

ESS types	Maturity	Duration time	Capacity (kWh)	Power range (MW)	Power density (W/kg)	Efficiency (%)	Lifetime (years)
PHS	Mature	1–24+ h	2×10^5–5×10^5	10–5000	-	70–85	40–60
Underground CAES	Developed	1–24+ h	2×10^5–10^6	5–300	-	41–75	20–40
Overground CAES	Developed	6–20 h	2–8.3	3–15	-	70–89	∼20
FES	Commercial	15 s–30 min	25–5k	0.01–0.25	700–12k	80–90	15–20
Supercapacitor	Developing	ms–min	10^{-3}–5	0.01–0.3	10–10^6	85–95	20–35
Lead-acid	Commercial	1–3 h	18–100k	0.1–150		85–80	5–15
Li-ion	Demonstration	min–h	250–25k	0.05–100	150–2k	85–95	20–25
NaS	Commercial	h	400–245k	10–34	150–230	75–90	10–15
VRB	Developing	5–10 h	4k–40k	0.01–10	-	60–75	10–20
Hydrogen fuel cell	Developing	s–24 h	<200k	0.3–50	5–800	30–50	5–15

Table 2.2: Energy storage system characteristics (continued) [21, 30, 31]

ESS types	Power cost ($/kW)	Energy cost ($/kWh)	Daily self-discharge	Operating temperature (°C)	Life cycles	Response time	Energy density (Wh/kg)
PHS	500–2k	5–100	Null	Ambient	-	min	0.5–1.5
Underground CAES	500–1.8k	50–400	∼0	Ambient	8k–13k	min	30–60 bar
Overground CAES	1k–1.55k	200–250	∼0	Ambient	0.5k–1.8k	s–min	140–300 bar
FES	100–300	1k–5k	1.3–100%	20–50+	20k–100k	s	5–80
Lead-acid	200-600	200-400	0.1–0.3%	−20–60	500–2000	ms	15-80
Li-ion	1.2k–4k	400–2.5k	0.15–0.3%	−20–60	1k–10k	ms	120–230
NaS	3.2k–4k	300–500	0.05–20%	300–350	2.5k–4k	ms	120–240
VRB	1.4k–3.7k	500–800	small	10–40	>12k	ms	25–35
Supercapacitor	100–300	300–2k	10–40%	−40–85	100k–500k	ms	0.05–15
Hydrogen fuel cell	400–2k	1–15	∼0	50–100, 600–1k	1k–10k	s	600–1.2k

Table 2.3 in terms of charging power, battery capacity, and range [32].

Table 2.3: EV types and characteristics [32]

Model	Charging power (kW)	Battery capacity (kWh)	Range (miles)
Nissan Leaf	6.6	30	107
Tesla model S	10	100	315
Chevrolet Bolt	7.2	60	238
BYD e6	8	64	260

Typically, three charging levels are defined by the EV industry [33], and Table 2.4 summarises the three typical charging levels [34].

Table 2.4: EV charging standards [34]

Charging level	Voltage and current	Rated power	Time required
Level 1 charging	220 V, 13 A	2.9 kW	6–7 h
Level 2 charging	220 V, 16 A	3.5 kW	4–5 h
	220 V, 32 A	7.0 kW	2–3 h
Level 3 charging	400 A	50.0 kW	0.5 h

- **Level 1 charging** is referred to as normal charging, which has relatively low charging power 220 V/13 A in most European countries, 230 V/13 A in the U.K., and 23 V/10 A in Switzerland. It usually uses a single-phase grounded outlet.

- **Level 2 charging** is normal charging, which has relatively high charging power. This charging method is usually used at private or public outlets. Three-phase distribution grids are used and the power ranges from 10 to 20 kW. It is reported that most EV owners are expected to charge their EVs overnight at home, and thus levels 1 and 2 are the primary charging options for owners.

- **Level 3 charging** is DC fast charging, under which EVs could be fully charged in less than one hour. Owing to the charger size and cooling systems in the charger, this type of charging usually uses external chargers. The charging power could reach more than 50 kW. These systems are typically equipped at gas stations and highway rest areas.

2.3.2 Vehicle-to-Grid Technology

The concept of V2G technology is defined as a system which could control the bidirectional energy flow between an EV and the power grid [35], when the EV is parked. Several entities are involved in the application of V2G, which include the grid (TSO and DSO), aggregator, and owners. The grid broadcasts a signal and sends requests to vehicles through a third-party aggregator. The aggregator determines the actual charging and discharging of each EV. On one hand, the aggregator should meet the owners' requirements in EV management; on the other hand, the aggregator should respond to the grid's signals.

The following sections discuss the application of V2G from the grid perspective.

Frequency Regulation

Studies have indicated that EVs could operate as ESS and contribute to the frequency regulation of the grid [36–39]. The DSO is responsible for keeping the distribution network operating at a constant frequency (50 or 60 Hz, depending on the country). With the cooperation of the charging and discharging of EVs to regulate the frequency, the active power imbalance issues of the generation and consumption could be mitigated.

In frequency regulation, three types of control methods are defined by the Union for the Coordination of Transmission of Electricity, which are primary, secondary, and tertiary control [40]. When the DSO announces regulation up signals, EVs are required to operate in discharging status. If regulation down is needed, EVs are required to charge their batteries. It has been reported that EVs are most profitable under primary control [41].

Spinning Reserve

Spinning reserve and regulation are regarded as ancillary services for the power grid. It has been reported that ancillary services account for approximately $ 12 billion in the U.S. annually (5–10% of electricity cost), with 80% of this from regulation [42].

Spinning reserve capacity is sold in units MWh, where 1 MWh means that 1 MW of reserve capacity is on stand-by for 1 h, and there is no actual energy produced. When the reserve is called, the generator should deliver the actual energy. Compared with regulation and reserve, the main difference is that regulation is called more often (400 times per day) with short duration (minutes at a time); in comparison, spinning reserve is called less frequently and it has a relatively long duration (minutes to hours).

Renewable Energy Sources Integration

Nowadays, researchers are interested in the operation of V2G with RESs. Amongst various RESs, wind power and solar power are potential solutions for GHG emission reduction. Meanwhile, RESs have the characteristics of being climate-dependent and highly stochastic [43]. EV aggregators acting as ESS have the advantages of no start-up and shut-down cost and fast response speed in solving the intermittency issue of RES.

Tavakoli *et al.* [10] consider the cooperation between a wind source company and EV aggregator. The results show that the EV aggregator could compensate wind power deviations. A comparative study has been done on the impact of energy exchange between a wind power generation company and EV aggregation for wind power deviation compensation. Mohamed *et al.* [44] proposed a real-time management strategy for an EV carpark with PV power systems. The model aim is to minimise the total charging cost of EVs and the impacts of EV charging on the power grid. The results show that the total feeder loss is reduced from 5.59% to 4.53%. Gao [45] presents V2G operation in distribution systems with integrated wind sources. An EV charging strategy is proposed for the aggregator to minimise the total operation cost of the grid and to provide frequency regulation services.

2.3.3 EV Energy Management Strategies

Different types of EV energy management strategies can be classified into two categories according to decision-making location. Decisions are made by a central operator (aggregator) in centralised strategies and by individual EVs in decentralised strategies

[46]. The concepts of centralised and decentralised control strategies are illustrated in Figure 2.4.

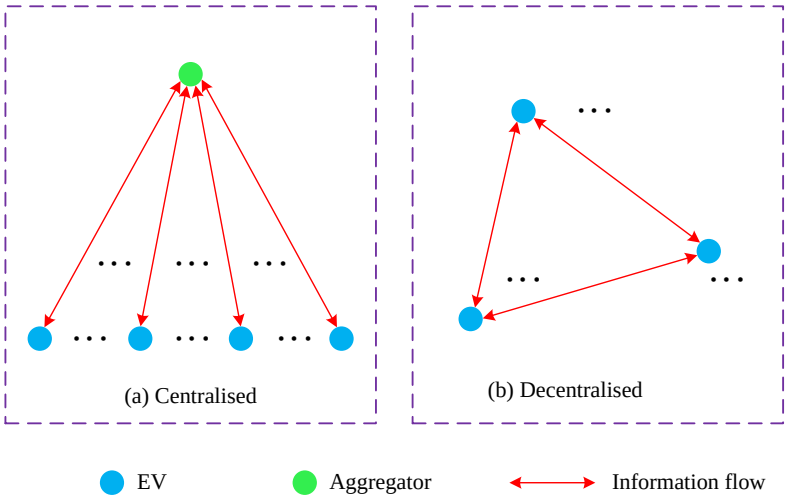

Figure 2.4: Centralised and decentralised strategies in EV energy management

Centralised strategies are utilised in commercial charging stations or carparks, where chargers are owned by the charging stations and carparks, and decentralised strategies are utilised by residential EV owners who own chargers by themselves.

Centralised Strategy

In centralised strategies, decisions are made by aggregators (at the system level), i.e. each EV sends its information to the aggregator, and then the EV aggregator determines the operation of the EVs over time. To form a scheduling strategy, the aggregator needs to centralise relevant information: EV battery information, EV driving patterns, DR signals, and power grid constraints. The aggregator directs and controls the charging/discharging of EVs, as shown on the left side of Figure 2.4. Centralised scheduling strategies include Linear Programming (LP) [10, 47–52], quadratic programming [53], dynamic programming [54, 55], and stochastic programming [48, 56–58].

Centralised strategies can usually find the globally optimal solution and manage EV stochastic behaviours well. However, centralised strategies rely on high communication

infrastructure between the EVs and aggregator, and high computational complexity is another problem with a large number of EVs. Moreover, maintaining EV end-user privacy is a problem, because EV users need to share their private driving information with the aggregator [46].

Decentralised Strategy

In decentralised strategies, the charging and discharging decisions are made by EVs autonomously based on information provided by the grid, e.g. price signals. Then, each EV scheduling result is submitted to the grid, individually. Normally, there are several iterations between the grid and EVs until an agreement has been reached [46].

Decentralised strategies have no scalability or user privacy issues, and the EV battery can be modelled in a detailed way based on decentralised strategies. However, a detailed representation of the EV battery requires high local intelligence. Moreover, the scheduling results of decentralised strategies cannot find the global optimal solution, as the optimisation usually gets trapped at a local optimal solution.

Table 2.5 summarises the main advantages and drawbacks of centralised and decentralised strategies.

Table 2.5: Advantages and disadvantages of centralised and decentralised methods

	Advantage	Disadvantage
Centralised	• Global optimal • Network capacity	• Complex communication infrastructure • Privacy violations • Optimisation complexity
Decentralised	• Less communication infrastructure • Protect privacy • Less complexity	• Uncertainty in the final results • Sub-optimal

2.3.4 Stakeholders' Interests in EV Energy Management

Numerous previous studies of the EV energy management are mainly categorised based on three stakeholders: EV owners, EV aggregator and the grid.

EV Owners

The EV owners are interested in minimising their charging fee for charging EVs, in addition, the driving limits and degradation of EV battery are also two important factors to be taken into consideration in EV energy management [59]. The smart charging strategy of EVs in response to the RTP has been studied in [11, 60, 61] to minimise the EV charging cost, including energy purchasing cost and the income of injecting energy back to the grid. The authors in [62, 63] developed home energy management systems structure, where household applications are scheduled in cooperation with EVs to minimise the total energy consumption cost based on DR programmes. In addition, the integration of DGs is considered. In [64], an accurate linear battery charging model is formulated, where the real-life battery charging constraints are imposed. The results demonstrated that the charging cost is reduced. Dynamic programming is used in [65] to minimise the EV owners' charging fee based on price signals without increasing battery degradation. The authors of [51] considered EV charging in an unbalanced electrical distribution system with distributed generation, to minimise the energy purchasing cost of EVs. In [66], the battery degradation cost is involved in an EV charging and discharging scheduling model. In the model, the degradation rate is related to the total discharging energy, and thus an iterative Mixed-Integer Linear Programming (MILP) algorithm is adopted. In addition, a sensitivity analysis of the charging and discharging strategy is carried out in terms of the discharging reward, charging period, and battery capital cost. In [67], an online constrained optimisation algorithm is proposed to minimise EV owners' charging fee, the power generation limits of the AC grid and power flow issues are considered in the EV energy management problem.

The common issue in these studies is that the relationship between EV owners with other stakeholders are ignored. In this thesis, the economic relationship between EV

owners with EV aggregator is discussed in details in chapter 4, and an owner-aggregator contract is designed in chapter 5.

EV Aggregator

The research on the EV aggregator profit maximisation problem has been widely studied.

In [68], the authors used a stochastic programming approach to examine the impact of different DR programs on EV parking lot profit. The results demonstrated that by participating in a selected combination of DR programmes, the parking lot profit can be significantly increased. Several studies have addressed the EV aggregator or ESS bidding strategy in electricity markets (regulation and reserve markets) [69, 70]. In [71], an aggregator providing ancillary services to the power grid is proposed. A robust algorithm is applied in the model by considering the uncertainty in energy and reserve prices based on LP. Furthermore, a battery degradation cost model is presented. The results showed that the aggregator revenue can be increased by 7.8% with the aid of ESS. In [72], ESS providing frequency regulation to power grids in cooperation with wind power is analysed. A real-time cooperative strategy of the ESS is proposed to maximise the profit in both energy and reserve markets. In this study, the optimal bidding of the ESS is implemented by assuming that all parameters are known in advance without uncertainty. Reference [73] considered the EV aggregator bidding strategy in both energy and reserve markets. In this study, the acceptance of the EV owners in providing reserve is modelled; however, the RT reserve deployment in impacting DA bidding is not well discussed. A two-stage stochastic programming model is proposed in [56] to minimise the net expected energy cost of the aggregator. The price deviation in the first stage (DAM) and several possible EV parking scenarios in the second stage (RTM) are considered in the model. However, the uncertainty in the reserve capacity deployment requirements at different times from the grid perspective is not considered. In [74, 75], the authors used a Robust Optimisation (RO) method to formulate the uncertainty in the prices, but the uncertainty in the grid's requirements is neglected. Kazemi *et al.* [76] addressed the uncertainty of ancillary services based on a RO method. It is assumed

that the ESS should deploy reserve in the RTM based on the RDR from the grid, and the uncertainty in the amount of the RDR is considered in the model. However, the authors only considered the amount of the RDR, and the impacts of the reserve being required to deploy at different times on the aggregator bidding and profit are neglected.

The common issue in these studies is that the uncertainty of reserve deployment requirements in terms of time and amount are not considered. In this thesis, the impact of the uncertainty of the RTM in DA bidding is taken into account, and the aggregator bidding strategy in the DAM is presented in chapter 5.

Grid

Considering the grid interest, EVs are regarded as ESS to provide ancillary services to the grid. In [45, 77, 78], the EVs charging and discharging behaviours are scheduled from the viewpoint of power grids to reduce the total operating cost or ensure the power grids stability by reducing power fluctuation level. The power grids constraints such as total load limits, voltage drop and phase balances are involved in these models. The cooperative EVs charging with power grids and transportation networks have been widely investigated [79]. The authors in [80] proposed a stochastic security constrained unit commitment model coupled with a traffic model, which jointly consider the EVs charging impact to both power grids and the traffic network. In [81], an EV charging station planning scheme is proposed by coupling transportation network and distribution network. A spatial-temporal model is built in [82] to investigate the optimisation of EVs in distribution systems, where the mobility of EVs in the transportation network is considered. Lian *et al.* [83] optimised the operation of ESS in response to frequency regulation signals from the grid. An economic analysis is performed based on the battery lifetime (degradation cost) and the U.K. frequency regulation market. A hierarchical framework of EV charging is proposed in [84] to minimise the system peak loads at the provincial and city levels. The interrelationship between various levels is identified in terms of energy transactions and information exchange. In [52], Micro Grid (MG) energy management systems were built involving household load, EVs, and renewable

sources. The model aimed to minimise the economic cost of energy exchange between the MG and the main grid.

Moreover, some researchers used MOO methods to address the trade-off between EV owners and the grid. Crow *et al.* [85] applied an augmented ε-constraint-based MOO method to tackle the conflict between owners and systems operator in economically charging and maintaining system load profiles. The battery degradation cost minimisation is considered in the model. In [86], the operation strategy of MGs involving PV and EVs is presented. The ε-constraint method followed by fuzzy decision-making is applied to jointly minimise the operation cost of EVs and voltage deviation.

The common issue in these studies is that several objectives are involved in one objective function, but the responsibility of each stakeholder is not clearly defined. A bi-level strategy is proposed in chapter 6, which clearly defines the responsibility of the TSO and EV aggregator.

Table 2.6 and 2.7 summarise the related works and the proposed work based on five aspects: stakeholder viewpoint, objective and optimisation algorithm.

Summary

A general summary can be made that previous studies mainly focus on the optimal operation of EV charging and discharging from the viewpoint of different stakeholders: EV owners, aggregator and the grid. However, there has been little work reported on investigating the relationship between these stakeholders from the perspective of the economic benefits. Because EVs belong to each EV owner, the economic benefits of each EV owner is an important part of the economic interactions among the stakeholders. Therefore, it is not practical to consider the energy and information interactions from the viewpoint of a single stakeholder.

Table 2.6: References summary of EV energy management strategies

	Reference	[11]	[51]	[52]	[49]	[57]	[45]	[48]	[44]	[50]	[58]	[56]	[53]	[87]	[71]
Stakeholder	EV owner	✓									✓	✓			
	Aggregator				✓	✓		✓	✓	✓			✓	✓	✓
	Grid		✓	✓			✓								
V2G	Unidirectional	✓			✓	✓			✓		✓			✓	✓
	Bidirectional		✓	✓			✓	✓		✓		✓	✓		
Service	Reserve											✓	✓		✓
	Regulation				✓		✓			✓					
	RES support		✓	✓			✓		✓					✓	
	Peak shaving								✓	✓					
	Market balancing					✓		✓			✓				
Objective	Min charging cost	✓						✓	✓		✓	✓	✓		
	Min systems cost		✓	✓			✓			✓					
	Max profit				✓	✓								✓	✓
Constraint	EV limits	✓	✓	✓	✓	✓	✓	✓	✓	✓	✓	✓	✓	✓	✓
	Distribution system limits		✓				✓		✓	✓					
	Transmission system limits														
	MG limits			✓										✓	
Method	MILP		✓	✓	✓					✓				✓	✓
	Heuristic algorithm	✓					✓						✓		
	Stochastic programming					✓		✓			✓	✓			
	Fuzzy agent								✓						

Table 2.7: References summary of EV energy management strategies (continued)

	Reference	[88]	[89]	[90]	[91]	[92]	[74]	[93]	[73]	[94]	[82]	[38]	[68]	[95]	[85]
Stakeholder	EV owner						✓	✓							✓
	Aggregator			✓		✓			✓			✓	✓	✓	
	Grid	✓	✓	✓	✓			✓		✓	✓				✓
V2G	Unidirectional	✓	✓	✓			✓			✓	✓				
	Bidirectional				✓	✓		✓	✓			✓	✓	✓	✓
Service	Reserve					✓			✓				✓		
	Regulation			✓		✓						✓			
	RES support		✓	✓	✓									✓	
	Peak shaving							✓		✓	✓		✓		✓
	Market balancing			✓											
Objective	Min charging cost	✓					✓	✓					✓		✓
	Min systems cost		✓	✓	✓	✓		✓		✓	✓			✓	
	Max profit								✓			✓	✓		
	Min curtailment	✓													
Constraint	Distribution system limits		✓	✓	✓	✓				✓	✓			✓	✓
	Transmission system limits	✓													
	MG limits														
Method	MILP			✓		✓		✓	✓		✓		✓		✓
	Heuristic algorithm	✓	✓		✓							✓			
	Stochastic programming														
	Robust optimisation						✓								
	Fuzzy agent									✓				✓	

2.4 Summary

In this chapter, different ESS including their characteristics, current status, and applications have been reviewed, and ESS will play a vital rule in future power grids. The utilisation of ESS in power grids is analysed from the viewpoints of generation, transmission, and distribution. The utilisation of various types of ESS is necessary, owing to the large penetration of renewable energy and distributed generation.

In addition, the application of EVs as dynamic ESS in power grids is reviewed. The EV energy management problem is reviewed in terms of centralised and decentralised strategies. Finally, EV energy management is reviewed according to three stakeholders in smart grids, i.e. the owners, aggregator and grid.

Chapter 3

Mathematical Modelling and Optimisation Techniques

3.1 Introduction

In this chapter, the mathematical modelling and optimisation techniques are introduced. Four models are presented in this chapter, which include the ESS, single EV, EV information, and DC-OPF models. Two programming methods are introduced in Section 3.2. In Section 3.3, the charging and discharging model of a Li-ion battery is formulated by taking charging power limits and SOC limits into account. The dynamic charging characteristics of the Li-ion battery are also involved in the model. After that, in Section 3.4, a single EV charging and discharging model is built based on the ESS model in Section 3.3. To involve the EV driving requirements in the EV charging and discharging modelling, the EV information model is introduced in Section 3.5. In order to enable EV participation in power grid operation, a transmission network is modelled in Section 3.6, based on the DC-OPF model.

To achieve the optimisation of these models, three optimisation techniques are utilised, namely MOO, stochastic programming, and RHO. Section 3.7 introduces two methods: WSM and ε-constraint method. Then, two optimisation methods, which

could be used to address uncertainties, are presented in Section 3.8 and 3.9. Stochastic programming method is introduced in Section 3.8, which formulates the uncertainty as several scenarios and involves the probability of each scenario in the optimisation. Section 3.9 discusses the RHO method, which is an iterative, online optimisation method. The optimisation results are fixed and updated in each iteration.

3.2 Programming Methods

Mixed-Integer Linear Programming

MILP is a mathematical optimisation method of a linear objective function, subject to linear equality and linear inequality constraints, and some variables are restricted to integers. The MILP problem can be formulated as follow:

$$\begin{aligned} \text{Minimise} \quad & \mathbf{c^T x} \\ \text{subject to} \quad & \mathbf{A x} \leq \mathbf{b} \\ & \mathbf{x}_i \in \mathbb{Z} \quad \forall i \in \mathcal{I} \end{aligned} \tag{3.1}$$

where $\mathbf{x}$ is the vector of variables to be optimised; $\mathbf{c}$ and $\mathbf{b}$ are vectors; and $\mathbf{A}$ is a matrix. $\mathcal{I}$ is a nonempty subset.

MILP is suitable for the modelling of the ESS and EV, because the charging status, discharging status and idling status can be represented by integer (binary) variables and the charging/discharging power can be represented by continuous variables.

Mixed-Integer Quadratic Programming

As a special type of mathematical programming problem, Mixed-Integer Quadratic Programming (MIQP) is a type of nonlinear programming. In MIQP, the objective function is to optimise a quadratic function, subject to linear constraints, with some

integer variables. The MIQP problem can be formulated as follow:

$$\begin{aligned} \text{Minimise} \quad & \frac{1}{2}\mathbf{x}^T\mathbf{Q}\mathbf{x} + \mathbf{c}^T\mathbf{x} \\ \text{subject to} \quad & \mathbf{A}\mathbf{x} \leq \mathbf{b} \\ & \mathbf{x}_i \in \mathbb{Z} \quad \forall i \in \mathcal{I} \end{aligned} \tag{3.2}$$

where $\mathbf{Q}$ is a real symmetric matrix.

MIQP is used to formulate the DC-OPF model, because the relationship between the generation cost with the output power of generators can be represented by a quadratic function, see Equation (3.38). The other models and optimisation techniques discussed in this thesis are formulated based on MILP method.

In this thesis, MILP and MIQP methods are used for the modelling and optimisation. The MILP and MIQP problems, including objective functions and constraints, are modelled and solved by the intlinprog and quadprog solvers in MATLAB. The modelling and optimisation are conducted on a PC with Intel Core i5 CPU, 3.20 GHz and 8.00 GB installed memory.

3.3 ESS Charging/Discharging Model

The concept of State of Charge (SOC) is used to measure the charge content of the battery, which is a dimensionless number ranging from 0 to 1. The battery SOC at time t is defined as

$$SOC(t) = \frac{Q_b + \Delta Q}{Q_0} = \frac{Q_b}{Q_0} + \frac{1}{Q_0}\int_0^t I(t)dt \tag{3.3}$$

where Q_0 and Q_b stand for the total capacity and the amount of charge at the initial time of the battery (with unit Ah). $I(t)$ denotes the charging current of the battery at time t.

The discretised form of Equation (3.3) is shown in Equation (3.4)

$$\begin{aligned} SOC_t &= \frac{Q_b}{Q_0} + \frac{\sum_1^t I_t \Delta t}{Q_0} \\ &= \mathrm{SOC^b} + \frac{\sum_1^t I_t V_b \Delta t}{Q_0 V_b} \\ &= \mathrm{SOC^b} + \frac{\sum_1^t p_t \Delta t}{E_0} \end{aligned} \tag{3.4}$$

where $\mathrm{SOC^b}$ is the battery SOC at the initial time, E_0 is the energy capacity of the battery, V_b is the battery voltage, p_t stands for the power flow into or out of (charging or discharging power) the battery at time t, and ΔT is the time interval.

For a typical ESS charging/discharging scheduling problem, the objective function is defined to minimise the total cost among times from 1 to M, which consists of two parts: 1) charging cost and discharging income J_1^{ess} and 2) battery degradation cost J_2^{ess}. The objective function is shown in (3.5a)

$$\text{Minimise} \quad J_1^{\mathrm{ess}} + J_2^{\mathrm{ess}} \tag{3.5a}$$

$$J_1^{\mathrm{ess}} = \sum_{t=1}^{M} (r_t^+ p_t^+ - r_t^- p_t^-) \Delta T \tag{3.5b}$$

$$J_2^{\mathrm{ess}} = \sum_{t=1}^{M} \mathrm{D^{ess}} (p_t^+ + p_t^-) \Delta T \tag{3.5c}$$

where r_t^+ and r_t^- are the charging and discharging RTP at time t, p_t^+ and p_t^- are the variables of charging and discharging power of the ESS at time t, and $\mathrm{D^{ess}}$ represents the degradation rate of the ESS.

3.3.1 Constant Maximum Charging Power Constraint

Constraints (3.6) and (3.7) ensure that, at each time t, the charging and discharging operations of the ESS p_t^+ and p_t^- are limited between zero and the maximum charging and discharging power

$$0 \leq p_t^+ \leq \overline{P}^{\mathrm{ess}} i_t^+ \qquad \forall t \tag{3.6}$$

$$0 \leq p_t^- \leq \overline{P}^{\text{ess}} i_t^- \qquad \forall t \tag{3.7}$$

where it is assumed that the ESS have the same maximum charging and discharging power, and the maximum power is assumed as a constant value $\overline{P}^{\text{ess}}$.

Constraint (3.8) prevents from the ESS charging and discharging simultaneously,

$$i_t^+ + i_t^- \leq 1 \qquad \forall t \tag{3.8}$$

where i_t^+ and i_t^- are both binary variables.

The relationship between the charging/discharging power of ESS with the battery SOC is described in (3.9) and (3.10)

$$SOC_t^{\text{ess}} = SOC_{t-1}^{\text{ess}} + \frac{(p_t^+ - p_t^-)\Delta T}{E^{\text{ess}}} \qquad \forall t, t \neq 1 \tag{3.9}$$

$$SOC_t^{\text{ess}} = \text{SOC}^{\text{b}} + \frac{(p_t^+ - p_t^-)\Delta T}{E^{\text{ess}}} \qquad t = 1 \tag{3.10}$$

Considering the battery capacity of the ESS, constraint (3.11) is used to prevent the battery from over charging or discharging

$$\underline{\text{SOC}} \leq SOC_t^{\text{ess}} \leq \overline{\text{SOC}} \qquad \forall t \tag{3.11}$$

where $\underline{\text{SOC}}$ and $\overline{\text{SOC}}$ stand for the upper and lower bound of the battery SOC, respectively.

Considering the ESS operation on the next day, constraint (3.12) guarantees that the battery SOC of the ESS at the end of the time ($t = M$) is not less than a specific value SOC^{e}:

$$SOC_t^{\text{ess}} \geq \text{SOC}^{\text{e}} \qquad t = M \tag{3.12}$$

3.3.2 Linear CC-CV Maximum Charging Power Constraint

In Section 3.3.1, the maximum charging power is assumed as a constant value, as shown in constraint (3.6). A more accurate linear Constant Current-Constant Voltage (CC-CV)

battery charging model is presented in this section, where the relationship between the maximum charging power and the SOC is represented in Figure 3.1.

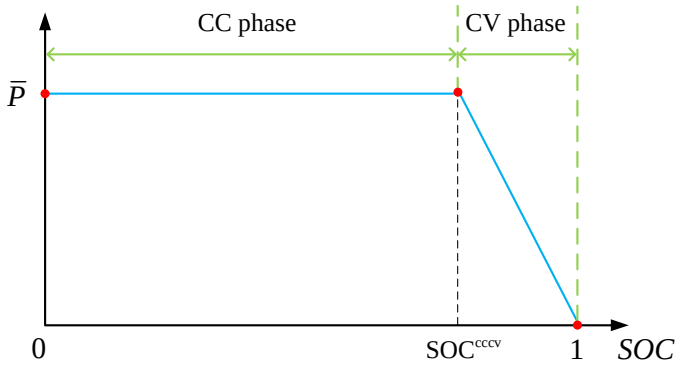

Figure 3.1: Linear CC-CV maximum charging power limits

It can be seen from the figure that the battery charging process consists of two parts: the CC phase and CV phase. In the CC phase, when the SOC is less than SOC^{cccv} ($0 \leq SOC < SOC^{cccv}$), the maximum charging power is assumed as a constant value, denoted by $\overline{P}$. In the CV phase, when $SOC^{cccv} \leq SOC \leq 1$, the maximum charging decreases linearly from $\overline{P}$ to 0 as the SOC increases from SOC^{cccv} to 1. The mathematical representation of the liner CC-CV battery charging model is shown in Equations (3.13) and (3.14):

$$0 \leq p_t^+ \leq \overline{P}^{ess} i_t^+ \qquad \forall t \tag{3.13}$$

$$0 \leq p_t^+ \leq \overline{P}^{ess} \frac{1 - SOC_t^{ess}}{1 - SOC^{cccv}} i_t^+ \qquad \forall t \tag{3.14}$$

where SOC^{cccv} represents the battery SOC at which the CC phase switches to the CV phase.

3.3.3 Dynamic Maximum Charging Power versus SOC Constraint

Detailed battery maximum charging power constraints are presented in this section. Figure 3.2 shows the piecewise linearised relationship between the maximum charging power and the SOC under normal charging mode. In the CC phase, the charging current

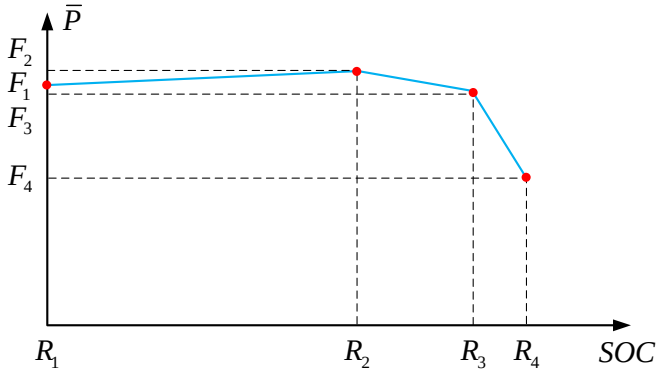

Figure 3.2: Piecewise linear approximation of the maximum charging power

is maintained at a constant value and the charging voltage increases gradually with the SOC. As a result, the maximum charging power slowly increases. In the CV phase, the charging voltage is maintained at a constant value and the charging current decreases. Thus, the charging power decreases as the SOC increases.

Figure 3.2 indicates that the nonlinear function is approximated by three segments. Therefore, the dynamic maximum charging power is modelled as follows:

$$0 \leq p_t^+ \leq \left(\frac{F_{s+1} - F_s}{R_{s+1} - R_s} SOC_{t-1}^{\text{ess}} + \frac{F_s R_{s+1}}{R_{s+1} - R_s} \right) i_t^+ \qquad \forall t, t \not= 1, s \tag{3.15}$$

$$0 \leq p_t^+ \leq \left(\frac{F_{s+1} - F_s}{R_{s+1} - R_s} \text{SOC}^{\text{b}} + \frac{F_s R_{s+1}}{R_{s+1} - R_s} \right) i_t^+ \qquad t = 1, \forall s \tag{3.16}$$

Equation (3.15) divides the battery SOC into $S - 1$ segments, where S is the number of the red breakpoints in Figure 3.2.

Because there are multiplication terms in (3.15) and (3.16), these two constraints can be linearised based on the big-M method as follows:

$$0 \leq p_t^+ \leq \frac{F_{s+1} - F_s}{R_{s+1} - R_s} SOC_{t-1}^{\text{ess}} + \frac{F_s R_{s+1}}{R_{s+1} - R_s} \qquad \forall t, t \not= 1, s \tag{3.17}$$

$$0 \leq p_t^+ \leq \frac{F_{s+1} - F_s}{R_{s+1} - R_s} \text{SOC}^{\text{b}} + \frac{F_s R_{s+1}}{R_{s+1} - R_s} \qquad t = 1, \forall s \tag{3.18}$$

$$0 \leq p_t^+ \leq \text{M}_{\text{big}} i_t^+ \qquad \forall t \tag{3.19}$$

where M_{big} is a sufficiently large constant value. The big-M method works as follow:

- When $i_t^+ = 0$, according to constraint (3.19), p_t^+ is forced to zero, and the ESS operate in discharging status or idling status.
- When $i_t^+ = 1$, constraint (3.19) is relaxed, such that constraints (3.15) and (3.16) are equivalent to (3.17) and (3.18). Under this circumstance, the ESS operate in charging status, and the charging power p_t^+ is limited by constraints (3.17) and (3.18).

3.4 Single EV Charging/Discharging Model

As a type of dynamic ESS, EVs could operate in V2G mode to minimise the charging fee while satisfying EV owners' driving requirements. The optimisation model of EVs is similar to the ESS model represented in Section 3.3. The optimisation model of a single EV is given as follows.

The objective function of EV n shown in (3.20a) has the same format as the ESS model, i.e. minimise the charging fee including the charging and discharging cost $J_{n,1}^{\text{ev}}$ and the battery degradation cost $J_{n,2}^{\text{ev}}$:

$$\text{Minimise} \quad J_{n,1}^{\text{ev}} + J_{n,2}^{\text{ev}} \tag{3.20a}$$

$$J_{n,1}^{\text{ev}} = \sum_{t=1}^{M} \left(r_t^+ p_{n,t}^+ - r_t^- p_{n,t}^- \right) \Delta T \tag{3.20b}$$

$$J_{n,2}^{\text{ev}} = \sum_{t=1}^{M} D^{\text{ev}} \left(p_{n,t}^+ + p_{n,t}^- \right) \Delta T \tag{3.20c}$$

where $p_{n,t}^+$ and $p_{n,t}^-$ denote the charging and discharging variables of EV n at time t and D_n^{ev} is the degradation rate of the EV battery.

The EV scheduling constraints are illustrated in Figure 3.3, and the mathematical formulations of these constraints are given in Equations (3.21)-(3.31).

Equations (3.21) and (3.22) mean that EV n can only be scheduled during the

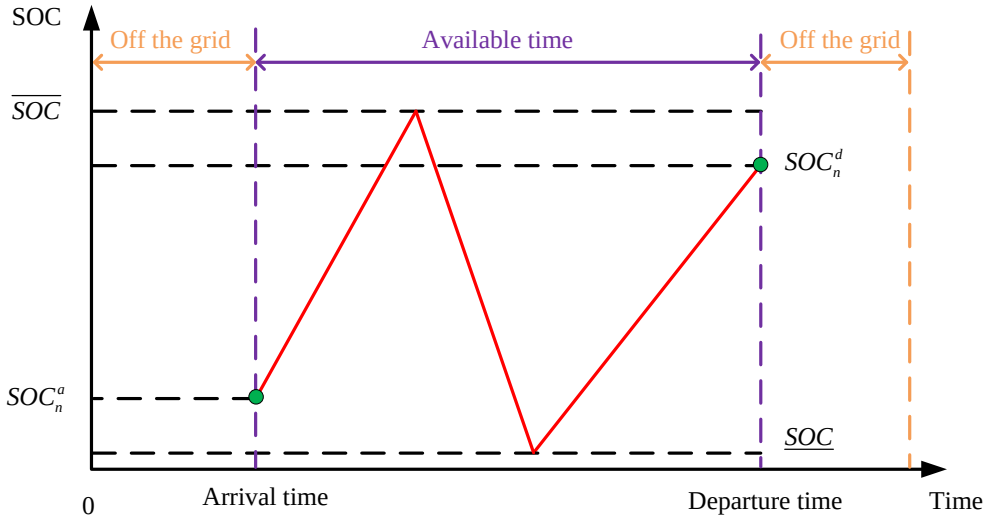

Figure 3.3: Single EV charging/discharging scheduling constraints

available time ($t_n^a \leq t < t_n^d$). The charging and discharging variables are forced to be zero when EV n is off the grid ($t < t_n^a$ or $t \geq t_n^d$).

$$i_{n,t}^{+} = \begin{cases} 0 & 1 \leq t < t_n^a \\ \{0,1\} & t_{n,t}^a \leq t < t_n^d \\ 0 & t_n^d \leq t \leq M \end{cases} \tag{3.21}$$

$$i_{n,t}^{-} = \begin{cases} 0 & 1 \leq t < t_n^a \\ \{0,1\} & t_{n,t}^a \leq t < t_n^d \\ 0 & t_n^d \leq t \leq M \end{cases} \tag{3.22}$$

$$i_{n,t}^{+} + i_{n,t}^{-} \leq 1 \quad \forall t \tag{3.23}$$

where $i_{n,t}^{+}$ and $i_{n,t}^{-}$ are binary variables, which indicate whether the EV n is in the charging status, discharging status, or idling status.

The dynamic maximum charging power limits are considered in the EV scheduling problem. The linearised maximum charging power limits are formulated in constraints

(3.24)-(3.26):

$$0 \leq p_{n,t}^{+} \leq \frac{F_{s+1}-F_s}{R_{s+1}-R_s} SOC_{n,t-1} + \frac{R_{s+1}F_s}{R_{s+1}-R_s} \qquad \forall s,t,t \neq t_n^a \tag{3.24}$$

$$0 \leq p_{n,t}^{+} \leq \frac{F_{s+1}-F_s}{R_{s+1}-R_s} SOC_n^a + \frac{R_{s+1}F_s}{R_{s+1}-R_s} \qquad \forall s,t=t_n^a \tag{3.25}$$

$$0 \leq p_{n,t}^{+} \leq \mathrm{M_{big}} i_{n,t}^{+} \qquad \forall t \tag{3.26}$$

$$0 \leq p_{n,t}^{-} \leq \overline{P}_n^{\mathrm{ev}} i_{n,t}^{-} \qquad \forall t \tag{3.27}$$

The relationship between the charging/discharging power and the SOC of the EV n during the available time is formulated in (3.28) and (3.29):

$$SOC_{n,t} = SOC_{n,t-1} + \frac{\left(p_{n,t}^{+} - p_{n,t}^{-}\right) \Delta T}{E_n^{\mathrm{ev}}} \qquad t_{n,t}^a < t < t_n^d \tag{3.28}$$

$$SOC_{n,t} = SOC_n^{\mathrm{a}} + \frac{\left(p_{n,t}^{+} - p_{n,t}^{-}\right) \Delta T}{E_n^{\mathrm{ev}}} \qquad t = t_n^a \tag{3.29}$$

Equation (3.30) indicates that the battery SOC is not taken into account (assumed to be zero) when EV is off the grid, and the battery SOC is bounded by $\overline{\mathrm{SOC}}$ and $\underline{\mathrm{SOC}}$ during available time (connected to the grid):

$$SOC_{n,t} = \begin{cases} 0 & t < t_n^a \\ \left[\underline{\mathrm{SOC}}, \overline{\mathrm{SOC}}\right] & t_n^a \leq t \leq t_n^d \\ 0 & t > t_n^d \end{cases} \tag{3.30}$$

To ensure the next day's driving requirements of EV owner n are satisfied, constraint (3.31) guarantees the EV battery SOC at the departure time is not less than the target value $\mathrm{SOC_n^d}$:

$$SOC_t \geq \mathrm{SOC_n^d} \qquad t = t_n^d \tag{3.31}$$

3.5 EV Information Model

The Truncated Gaussian Distribution (TGD) has been widely used to model EV transportation behaviours [68, 78, 80]. To model EV transportation behaviours, it is assumed that the arrival time (t_n^{a}), departure time (t_n^{d}), and battery SOC at arrival time (initial SOC, SOC_n^{a}) follow TGDs.

Equations (3.32)–(3.34) are used to generate the arrival/departure time and the initial SOC of the EV n,

$$t_n^a = f(x) = f_{TG}\left(x; \mu_a, \sigma_a^2, \left(t_n^{a,\min}, t_n^{a,\max}\right)\right) \quad \forall n \tag{3.32}$$

$$t_n^d = f(x) = f_{TG}\left(x; \mu_d, \sigma_d^2, \left(t_n^{d,\min}, t_n^{d,\max}\right)\right) \quad \forall n \tag{3.33}$$

$$SOC_n^a = f(x) = f_{TG}\left(x; \mu_{soc}, \sigma_{soc}^2, \left(SOC_n^{a,\min}, SOC_n^{a,\max}\right)\right) \quad \forall n \tag{3.34}$$

where f_{TG} denotes the TGD. The mean value and the variances of the random variable are represented by μ and σ^2, respectively. $t_n^{a,\min}$ and $t_n^{a,\max}$ represent the minimum and maximum arrival time. $t_n^{d,\min}$ and $t_n^{d,\max}$ represent the minimum and maximum departure time. $SOC_n^{a,\min}$ and $SOC_n^{a,\max}$ represent the minimum and maximum initial SOC.

Equation (3.35) guarantees the generated EV information is logical. That is, the departure time should be later than the arrival time:

$$t_n^d > t_n^a \quad \forall n \tag{3.35}$$

In addition, the generated EV information should be enough for the EV to be charged to the target SOC during parking time:

$$SOC_n^a + \frac{\overline{P}_n^{\mathrm{ev}}\left(t_n^d - t_n^a\right)}{E_n^{\mathrm{ev}}} \geq \mathrm{SOC_n^d} \quad \forall n \tag{3.36}$$

If the target SOC is not met, the EV may adopt as-fast-as-it-can mode, which means

the EV should operate in charging status until the departure time. This kind of EVs are not considered in this thesis, because these EVs have no flexibility and can not be scheduled.

3.6 DC-Optimal Power Flow Model

The OPF is a classic nonlinear optimisation problem, that determines the best operating level of generators or the minimal power losses in power grids to meet the load demand, subject to physical constraints [96, 97]. The concept of DC-OPF is originally from the 1960s and it denotes the linearised form of AC-OPF [98], where the reactive power and sinus terms are not considered in the DC-OPF.

In the DC-OPF model, the objective function is usually defined as the minimisation of the total generation cost of all generators in the power grid. The optimisation is subject to the power network constraints and the equipment operation limits. The objective function of the DC-OPF model is written as:

$$\text{Minimise} \qquad \sum_{i \in \boldsymbol{G}} f\left(p_i^{\mathrm{G}}\right) \tag{3.37}$$

which is the summation of all generators costs in the system, and the generation cost of the generator at bus i is calculated based on Equation (3.38):

$$f\left(p_i^{\mathrm{G}}\right) = a_i {p_i^{\mathrm{G}}}^2 + b_i p_i^{\mathrm{G}} + c_i \quad \forall i \in \boldsymbol{G} \tag{3.38}$$

where p_i^{G} represents the output power of the generator at bus i.

The generation limit constraint of the generator is formulated in (3.39):

$$\underline{P}_i^{\mathrm{G}} \leq p_i^{\mathrm{G}} \leq \overline{P}_i^{\mathrm{G}} \quad \forall i \in \boldsymbol{G} \tag{3.39}$$

where $\underline{P}_i^{\mathrm{G}}$ and $\overline{P}_i^{\mathrm{G}}$ are the minimum and maximum generation limits of the generator at bus i, respectively.

The equality constraint (3.40) stands for the power balance of the system, which means that at each bus i, the total generation minus the power flow from bus i to another bus j equals to the load demand:

$$p_i^{\mathrm{G}} - \sum_{i,j} P_{i,j}^{\mathrm{T}} = P_i^{\mathrm{L}} \qquad \forall i \tag{3.40}$$

where $P_{i,j}^{\mathrm{T}}$ stands for the real power flow on the transmission line from bus i to bus j and P_i^{L} denotes the load demand at bus i.

To avoid the transmission line overloading, constraint (3.41) represents that the power capacity is limited by the transmission line capacity:

$$-F_{i,j}^{\mathrm{T}} \leq P_{i,j}^{\mathrm{T}} \leq F_{i,j}^{\mathrm{T}} \qquad \forall i \tag{3.41}$$

where $F_{i,j}^{\mathrm{T}}$ stands for the capacity of the transmission line between bus i and j.

As mentioned before, the DC-OPF model is a linear approximation of the AC-OPF model. To achieve the approximation, the small-angle approximation and other relaxation methods are applied [96, 99]. In order to determine the real power flow on the transmission line $P_{i,j}^{\mathrm{T}}$, three assumptions are made in the DC-OPF:

- The shunt conductance of the transmission line is negligible.
- The ohmic resistance of the transmission line is much smaller than the reactance; therefore, the resistance can be ignored.
- The voltage at each bus is assumed as $V_i = V_j = 1$ p.u., and the voltage angle $\sin\theta$ is small enough, so that $\sin\theta \approx \theta$.

Based on these assumptions, the real power flow on the transmission line between bus i and bus j is simplified as in Equation (3.42):

$$P_{i,j}^{\mathrm{T}} = -\frac{\sin\left(\theta_j - \theta_i\right)}{X_{i,j}} \approx \frac{\theta_i - \theta_j}{X_{i,j}} \tag{3.42}$$

Thus, the power flow in branch i, j can be represented by the voltage angles in busses i and j (details deductions steps can be found in reference [100]).

Finally, the power balance constraint and the transmission line capacity limits shown in Equations (3.40) and (3.41) are linearised, and the linearised constraints are written as follows:

$$p_i^{\mathrm{G}} - \sum_{i,j} \frac{\theta_i - \theta_j}{X_{i,j}} = P_i^{\mathrm{L}} \quad \forall i \tag{3.43}$$

$$-F_{i,j} \leq \frac{\theta_i - \theta_j}{X_{i,j}} \leq F_{i,j} \qquad \forall i \tag{3.44}$$

3.7 Multi-Objective Optimisation

MOO is an area of multiple-criteria decision-making method, which involves more than one objective function to be optimised (maximised or minimised), subject to a set of constraints. In MOO, the multiple objectives do not coincide, which means that an optimal solution for one objective is sub-optimal for another. Unlike single-objective optimisation, MOO provides a set of solutions which reflects the trade-off between different objectives. Thus, from the viewpoint of the decision-maker, MOO provides a better understanding of the system. MOO has been applied in many fields in engineering and the sciences. For example, in the transportation sector, the designer needs to balance the trade-off of two objectives by maximising the performance while minimising the energy and emission of the vehicle.

The general MOO problem is expressed in (3.45), which has L objective functions:

$$\begin{aligned}
\text{Minimise} \quad & F(\mathbf{X}) = [f_1(\mathbf{X}), f_2(\mathbf{X}), \cdots, f_L(\mathbf{X})] \\
\text{subject to} \quad & g_j(\mathbf{X}) \geq 0 \qquad j = 1, 2, \cdots, J \\
& h_k(\mathbf{X}) = 0 \qquad k = 1, 2, \cdots, K \\
\text{with} \quad & \mathbf{X} = [x_1, x_2, \cdots, x_i, \cdots, x_I] \\
& \underline{x}_i \leq x_i \leq \overline{x}_i \qquad i = 1, 2, \cdots, I
\end{aligned} \tag{3.45}$$

where F represents the objective functions, $\mathbf{X}$ is an I-dimensional vector representing the decision variables, and the variables are bounded by $\overline{x}_i$ and $\underline{x}_i$. There are J inequality constraints and K equality constraints in this MOO problem.

In contrast with single-objective optimisation problems, there is no unique optimal solution for MOO problems. Instead, there is a set of acceptable trade-off optimal solutions: a Pareto front [101]. Figure 3.4 illustrates the concept of the Pareto front of the bi-objective optimisation problem $f_1(\mathbf{X})$ and $f_2(\mathbf{X})$ (both for minimisation). As

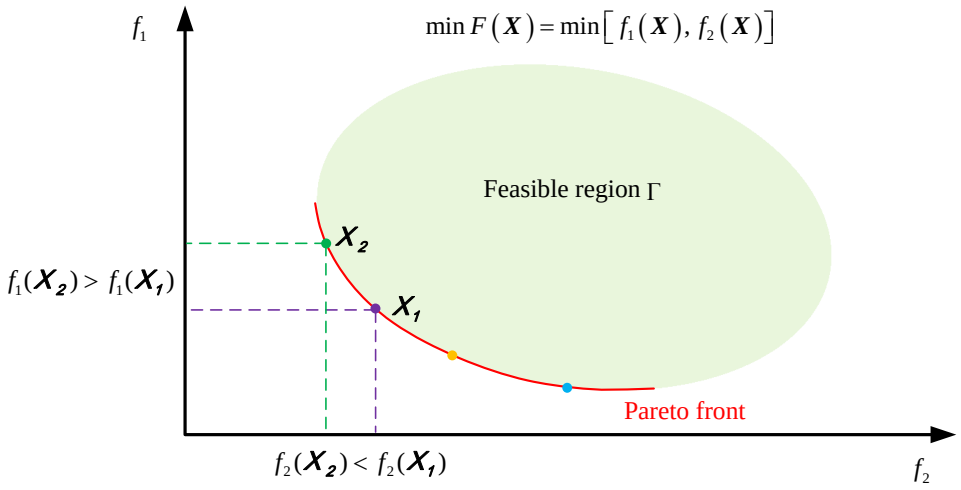

Figure 3.4: Pareto front of a bi-objective optimisation problem (both minimisation)

shown in Figure 3.4, the green area represents the feasible region Γ of the bi-objective optimisation problem and the red curve represents the Pareto front. Any point in the Pareto front is considered as **Pareto optimal**, where Pareto optimal is defined as follows:

Definition 3.7.1. A point $\boldsymbol{X_1} \in \Gamma$ is Pareto optimal if and only if there does not exist another point $\mathbf{X}_2 \in \Gamma$ such that $f_l(\mathbf{X}_2) \leq f_l(\mathbf{X}_1)$ for all l and $f_l(\mathbf{X}_2) < f_l(\mathbf{X}_1)$ for at least one l [102].

3.7.1 Weighted Sum Method

The most common approach to solve a MOO problem is the WSM. The WSM assigns a weight w_l to each objective function and minimises the sum of all objective functions with weights, i.e., $\sum_{l=1}^{L} w_l f_l(\mathbf{X})$, subject to the optimisation constraints.

The general mathematical formulation of the WSM is shown in (3.46):

$$\begin{aligned}
\text{Minimise} \quad & F(\mathbf{X}) = \sum_{l=1}^{L} w_l f_l(\mathbf{X}) \\
\text{subject to} \quad & g_j(\mathbf{X}) \geq 0 \qquad j = 1, 2, \cdots, J \\
& h_k(\mathbf{X}) = 0 \qquad k = 1, 2, \cdots, K \\
\text{with} \quad & \mathbf{X} = [x_1, x_2, \cdots, x_i, \cdots, x_I] \\
& \underline{x}_i \leq x_i \leq \overline{x}_i \qquad i = 1, 2, \cdots, I \\
& \sum_{l=1}^{L} w_l = 1 \\
& 0 \leq w_l \leq 1 \qquad \forall l
\end{aligned} \tag{3.46}$$

where w_l is the weight of the objective function $f_l(\mathbf{X})$. The value of each weight is defined before the optimisation and it is chosen in proportion to the relative importance of the objective. The value of weights ranges from 0 to 1 and the total sum of all weights equal to 1.

The advantages of the WSM are simple and straightforward; however, it also has some disadvantages. First, the value of weights are difficult to choose without prior information. Second, it is impossible to obtain the Pareto front if the MOO problem is non-convex. Figure 3.5 illustrates the feasible region and the Pareto front of a non-convex bi-objective optimisation problem. It can be seen from the figure that, the Pareto front between $F(\boldsymbol{X_1})$ and $F(\boldsymbol{X_2})$ is not accessible using the WSM.

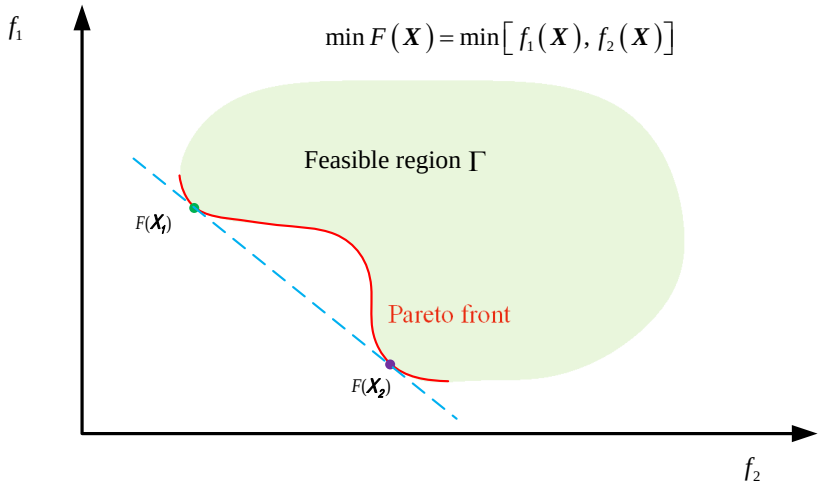

Figure 3.5: WSM for a non-convex bi-objective optimisation problem

3.7.2 ε-Constraint Method

Another common approach to solve MOO problems is the ε-constraint method. This method is designed to optimise the primary objective (single objective function) while treating other objective functions in the form of inequality constraints. The parameter ε_l is utilised to set the bound of the inequality constraints, which indicates the worst value that $f_l(\mathbf{X})$ can take. The mathematical formulation of the ε-constraint method is given in (3.47):

$$\begin{aligned}
\text{Minimise} \quad & f_{l'}(\mathbf{X}) && \forall l' \in \{1, 2, \cdots, L\} \\
\text{subject to} \quad & f_l(\mathbf{X}) \leq \varepsilon_l && \forall l, l \neq l' \\
& g_j(\mathbf{X}) \geq 0 && j = 1, 2, \cdots, J \\
& h_k(\mathbf{X}) = 0 && k = 1, 2, \cdots, K \\
\text{with} \quad & \mathbf{X} = [x_1, x_2, \cdots, x_i, \cdots, x_I] \\
& \underline{x}_i \leq x_i \leq \overline{x}_i && i = 1, 2, \cdots, I
\end{aligned} \tag{3.47}$$

where $f_{l'}(\mathbf{X})$ is the primary objective function, which must be optimised.

The ε-constraint method overcomes the disadvantage of the WSM; it is able to identify the Pareto front even though the MOO problem is non-convex. An example

is given in Figure 3.6. In this bi-objective optimisation problem, $f_1(\mathbf{X})$ is chosen as

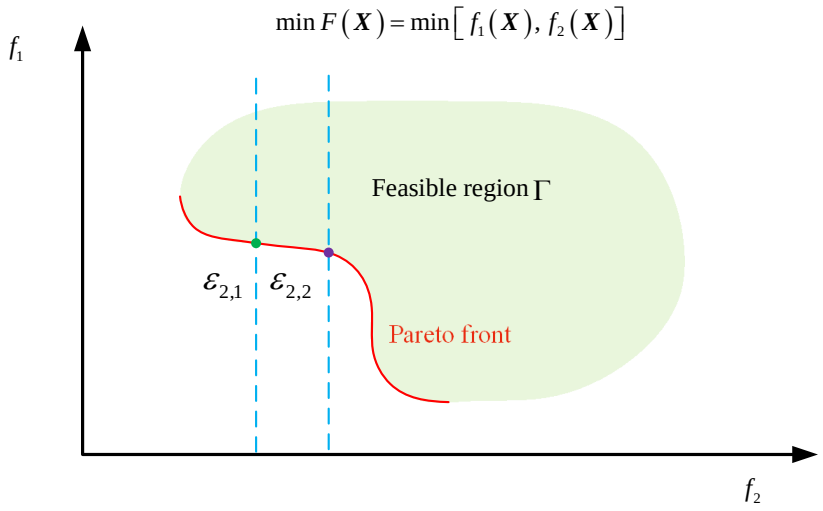

Figure 3.6: ε-constraint method for a non-convex bi-objective optimisation problem

the primary objective function and $f_2(\mathbf{X})$ is treated as constraint, i.e. $f_2(\mathbf{X}) \leq \varepsilon_2$. By setting different value of ε_2 ($\varepsilon_{2,1}$ and $\varepsilon_{2,2}$ in the figure), the Pareto front is obtained.

The advantage of the ε-constraint method is clear; this method is applicable to either convex or non-convex MOO problems. However, one issue of this method is that there is no feasible solution for some values of ε_l, e.g., if ε_l is too small, there may be no feasible solution.

3.8 Stochastic Programming

Stochastic programming is an optimisation approach that involves uncertainty. In the deterministic optimisation problem, all parameters are assumed to be known without uncertainty. However, real-world problems usually include some unknown parameters, and the optimisation problem can be solved by using RO when the parameters are known within certain bounds. Stochastic programming takes advantage of the probability distributions of the unknown parameters, and minimises/maximises the expectation of the objective function. Stochastic programming has been applied in broad areas.

The most common stochastic programming problem is two-stage stochastic programming, the general mathematical formulation of which is given in (3.48):

$$\begin{aligned} \text{Minimise} \quad & \boldsymbol{c^T x} + \mathbb{E}\left[Q\left(\boldsymbol{x}, \boldsymbol{\xi}\right)\right] \\ \text{subject to} \quad & \boldsymbol{Ax} \leq \boldsymbol{b} \\ & \boldsymbol{x} \geq 0 \end{aligned} \tag{3.48}$$

where the $Q\left(\boldsymbol{x}, \boldsymbol{\xi}\right)$ is an objective function as follows:

$$\begin{aligned} \text{Minimise} \quad & Q\left(\boldsymbol{x}, \boldsymbol{\xi}\right) = d(\xi)^T \boldsymbol{y} \\ \text{subject to} \quad & T(\xi)\boldsymbol{x} + W(\xi)\boldsymbol{y} \leq h(\xi) \\ & \boldsymbol{y} \geq 0 \end{aligned} \tag{3.49}$$

In (3.48), the objective function consists of two parts: the first-stage cost $\boldsymbol{c^T x}$ plus the expected cost in the second stage $\mathbb{E}\left[Q\left(\boldsymbol{x}, \boldsymbol{\xi}\right)\right]$. In the first stage, $\boldsymbol{x}$ is the *here-and-now* variable which should be determined before the realisation of the uncertain data $\boldsymbol{\xi}$. In the second stage, $\boldsymbol{y}$ is the *wait-and-see* variable, and $\boldsymbol{y}$ can be optimised only after the uncertain data $\boldsymbol{\xi}$ is realised.

Generally, the uncertain data $\boldsymbol{\xi}$ is described by a finite number of scenarios Ω and the probability of each scenario is written as $\pi_\omega, \forall\omega = \{1, 2, \cdots, \Omega\}$. The concept of the probability of each scenario is illustrated in Figure 3.7.

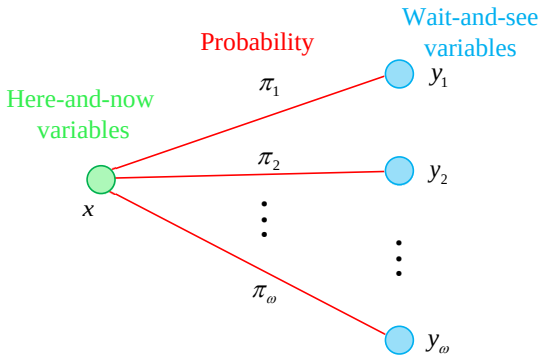

Figure 3.7: Two-stage stochastic programming

After that, the expected cost in the second stage is written as:

$$\mathbb{E}\left[Q\left(\boldsymbol{x}, \boldsymbol{\xi}\right)\right] = \sum_{\omega=1}^{\Omega} \pi_{\omega} \boldsymbol{d}_{\boldsymbol{\omega}}^{\boldsymbol{T}} \boldsymbol{y}_{\boldsymbol{\omega}} \tag{3.50}$$

Finally, the two-stage stochastic programming problem can be represented by a linear deterministic equivalent problem with a finite number of scenarios. The mathematical formulation of the linear deterministic equivalent problem is given in (3.51):

$$\begin{aligned} \text{Minimise} \quad & \boldsymbol{c}^{\boldsymbol{T}} \boldsymbol{x} + \sum_{\omega=1}^{\Omega} \pi_{\omega} \boldsymbol{d}_{\omega}^{\boldsymbol{T}} \boldsymbol{y}_{\omega} \\ \text{Subject to} \quad & \boldsymbol{A}\boldsymbol{x} \leq \boldsymbol{b} \\ & \boldsymbol{T}_{\omega}\boldsymbol{x} + \boldsymbol{W}_{\boldsymbol{\omega}}\boldsymbol{y}_{\omega} \leq \boldsymbol{h}_{\omega}, \qquad \forall \omega \\ & \boldsymbol{x} \geq 0 \\ & \boldsymbol{y}_{\omega} \geq 0 \qquad \forall \omega \end{aligned} \tag{3.51}$$

3.9 Rolling-Horizon Optimisation

To take the uncertainty into consideration, an Model Predictive Control (MPC)-based RHO method is introduced in this section. The RHO method solves a deterministic optimisation problem iteratively by advancing the optimisation horizon. At time t, the RHO optimises the objective function subject to constraints in terms of the predicted system information in the range $[t, t + H]$, where H is the optimisation horizon. Owing to the uncertainty of the predicted information, only the first step of the optimisation result is implemented, and the system states are updated. After that, the RHO repeats the optimisation from a new state, i.e. from $t+1$ to $t+H+1$, and the system information must be re-predicted. The prediction horizon keeps advancing; thus, the RHO is also known as **Receding-Horizon Optimisation**. The RHO method has been applied in several areas and it has shown good performance in managing uncertainties. However, the RHO method cannot achieve the globally optimal solution. Figure 3.8 illustrates the concept of the RHO method.

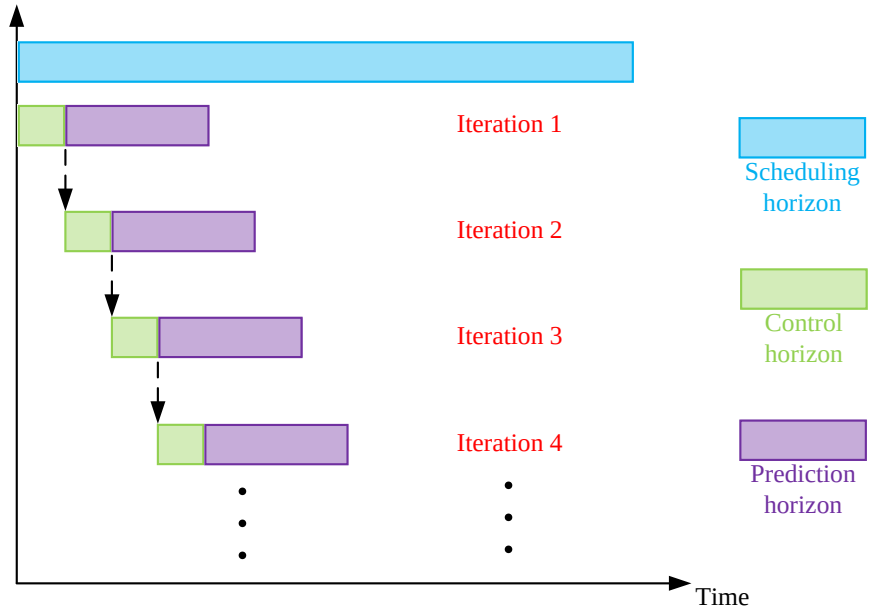

Figure 3.8: Illustration of the rolling-horizon optimisation method

The iterative process of the RHO is given as follows:

1. Initialise the start time $t_0 = 1$ (initial state of the system), prediction horizon H and number of iteration times;

2. The RHO mathematical formulation between $[t_0, t_0 + H]$ is given in (3.52):

$$\begin{aligned} \text{Minimise} \quad & f(x_{t_0}) + \sum_{t=t_0+1}^{t_0+H} \hat{f}(\hat{x}_t) \\ \text{subject to} \quad & g_j(\boldsymbol{X}) \geq 0 \qquad j = 1, 2, \cdots, J \\ & h_k(\boldsymbol{X}) = 0 \qquad k = 1, 2, \cdots, K \\ & x_{t_0} \geq 0 \\ & \hat{x}_t \geq 0 \qquad t = t_0 + 1, \cdots, t_0 + H \\ \text{with} \quad & \boldsymbol{X} = [x_{t_0}, \hat{x}_{t_0+1}, \cdots, \hat{x}_{t_0+H}] \end{aligned} \tag{3.52}$$

3. Implement the optimisation result x_{t_0} at the current time t_0 and advance the

optimisation horizon

$$t_0 = t_0 + 1 \tag{3.53}$$

4. Start the next iteration: repeat step 2 until the end.

3.10 Summary

This chapter introduces several models, including the ESS charging/discharging model, single EV charging/discharging model, EV information model, and DC-OPF model. The relationship between the charging/discharging power and the power limits, battery SOC, and dynamic characteristics of EVs are modelled in Section 3.3 and 3.4. EV driving behaviours are modelled based on TGD in Section 3.5, which are used to simulate the dynamic characteristics of EV fleets. A transmission power network model is built in Section 3.6, which enables the integration of EVs into the grid.

Finally, three optimisation techniques are reviewed, namely MOO in Section 3.7, stochastic programming in Section 3.8, and RHO in Section 3.9.

Chapter 4

Stakeholders' Interest Inconsistency between EV Owners and Aggregator

4.1 Introduction

In this chapter, the relationship between EV owners and EV aggregator is analysed considering these two stakeholders' interest, i.e., charging fee minimisation and profit maximisation.

Multi-stage scheduling strategy is common in EV energy management for EV aggregator profit maximisation. In [87], a two-stage scheduling strategy is proposed to maximise EV parking deck revenue. A marginal electricity price is determined in the first stage to maintain the parking deck revenue, and in the second stage a MPC-based online method is used to accommodate the uncertainty in EV driving behaviours. In [103], the authors concentrated on two objectives: maximising parking lot revenue and maximising the number of EVs fulfilling their requirements in a two-layer (DA and RT) parking lot recharging system. In [68], the objective function consists of several terms to maximise the aggregator revenue, which include the income of selling energy

to EV owners and the cost of purchasing energy from EV owners. However, it is not reasonable to merge the EV owners' benefits with the EV aggregator benefits in one objective function, as the different stakeholders' economic interests are not the same. In [49], the authors jointly considered the EV aggregator and EV owner by involving EV owner's charging fee limit as the key constraint in aggregator scheduling. However, the EV owner's charging fee is a parameter and the rationale of providing this parameter is not provided. In [104], a rebate factor is introduced in the model to encourage EV owners to participate in the power grid operation. However, the value of the rebate factor is not determined, and the charging fee of EV owners participating in the power grid operation is not discussed (the EV owners' economic interests are not evaluated).

In this thesis, a three-stage EV energy management strategy is introduced. The proposed strategy aims to maximise the EV aggregator profit without sacrificing EV owners' economic benefits. In the first stage, the charging and discharging operations of EVs are scheduled from EV owners' viewpoint (self-scheduling), with the objective to minimise the charging fee of each EV owner, including the charging/discharging cost and battery degradation cost. The second stage of the strategy aims to maximise the EV aggregator profit versus rebate values by taking EV owners' economic benefits into account. The third stage is to apply the optimal rebate value from the second stage in the real-time scheduling strategy. Considering the uncertainty in EV owners' driving behaviours, an MPC-based RHO method is applied in the third stage. These three stages are linked as follow: the first-stage scheduling results of EV owner charging cost are involved as constraints in the second-stage scheduling; then, the optimal rebate value is determined in the second-stage scheduling, which is applied in the third-stage scheduling.

The main contributions of this case study are highlighted as follows:

- The economic relationship between EV owners and the aggregator is analysed by the utilisation of MOO method; the Pareto optimal results is obtained based on the WSM.

- The economic inconsistency issue is considered, i.e. the economic interests of the EV owners and EV aggregator are analysed and the economic inconsistency issue between these two stakeholders is presented. Moreover, a sensitivity analysis of the factors impacting the economic inconsistency is presented.

- To mediate the economic inconsistency issue between the aggregator and EV owners, a rebate factor is introduced. The optimal rebate value is found in the second-stage scheduling, which maximises the aggregator profit under the condition that there is no charging fee increment for EV owners compared with the results from the first-stage scheduling.

4.2 Three-Stage Scheduling Strategy

This section introduces a three-stage scheduling strategy. The first and second stages are day-ahead strategies and the third stage is a real-time strategy. The concepts of first and second stages are illustrated in Figure 4.1.

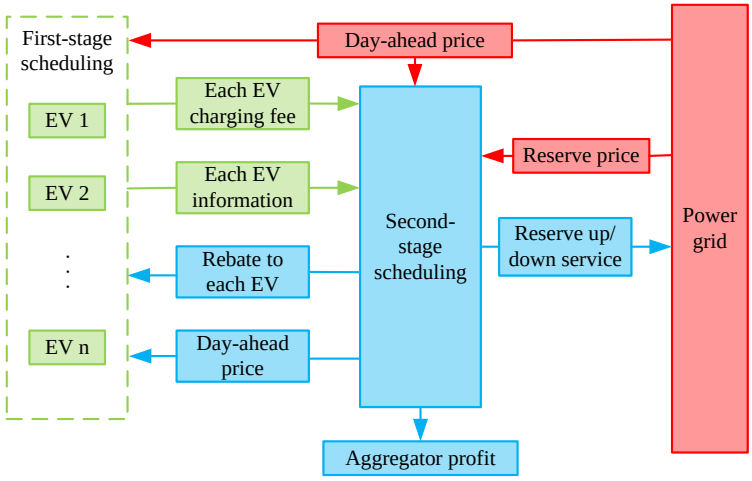

Figure 4.1: A block-diagram illustration for First- and Second-stage scheduling strategy

In the first stage, the interaction between the EV owners and the grid is formulated. A day-ahead scheduling strategy (self-scheduling strategy) is presented with the aim to minimise each EV owner's charging fee based on RTP. After that, the energy and

reserve interactions among the EV owners, aggregator, and the grid are modelled in the second stage, where the EV aggregator participates in both energy and reserve markets. As a coordinator between the grid and EV owners, the EV aggregator obtains EV information (arrival time, departure time, and initial SOC) and charging fee from the EV owners. Then, the EV aggregator schedules all EVs' charging and discharging operations based on RTP and reserve up/down prices. At the same time, the reserve up/down capacities of the aggregator are determined and submitted to the grid. Finally, the aggregator gains profit from the grid.

The relationship between energy scheduling and the reserved energy is illustrated in Figure 4.2. The figure shows a typical single EV under V2G mode during the

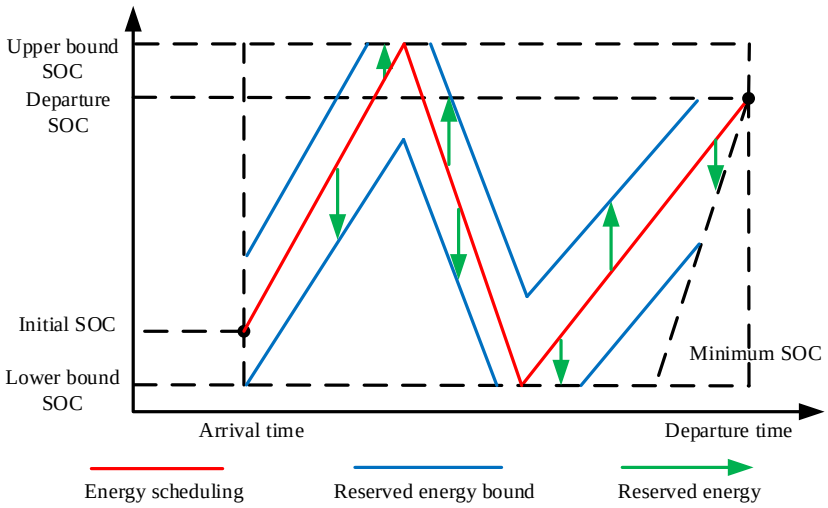

Figure 4.2: Energy scheduling and corresponding reserved energy

available time; the reserved energy (in kWh) shows the ability of the EV to increase or decrease the current consumption energy temporarily based on the requirements of the grid. At each time, there are three corresponding modes for each single EV: operating power (charging, discharging, or idling modes), reserve up capacity and reserve down capacity. By evaluating reserve up and down capacities at each time, the flexibility of the EV is determined. The EV aggregator submits reserve up and down capacities with multiple EVs together to the grid and thus participates in the power grid reserve

market. The system operator could call for reserve, that is reserve deployment, from the EV aggregator and thus maintain the power grid stability.

Figure 4.3 shows the relationship between the operating power, reserve up capacity and reserve down capacity without considering the battery SOC or EV owner driving requirements. The reserve down capacity (in kW) is defined as the difference between the maximum charging power and the current operation power and the reserve up capacity (in kW) is the difference between maximum discharging power and the current operation power.

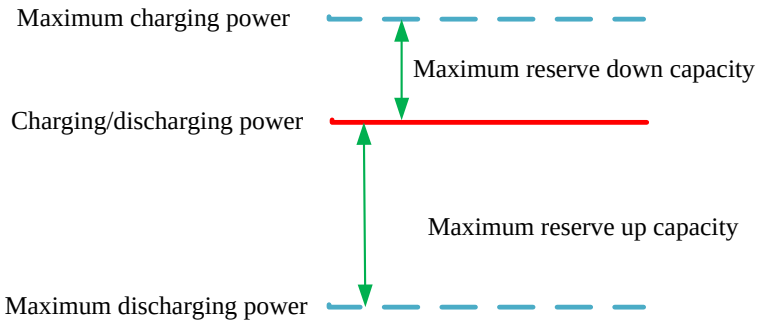

Figure 4.3: Relationship between charging/discharging power with reserve up/down capacity (without SOC and driving constraints)

4.2.1 First Stage: EV Owners' Scheduling Strategy

The first stage is to minimise the day-ahead charging fee of each EV owner under V2G, based on RTP and day-ahead EV information. The EV owners' charging fee consists of three parts: 1) charging cost for purchasing energy from the grid, 2) discharging income for selling energy back to the grid, and 3) corresponding battery degradation cost both for charging and discharging. Because EV operations are independent of each other [87], the objective function of each EV owner can be integrated as follows:

$$\text{Minimise} \quad J_1^{\text{ev}} + J_2^{\text{ev}} \tag{4.1a}$$

$$J_1^{\text{ev}} = \sum_{t=1}^{M} \sum_{n=1}^{N} \left(r_t^+ p_{n,t}^{+,e} - r_t^- p_{n,t}^{-,e} \right) \Delta T \tag{4.1b}$$

$$J_2^{\text{ev}} = \sum_{t=1}^{M} \sum_{n=1}^{N} D^{\text{ev}} \left(p_{n,t}^{+,e} + p_{n,t}^{-,e} \right) \Delta T \tag{4.1c}$$

where J_1^{ev} is the charging cost/discharging income and J_2^{ev} is the corresponding battery degradation cost. M is the total number of time intervals; N is the total number of EVs; r_t^+ are r_t^- are purchasing and selling RTP information of owners obtained from power grids at time t; $p_n^{+,e}$ and $p_n^{-,e}$ are continuous variables, which stand for the charging and discharging powers of EV n, respectively. D^{ev} is the degradation rate of the EV battery with the unit \$/kWh and ΔT is the time interval. To enhance the energy interactions between EVs and the grid, EV owners will be rewarded for discharging according to a feed-in-policy [66], that is $r_t^- = r_t^+ + \hat{r}$, where $\hat{r}$ is a positive real number representing the V2G reward tariff in \$/kWh to encourage EV owners to inject energy back to the grid (discharge).

The availability of EVs is represented in (4.2) and (4.3), which indicate that the charging and discharging powers of EVs can only be scheduled during available time (after arrival and before departure).

$$p_{n,t}^{+,e} = \begin{cases} 0 & 1 \le t < t_n^{a,d} \quad \text{Before arrival} \\ \left(0, \overline{P}_n^{\text{ev}} i_{n,t}^{+,e}\right] & t_n^{a,d} \le t < t_n^{d,d} \quad \text{Charging} \\ 0 & t_n^{a,d} \le t < t_n^{d,d} \quad \text{Idling or discharging} \\ 0 & t_n^{d,d} \le t \le M \quad \text{After departure} \end{cases} \quad \forall n, t \tag{4.2}$$

$$p_{n,t}^{-,e} = \begin{cases} 0 & 1 \le t < t_n^{a,d} \quad \text{Before arrival} \\ \left(0, \overline{P}_n^{\text{ev}} i_{n,t}^{-,e}\right] & t_n^{a,d} \le t < t_n^{d,d} \quad \text{Discharging} \\ 0 & t_n^{a,d} \le t < t_{d,n}^{d,d} \quad \text{Idling or charging} \\ 0 & t_n^{d,d} \le t \le M \quad \text{After departure} \end{cases} \quad \forall n, t \tag{4.3}$$

where $i_{n,t}^{+,e}$ and $i_{n,t}^{-,e}$ are binary variables representing the charging ($i_{n,t}^{+,e}$=1, $i_{n,t}^{-,e}$=0), discharging ($i_{n,t}^{+,e}$=0, $i_{n,t}^{-,e}$=1) and idling ($i_{n,t}^{+,e}$=0, $i_{n,t}^{-,e}$=0) status of the EV during available

time. $t_n^{d,d}$ and $t_n^{d,d}$ are day-ahead EV information for the arrival time and departure time of EV n. These two constraints suggest that the charging and discharging operations of EVs are restricted between 0 and $\overline{P}_n^{\text{ev}}$ when EVs are connected to the grid. When EVs are off the grid, they cannot be scheduled and thus the charging/discharging power are both set to 0.

Constraint (4.4) ensures that an EV only has one status during operation, i.e. an EV cannot operate in the charging and discharging status simultaneously.

$$i_{n,t}^{+,e} + i_{n,t}^{-,e} \leq 1 \quad \forall t, \forall n \tag{4.4}$$

The relationship between charging/discharging power and the EV battery SOC is described in (4.5), where E_n^{ev} is the battery capacity of EV n.

$$SOC_n^t = SOC_n^{t-1} + \frac{\left(p_{n,t}^{+,e} - p_{n,t}^{-,e}\right) \Delta T}{E_n^{\text{ev}}} \quad t_n^{a,d} < t < t_n^{d,d}, \forall n \tag{4.5}$$

$$SOC_n^t = SOC_n^{a,d} + \frac{\left(p_{n,t}^{+,e} - p_{n,t}^{-,e}\right) \Delta T}{E_n^{\text{ev}}} \qquad t = t_n^{a,d}, \forall n \tag{4.6}$$

In constraint (4.7), $\underline{\text{SOC}}$ and $\overline{\text{SOC}}$ are the lower and upper bounds on the EV battery SOC, to prevent the battery from over discharging or charging. Furthermore, constraint (4.6) defines the initial SOC as equal to $SOC_n^{a,d}$, where $SOC_n^{a,d}$ is obtained from the EV information of EV n. To guarantee the EV owners' driving requirements, each EV should be charged to a level no less than the desired SOC value SOC^{d}. It is assumed that SOC^{d} is a constant for all EVs.

$$\underline{\text{SOC}} \leq SOC_n^t \leq \overline{\text{SOC}} \qquad \forall t, \forall n \tag{4.7}$$

$$SOC_n^t \geq \text{SOC}^{\text{d}} \qquad t = t_{d,n}^d, \forall n \tag{4.8}$$

Battery degradation is an important parameter to be considered under V2G for EV owners. It is assumed that the EV charging and discharging behaviours could both lead

to battery degradation, and the cost is formulated in the second part of the objective function (4.1c), in which D^{ev} represents the corresponding battery degradation rate due to EV charging and discharging behaviours. It is calculated based on the battery capital cost, cycle time, and DOD, which has been discussed in detail in [41]:

$$D^{\text{ev}} = \frac{C_{cap}}{L_c E_n^{\text{ev}} DoD} \tag{4.9}$$

where C_{cap}, L_c, and E_n^{ev} are the initial investment cost of the battery ($), battery lifetime in cycles, and battery capacity (kWh).

4.2.2 Second Stage: Optimal Rebate for EV Aggregator

The second stage aims to maximise the day-ahead aggregator profit from the EV aggregator's viewpoint. According to the day-ahead EV information $\left[t_n^{a,d}, t_n^{a,d}, SOC_n^{a,d}\right]$, the objective function of the EV aggregator is formulated in (4.10a):

$$\text{Maximise} \quad I_{res}^d - C_{gri}^d + I_{own}^d - C_{reb}^d \tag{4.10a}$$

which consists of four terms: 1) reserve income I_{res}^d for providing reserve up/down services for power grid; 2) C_{gri}^d represents the cost of aggregator–grid energy interactions (purchasing and selling energy); 3) I_{own}^d stands for the income of aggregator–owner energy interactions; and 4) C_{reb}^d is the rebate fee provided by the aggregator to each EV owner to guarantee their economic benefits.

The first term of (4.10a) is the reserve profit, which is obtained based on reserve up/down prices, as shown in (4.10b):

$$I_{res}^d = \sum_{t=1}^{M} \sum_{n=1}^{N} \left(r_t^{up} p_{n,t}^{up} + r_t^{dw} p_{n,t}^{dw} \right) \Delta T \tag{4.10b}$$

where r_t^{up} and r_t^{dw} are the reserve up and down prices at time t, and $p_{n,t}^{up}$ and $p_{n,t}^{dw}$ are variables of the day-ahead reserve up and down capacities for EV n at time t,

respectively.

The second term of (4.10a) is the energy interaction between the EV aggregator and the grid, which includes the purchasing fee and selling income, and is given in (4.10c):

$$C^{d}_{gri} = \sum_{t=1}^{M}\sum_{n=1}^{N}\left(r^{+}_{t}p^{+,d}_{n,t} - r^{-}_{t}p^{-,d}_{n,t}\right)\Delta T \tag{4.10c}$$

The third term of (4.10a) describes the energy interaction between the EV aggregator and EV owners, including purchasing fee and selling income, which is given in (4.10d):

$$I^{d}_{own} = \sum_{t=1}^{M}\sum_{n=1}^{N}\left(r^{+}_{t}p^{+,d}_{n,t} - r^{-}_{t}p^{-,d}_{n,t}\right)\Delta T \tag{4.10d}$$

The last term of (4.10a) is the rebate fee for all EV owners provided by the aggregator. It represents the economic interaction between the aggregator and each EV owner, which means that EV owners will receive rebate income both for charging and discharging under aggregator scheduling. The equation is formulated in (4.10e):

$$C^{d}_{reb} = \sum_{t=1}^{M}\sum_{n=1}^{N}\alpha\left(p^{+,d}_{n,t} + p^{-,d}_{n,t}\right)\Delta T \tag{4.10e}$$

where α stands for the rebate factor with the unit \$/kWh.

From the EV aggregator's viewpoint, the scheduling has common constraints with self-scheduling subject to (4.2)–(4.8), by substituting variables $p^{+,e}_{n,t}$ and $p^{-,e}_{n,t}$ by $p^{-,d}_{n,t}$ and $p^{-,d}_{n,t}$. Moreover, there are several constraints on the aggregator for providing reserve service to the grid.

The reserve capacity is limited by the operating status and maximum charging and discharging power. Constraint (4.11) shows that the sum of reserve down capacity and operating power should be no more than the maximum charging power. The reserve up capacity is determined based on (4.12); it shows that the difference between the operating status and reserve up capacity should not be less than the maximum

discharging power.

$$p_{n,t}^{+,d} - p_{n,t}^{-,d} + p_{n,t}^{dw} \leq \overline{P}_n^{\mathrm{ev}} \quad \forall t, \forall n \tag{4.11}$$

$$p_{n,t}^{+,d} - p_{n,t}^{-,d} - p_{n,t}^{up} \geq -\overline{P}_n^{\mathrm{ev}} \quad \forall t, \forall n \tag{4.12}$$

Constraint (4.13) and (4.14) define the range of the reserve up and down capacity of the EV.

$$p_{n,t}^{up} = \begin{cases} 0 & 1 \leq t < t_n^{a,d} \quad \text{Before arrival} \\ \left[0, 2\overline{P}_n^{\mathrm{ev}}\right] & t_n^{a,d} \leq t < t_n^{d,d} \\ 0 & t_n^{d,d} \leq t \leq M \quad \text{After departure} \end{cases} \qquad \forall n, t \tag{4.13}$$

$$p_{n,t}^{dw} = \begin{cases} 0 & 1 \leq t < t_n^{a,d} \quad \text{Before arrival} \\ \left[0, 2\overline{P}_n^{\mathrm{ev}}\right] & t_n^{a,d} \leq t < t_n^{d,d} \\ 0 & t_n^{d,d} \leq t \leq M \quad \text{After departure} \end{cases} \qquad \forall n, t \tag{4.14}$$

The reserve up and down capacities not only depend on the operation status, but also relate to the upper and lower bounds of the battery SOC, which are shown in (4.15) and (4.16):

$$SOC_n^{t-1} + \frac{\left(p_{n,t}^{+,d} - p_{n,t}^{-,d} + p_{n,t}^{dw}\right) \Delta T}{E_n^{\mathrm{ev}}} \leq \overline{\mathrm{SOC}} \qquad \forall t, \forall n \tag{4.15}$$

$$SOC_n^{t-1} + \frac{\left(p_{n,t}^{+,d} - p_{n,t}^{-,d} - p_{n,t}^{up}\right) \Delta T}{E_n^{\mathrm{ev}}} \geq \underline{\mathrm{SOC}} \qquad \forall t, \forall n \tag{4.16}$$

In addition, the reserve up capacity is also limited by the driving requirement of EV owners, such that the minimum SOC at each time is involved to ensure that the battery SOC is not less than $\mathrm{SOC}^{\mathrm{d}}$ at the departure time, as shown by the constraints in (4.17):

$$SOC_n^{t-1} + \frac{\left(p_{n,t}^{+,d} - p_{n,t}^{-,d} - p_{n,t}^{up}\right) \Delta T}{E_n^{\mathrm{ev}}} \geq \mathrm{SOC}^{\mathrm{d}} - \frac{\overline{P}_n^{\mathrm{ev}}(M-t)\Delta T}{E_n^{\mathrm{ev}}} \qquad \forall t, \forall n \tag{4.17}$$

where the right-hand side of the operator in (4.17) determines the minimum SOC during the available time. The concepts of upper and lower bound and minimum SOC at each time are illustrated in Figure 4.2.

To guarantee EV owners' economic benefits, a rebate factor is introduced in the model to ensure that the charging fee does not exceed the day-ahead self-scheduling charging fee for all EV owners. The constraint is shown in (4.18):

$$\begin{aligned}\sum_{n=1}^{N}\sum_{t=1}^{M}\left(r_t^{+}p_{n,t}^{+,d}-r_t^{-}p_{n,t}^{-,d}\right)\Delta T+\sum_{n=1}^{N}\sum_{t=1}^{M}D^{\mathrm{ev}}\left(p_{n,t}^{+,d}+p_{n,t}^{-,d}\right)\Delta T \\ -\sum_{n=1}^{N}\sum_{t=1}^{M}\alpha\left(p_{n,t}^{+,d}+p_{n,t}^{-,d}\right)\Delta T\leq(1-\beta)\left(J_1^{\mathrm{ev}*}+J_2^{\mathrm{ev}*}\right)\quad\forall n\end{aligned} \tag{4.18}$$

where β is a discount parameter offered by the EV aggregator to provide a lower charging cost (compared with the self-scheduling result of $J_1^{\mathrm{ev}*}+J_2^{\mathrm{ev}*}$) for EV owners, which can thus attract more EVs to participate in aggregator scheduling.

The scheduling result of the second stage is to obtain the optimal rebate value α^* which maximises the aggregator profit without sacrificing each EV owner's economic benefits. In addition, a non-optimal rebate factor in a range will still work for the model, and only slightly affect the profit of the aggregator.

4.2.3 Third Stage: Real-time Aggregator Scheduling Strategy

This section presents the aggregator profit maximisation strategy in a real-time scenario. The optimal rebate value α^* obtained from the second stage is involved in this stage. Because EV owner driving behaviours are difficult to predict, the strategy needs to be rescheduled based on the dynamic real-time EV information. In this case, an MPC-based algorithm is proposed in the third stage, i.e. the EV aggregator schedules the operation behaviours based on real-time EV information, and only the first step is dispatched to each EV. After that, EVs update their information. Finally, the EV aggregator repeats the next step of scheduling.

In this stage, all variables and parameters are of two types, i.e. fixed or predicted EV

information. $\left[p^{+}_{\bar{n},t}, p^{-}_{\bar{n},t}, p^{up}_{\bar{n},t}, p^{dw}_{\bar{n},t}\right]$ are variables of fixed EV information $\left[t^{a}_{\bar{n}}, t^{d}_{\bar{n}}, SOC^{a}_{\bar{n}}\right]$, and $\left[p^{+}_{\dot{n},t}, p^{-}_{\dot{n},t}, p^{up}_{\dot{n},t}, p^{dw}_{\dot{n},t}\right]$ are variables of predicted EV information $\left[t^{a}_{\dot{n}}, t^{d}_{\dot{n}}, SOC^{a}_{\dot{n}}\right]$. Here, $\bar{n}$ and $\dot{n}$ represent the fixed EV and predicted EV, respectively. Note that all variables and parameters in the third stage have the same format as those in the second stage and the objective function is given in (4.19):

$$\begin{aligned} \text{Maximise} \quad & \bar{I}_{res} - \bar{C}_{gri} + \bar{I}_{own} - \bar{C}_{reb} \\ & + \dot{I}_{res} - \dot{C}_{gri} + \dot{I}_{own} - \dot{C}_{reb} \end{aligned} \tag{4.19}$$

where the first four terms represent the aggregator profits for the fixed EV information and the last four terms are the aggregator profit for the predicted EV information.

The scheduling strategy is implemented as follows.

1. EV owners receive the day-ahead price from the power grid for day-ahead self-scheduling and obtain each owner charging cost based on the objective function (4.1a), subject to (4.2)–(4.9). It is assumed that the da-ahead price is the same with RTP.

2. The EV aggregator receives the day-ahead price, reserve price, day-ahead EV information, and owners' charging fee for day-ahead scheduling with the objective function (4.10a), subject to (4.2)–(4.9) and (4.11)–(4.18). The optimal rebate value α^{*} is obtained.

3. Initialise the beginning time $t_0 = 1$, and determine the charging fee of fixed EVs $\bar{J}^{\text{ev}*}_{1,t_0}$, $\bar{J}^{\text{ev}*}_{2,t_0}$ and predicted EVs $\dot{J}^{\text{ev}*}_{1,t_0}$, $\dot{J}^{\text{ev}*}_{2,t_0}$.

4. The EV aggregator schedules all EVs from t_0 to the end based on the RTP, reserve price and dynamic real-time EV information.

5. Implement the scheduling results of the first step to the fixed EVs and update their EV information based on (4.20) and (4.21):

$$SOC^{a}_{\bar{n}} = SOC^{a}_{\bar{n}} + \frac{\left(p^{+}_{\bar{n},t_0} - p^{-}_{\bar{n},t_0}\right) \Delta T}{E_{\bar{n}}} \tag{4.20}$$

$$\begin{aligned}(1-\beta)\left(\bar{J}^{\mathrm{ev}*}_{1,t_0+1}+\bar{J}^{\mathrm{ev}*}_{2,t_0+1}\right) = (1-\beta)\left(\bar{J}^{\mathrm{ev}*}_{1,t_0}+\bar{J}^{\mathrm{ev}*}_{2,t_0}\right) &- \sum_{\bar{n}}^{\bar{N}}\left(r^{+}_{t}p^{+}_{\bar{n},t_0}-r^{-}_{t}p^{-}_{\bar{n},t_0}\right)\Delta T \\ &+ \sum_{\bar{n}}^{\bar{N}} D^{\mathrm{ev}}\left(p^{+}_{\bar{n},t_0}+p^{-}_{\bar{n},t_0}\right)\Delta T \\ &- \sum_{\bar{n}}^{\bar{N}} \alpha^{*}\left(p^{+}_{\bar{n},t_0}+p^{-}_{\bar{n},t_0}\right)\Delta T \quad \forall\bar{n}\end{aligned} \tag{4.21}$$

where $\bar{J}^{\mathrm{ev}*}_{1,t_0+1}$ and $\bar{J}^{\mathrm{ev}*}_{1,t_0+1}$ represent the new values of EV owners' charging fee during the update.

6. Re-predict the EV information $\left[t^{a}_{\dot{n}}, t^{d}_{\dot{n}}, SOC^{a}_{\dot{n}}\right], \forall\dot{n}=1...\dot{N}$ for EVs which are not connected the grid. Update the charging fee of predicted EVs $\dot{J}^{\mathrm{ev}*}_{1,t_0+1}$, $\dot{J}^{\mathrm{ev}*}_{2,t_0+1}$.

7. Update the dynamic real-time EV information and the time based on (4.22). After that, repeat the RHO process from Step 4.

$$t_0 = t_0 + 1 \tag{4.22}$$

To summarise, the proposed three-stage scheduling strategy is illustrated by a flowchart given in Figure 4.4.

In the first and second stages, the scheduling strategies are carried out based on day-ahead EV information. In the third stage, because EV driving behaviours are difficult to predict, a real-time EV information model is presented. An assumption is made that the information of EVs already in the gird and those that will connect to the grid in the following time interval ΔT will not change. Otherwise, EV information is generated based on the TGD (EVs that are off the grid). The concept of the real-time EV information model is shown in Figure 4.5.

In Figure 4.5, the arrival time of EV 1 is earlier than the current time (i.e. $t^{a}_{1} < t_0$), therefore EV 1 is already in the grid and its EV information is fixed. In contrast, EV 2 is not in the grid, as the predicted arrival time is later the current time (i.e. $t^{a}_{2} > t_0 + 1$).

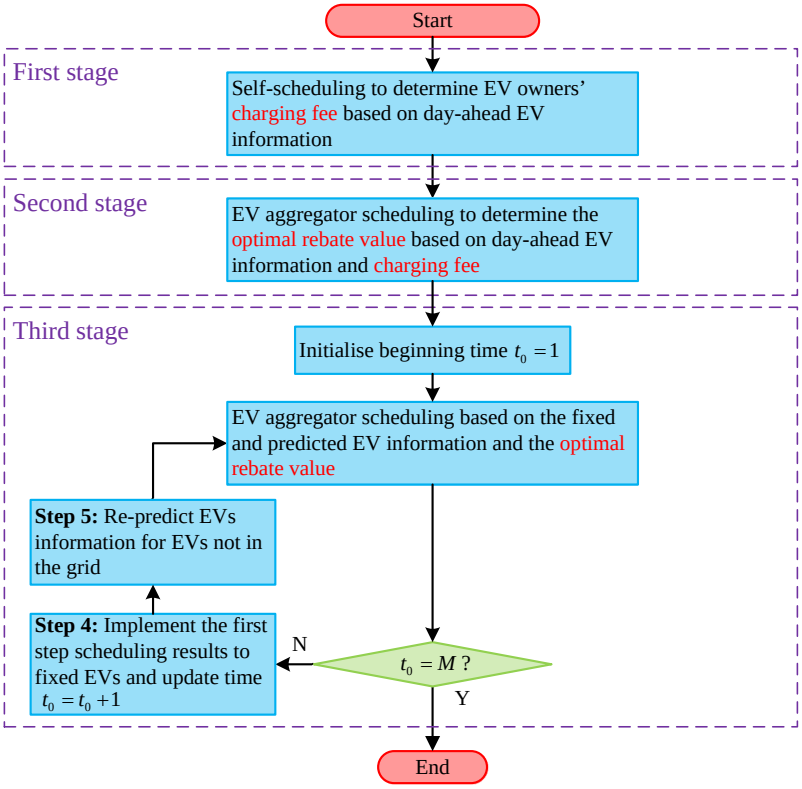

Figure 4.4: Flowchart of the three-stage scheduling strategy

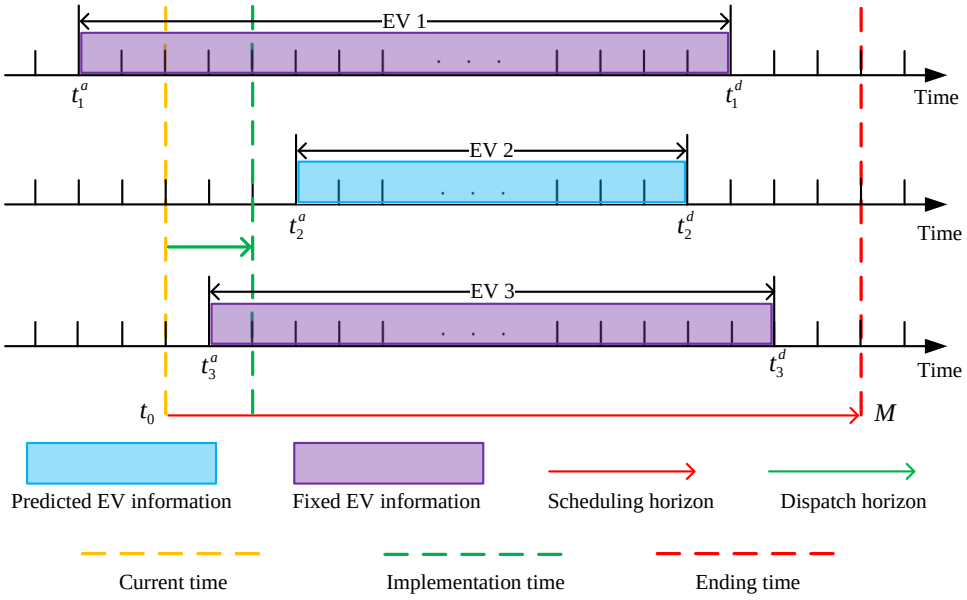

Figure 4.5: Real-time EV information model

Thus, the EV information of EV 2 is not fixed and it must be re-predicted for the next scheduling round. For EV 3, it is assumed that the EV information can be predicted accurately in the following ΔT period, and thus its information is also fixed because the arrival time is between the current time and the next scheduling time ($t_3^a = t_0 + 1$).

4.3 Numerical Examples

4.3.1 Pareto Front of Stakeholders' Interests

In this section, WSM is utilised to demonstrate the economic inconsistency issue between the stakeholders. According to the WSM model discussed in Section 3.7.1, the objective function is formulated by multiplying a weight factor w by each objective (charging fee minimisation for EV owners and profit maximisation for the EV aggregator), as given in (4.23):

$$\text{Maximise} \quad w_1 \left(I_{res}^d - C_{gri}^d + I_{own}^d \right) - w_2 \left(J_1^{\text{ev}} + J_2^{\text{ev}} \right) \tag{4.23}$$

subject to: (4.2)–(4.8), (4.11)–(4.17), and all variables in (4.1b)–(4.8) are substituted by $p_{n,t}^{+,d}, p_{n,t}^{-,d}$.

The Pareto optimal of this optimisation problem is shown in Figure 4.6, based on the WSM. It suggests the relationship between the aggregator profit and the EV owners' charging fee.

It can be seen from the figure that both the aggregator profit and EV owners' charging fee increase as the weight w_1 increases from 0 to 1 (detailed numerical results is available in Table C.1 in Appendix C). The marginal point is defined in this figure, where the EV owners' charging fee under aggregator scheduling is the same as the self-scheduling charging fee. On the right-hand side of the marginal point, the owners' charging fee is higher than self-scheduling results, while on the left-hand side, the EV owners' charging fee is less than self-scheduling results. The marginal point is achieved when the weights are chosen as $w_1 = 0.33$ and $w_2 = 0.67$; at this point, the EV owners'

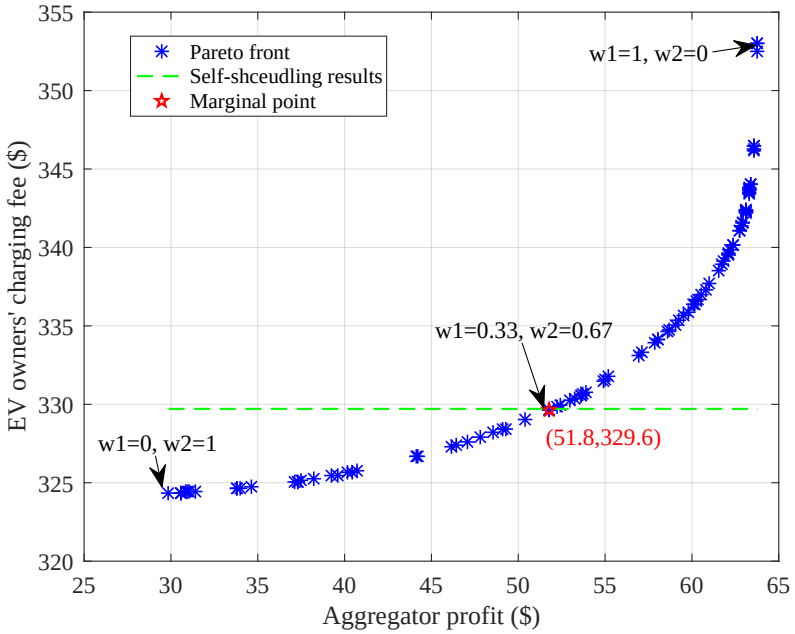

Figure 4.6: Pareto front of aggregator profit and EV owners' charging fee with demonstration of the self-scheduling results

charging fee is $ 329.60 and the aggregator profit is $ 51.80.

In addition, the results shown in Figure 4.6 suggest that on the right-hand side of the marginal point, the EV owners' charging fee significantly increases when w_1 or ε increase. On the left-hand side of the marginal point, the aggregator profit significantly reduces when w_1 or ε decrease. These results could be used as a reference in balancing the economic interests of the two stakeholders and thus design a reasonable settlement mechanism between EV owners and the aggregator.

4.3.2 Economic Interests of EV Owners

The EV owners (self) scheduling results in the first stage are depicted in Figure 4.7. It can be seen from the figure that EVs have less charging power at the beginning (13:00–17:00), because most EVs are off the grid, i.e. most EVs are not available during this time. For the available EVs, they operate in charging status because the charging price is relatively low (price is available in Figure B.1 in Appendix B). To operate

in charging status during these times, it could cause EVs to store enough energy to discharge in the following peak hours and thus earn profit. After that, during peak hours (18:00–21:00), EVs operate in discharging status to inject energy back to the grid to receive profit. However, the maximum discharging power appears at 19:00, with a

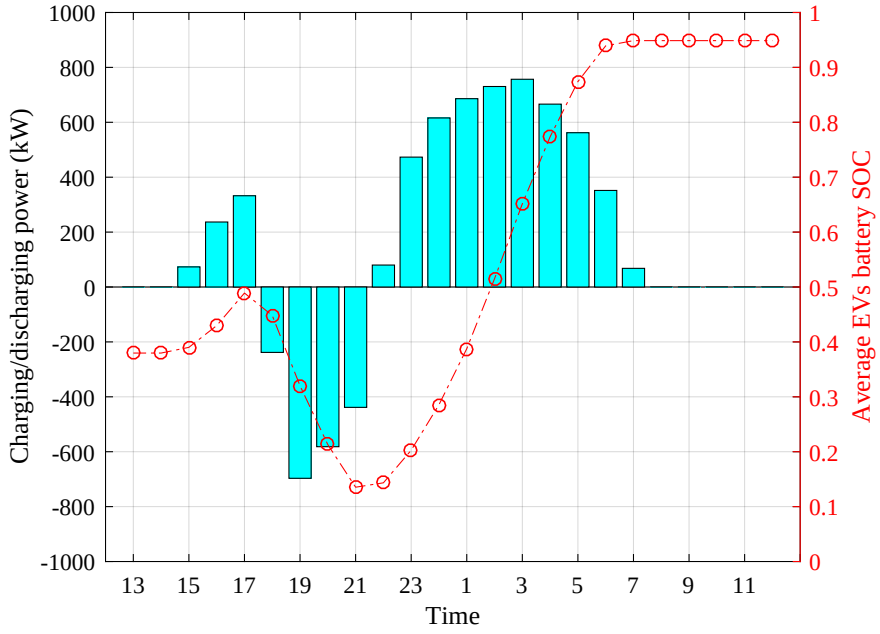

Figure 4.7: Charging/discharging results of EVs and the average EV battery SOC results under self-scheduling strategy

value of 684 kW, which is lower than the peak charging power (784 kW) at 3:00. There are two reasons for this; first, there are still some EVs off the grid at 19:00, and second, some EV battery SOC values are too low to operate in discharging status. During the period 22:00–7:00, most EVs operate in charging status because these periods are in off-peak hours. Finally, after 7:00, no EV operates in charging or discharging status, because the battery SOC is enough to satisfy owners' driving requirements.

The average battery SOC of the available EVs is also presented in Figure 4.7. It can be seen from the figure that at each time, the SOC is strictly bounded between 0.1 and 1, which guarantees that EVs will not be overcharged or discharged. Moreover, in the morning of the next day (around 7:00), the average SOC reaches 0.95, which guarantees

EV owners' next-day driving requirements.

The impact of the battery degradation rate on the self-scheduling results is shown in Figure 4.8. To examine the charging fee of EV owners operating under V2G, different

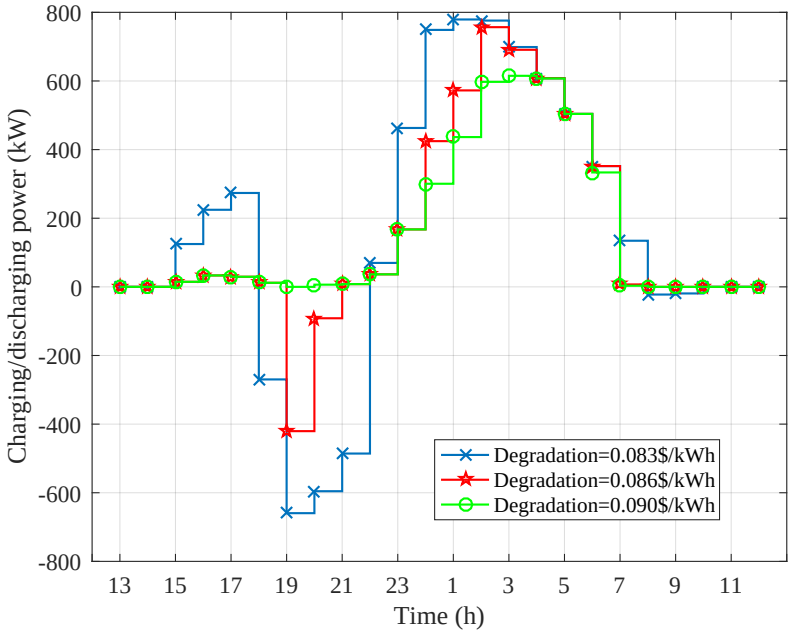

Figure 4.8: EV owners self scheduling results versus degradation rate

degradation rates are used in the model. Compared with the RTP information, it can be observed that all EVs operate in charging status during off-peak hours (low price) and operate in discharging status during peak hours (high price) under degradation rates of 0.083 $/kWh and 0.086 $/kWh. However, there are no discharging behaviours for all EVs under a degradation rate 0.090 $/kWh. This is because the V2G reward tariff cannot cover the degradation cost for EV owners to operate under V2G.

Furthermore, Table 4.1 shows the total charging fee for all EVs including the charging cost, discharging income and degradation cost versus degradation rate. It can be seen from the table that the charging fee and discharging income both decrease with increased degradation rate. This is because frequent energy interaction between EVs and the grid leads to an increase in degradation cost. Therefore, the degradation rate has a

Table 4.1: EV owners' charging fee versus degradation rate

Degradation rate ($/kWh)	0.083	0.086	0.090
Charging cost ($)	51.98	34.78	30.39
Discharging income ($)	377.14	93.99	0
Degradation cost ($)	654.86	407.79	333.45
Total fee ($)	329.71	348.58	363.84

significant influence in EV charging and discharging scheduling, and EV owners would like to be involved under V2G under the condition that the V2G reward tariff provided by the power grid can cover their battery degradation cost.

4.3.3 Economic Interests of EV Aggregator

In this section, only the EV aggregator economic interests are taken into account (ignore the economic interaction between aggregator and EV owners), so that the rebate factor in (4.10a) and EV charging cost constraint (4.18) are not considered in EV aggregator scheduling. In this case, the objective function of maximising EV aggregator profit without rebate factor is given in (4.24):

$$\text{Maximise} \quad I^d_{res} - C^d_{gri} + I^d_{own} \tag{4.24}$$

Because it is assumed that the RTP between owner–aggregator and aggregator–grid are the same, two terms in (4.24) can be cancelled with each other (i.e. $-C^d_{gri}+I^d_{own} = 0$). The aggregator scheduling results for the reserve up/down capacities are illustrated in Figure 4.9. It can be seen from the figure that the reserve up/down capacities are scheduled based on the corresponding prices, which describes the response ability of the EV aggregator in meeting temporary power grid requirements. That is, the reserve up/down capacities enable the aggregator to decrease or increase its current operating power based on power grid demands. Figure 4.10 shows both charging and discharging operations and reserve capacity results over twenty-four hours. The EV aggregator enables the power grid to call for the reserve to absorb or inject energy back temporarily and thus improves the power grids stability. Therefore, the EV aggregator gains profit

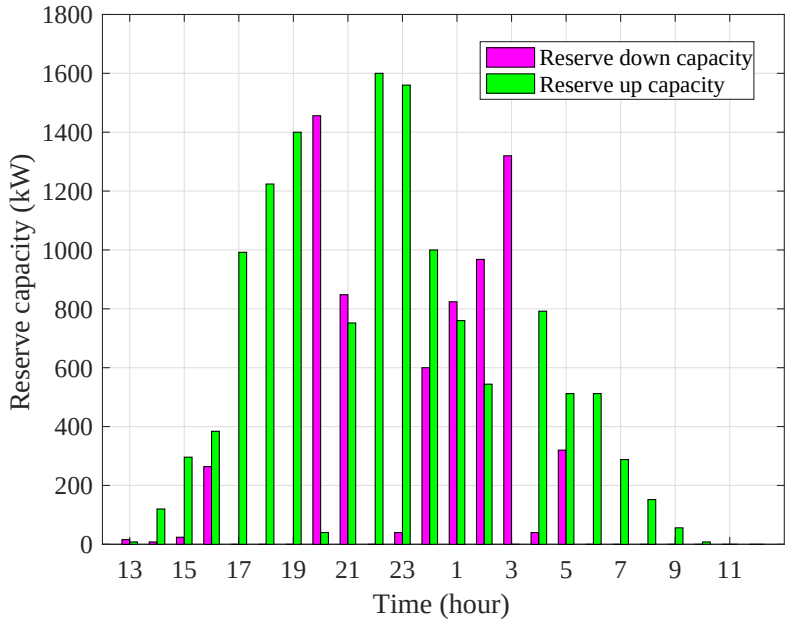

Figure 4.9: Aggregator scheduling results for reserve up/down capacities

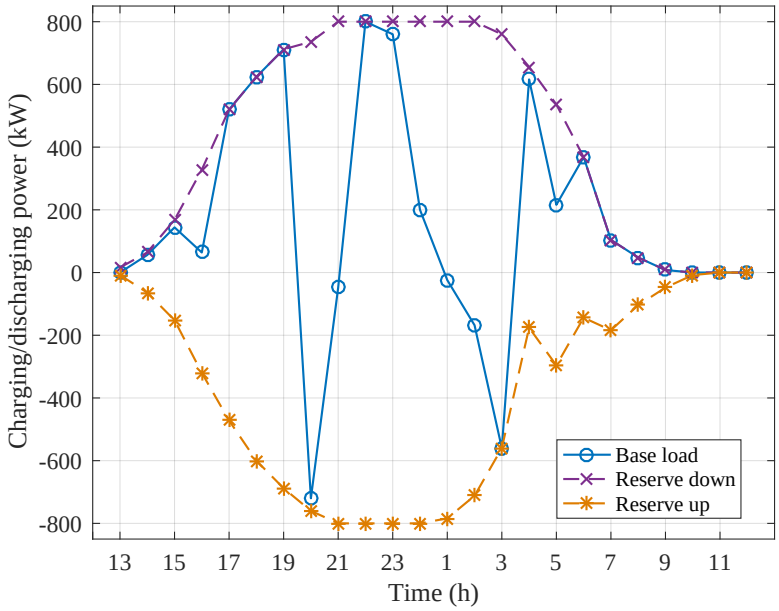

Figure 4.10: Charging/discharging power and reserve up/down capacity for the EV aggregator profit maximisation results

by providing reserve up/down capacities to the power grid.

4.3.4 Economic Inconsistency Between Stakeholders

In this section, the economic inconsistency issue is presented, which is described as the total charging fee increment rate. A sensitivity analysis of the impacting economic inconsistency is illustrated in terms of the degradation rate, maximum charging/discharging power, and battery capacity.

The total charging fee for EV owners self-scheduling and aggregator scheduling associated with different battery degradation rates are summarised in Table 4.2. It can be observed from the table that the total charging fee for self and aggregator scheduling both increase with increased degradation rate. Moreover, the economic inconsistency issue becomes significant with a higher degradation rate (from +9.87% to +14.41%). This is because the frequent energy interaction between the EV and power grids causes a high battery degradation cost.

Table 4.2: Economic inconsistency versus degradation rate

Degradation rate ($/kWh)	0.083	0.086	0.090
Self scheduling ($)	329.71	348.58	363.83
Aggregator scheduling ($)	362.26	385.42	416.29
Increment rate	+9.87%	+10.56%	+14.41%

The impact of the different charging and discharging power of EVs in influencing the economic inconsistency issue is shown in Table 4.3. The results in this table suggest that the economic inconsistency becomes significant (from +9.87% to +13.14%) as the charging and discharging power increase.

Table 4.3: Economic inconsistency versus power

Charging/discharging power (kW)	8	10	12
Self scheduling ($)	329.71	325.16	322.14
Aggregator scheduling ($)	362.26	362.48	364.46
Increment rate	+9.87%	11.48%	+13.14%

In addition, the impacts of different battery capacity values are examined in the

model. The scheduling results shown in Table 4.4 indicate that as the battery capacity increases, the economic inconsistency issue is reduced; that is, the charging cost increment rate decreases from +9.87% to +8.14%.

Table 4.4: Economic inconsistency versus capacity

Battery capacity (kWh)	64	72	80
Self scheduling ($)	329.71	375.12	420.87
Aggregator scheduling ($)	362.26	409.00	455.11
Increment rate	+9.87%	+9.03%	+8.14%

4.3.5 Optimal Rebate Value

In the previous section, the existence of economic inconsistency between EV owners and the aggregator is demonstrated, and the impacting factors are analysed. That is, the EV owners' charging fee increases under aggregator scheduling compared with EV owners' self-scheduling. In order to mediate the economic inconsistency issue, a rebate factor is proposed in the model in the second-stage scheduling. This enables the model to jointly consider the two stakeholders' economic interests.

The relationship between the maximum EV aggregator profit and the value of the rebate factor is described in Figure 4.11 and Figure 4.12. These figures suggest that there exists an optimal rebate factor value which can achieve maximised aggregator profit. The maximum aggregator profit is obtained as $\alpha^* = 0.0046$ \$/kWh and $\alpha^* = 0.0056$ \$/kWh under different discount values. For a relatively smaller rebate factor, EV charging and discharging operations mainly depend on the self-scheduling, which restricts the aggregator from responding to the power grid, and the aggregator has a lower flexibility to schedule EVs based on the reserve up/down prices. On the contrary, for a relatively higher rebate value, the aggregator has more incentive to involve EVs in the reserve market. However, a higher rebate value requires a greater rebate fee to EV owners from the EV aggregator, and thus reduces the aggregator profit.

In Figure 4.13, ten EV owners' charging fee are presented both under self and aggregator scheduling, with different values of the discount and corresponding optimal

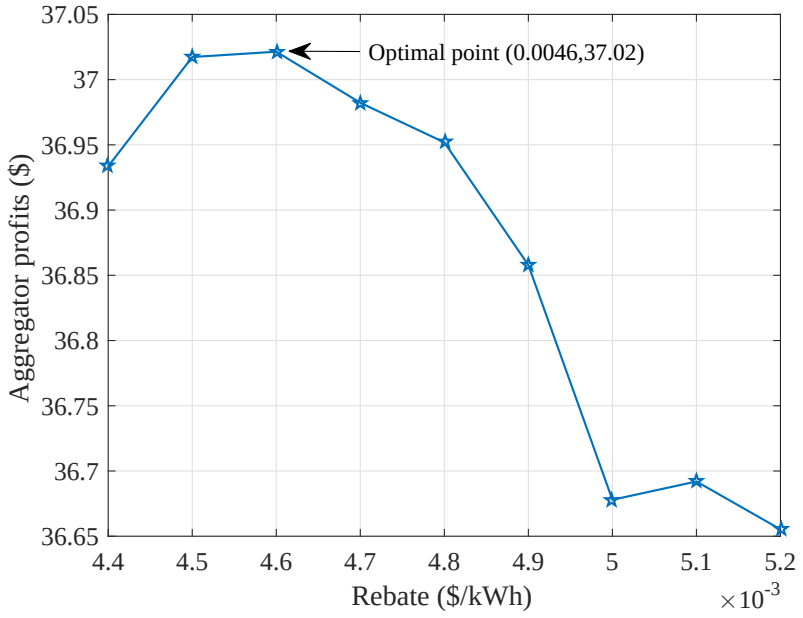

Figure 4.11: Maximum aggregator profit versus rebate values ($\beta = 5\%$)

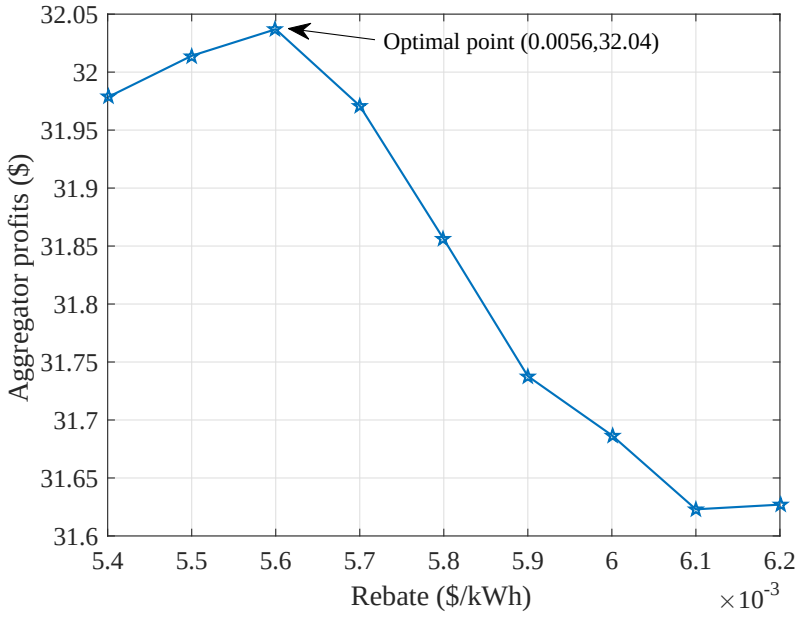

Figure 4.12: Maximum aggregator profit versus rebate values ($\beta = 7.5\%$)

rebate values. It can be found from the figure that each EV owner charging fee under aggregator scheduling is less than the that under self-scheduling (5% and 7.5% discount). The results verified the effectiveness of the proposed rebate factor in the second-stage scheduling. These results demonstrate that the proposed strategy motivates EV owners to participate in aggregator scheduling, owing to the lower charging cost under aggregator scheduling than self-scheduling. However, the aggregator profit significantly decreases under a higher discount ($ 37.02 with 5% discount and $ 32.04 with 7.5% discount in Figure 4.11 and 4.12).

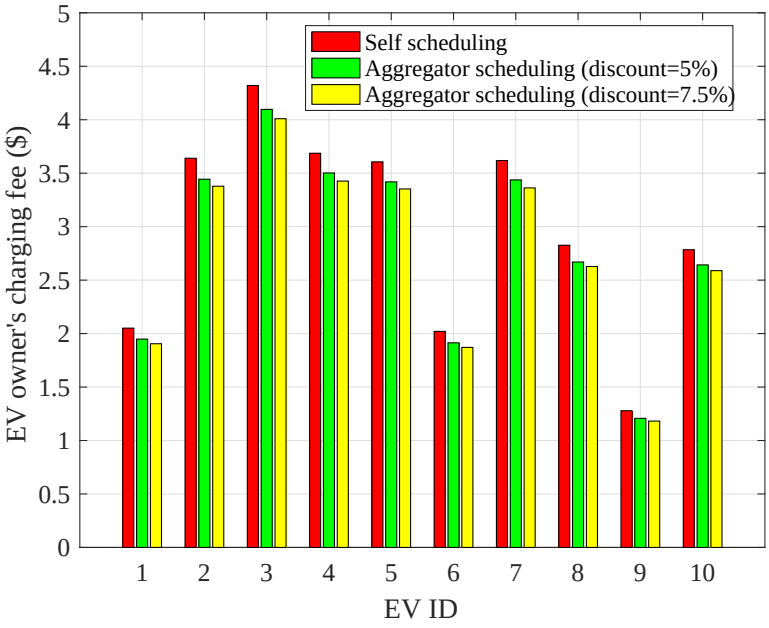

Figure 4.13: EV owners' charging fee (self and aggregator scheduling) versus discount values

4.3.6 MPC based Real-Time Scheduling Strategy

In the third-stage scheduling, the stochastic driving behaviours of EV owners are considered in the model. That is, EV information cannot be predicted accurately, and thus dynamic real-time EV information (fixed and predicted) is adopted during the scheduling. The day-ahead and real-time scheduling results are presented in Figure 4.14

with degradation rate $D^{\text{ev}} = 0.083$ \$/kWh and discount $\beta = 5\%$. Because the day-ahead EV information is fixed, the results of the second-stage scheduling (day-ahead aggregator profit maximisation) are deterministic. On the contrary, the dynamic real-time EV information must be re-predicted owing to the prediction errors. In this case, the real-time scheduling results are not the same as the day-head results. In Figure 4.14, the

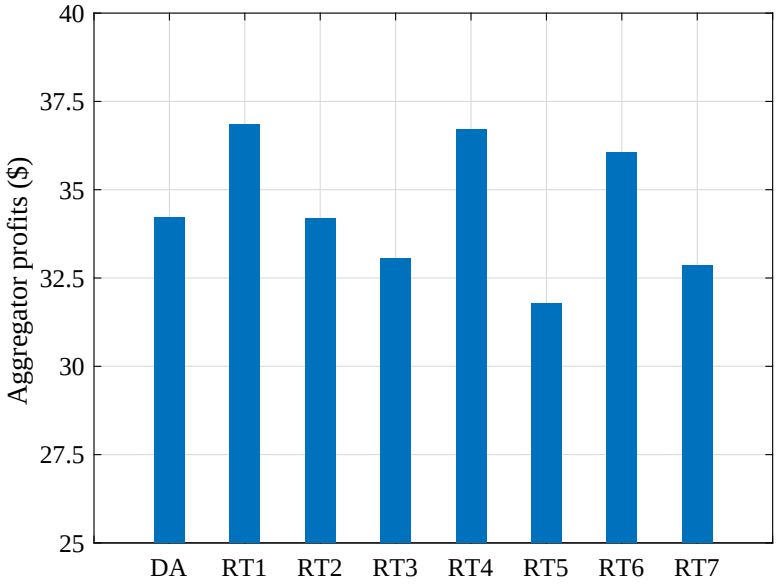

Figure 4.14: DA and RT aggregator profit in a week

real-time scheduling strategy is repeated seven times to represent the daily aggregator profit in a week, i.e. from RT1 to RT7. It is assumed that the day-ahead EV information in the whole week is the same. Based on the results, the daily RT aggregator profits in a week are \$ 36.85, \$ 34.19, \$ 33.05, \$ 36.70, \$ 31.79, \$ 36.05, and \$ 32.87, which are not equal to the DA aggregator profit of \$ 34.22, because the real-time EV information is stochastic.

4.4 Summary

In this chapter, a three-stage EV energy management strategy is proposed considering two stakeholders' (EV owner and aggregator) interest: to minimise each EV owners' charging fee and maximise aggregator profit. The energy, reserve, and economic interactions among the power grid, EV aggregator, and EV owners are discussed. The EV owners minimise their charging fee in the energy market based on RTP and V2G reward tariffs provided by the power grid. The aggregator maximises its profit by participating in the reserve market. Because the two stakeholders have different objectives, the economic inconsistency issue is analysed.

The main outcomes of this chapter are summarised as follow:

- The model is simulated from the viewpoint of two stakeholders. In the first-stage scheduling, each EV owner charging fee is minimised and the influence of the battery degradation rate on the charging fee of the EV owner participating in V2G is evaluated. By implementing a sufficient V2G reward tariff, EV owners are willing to participate in V2G to enhance the energy interaction between the power grid and EVs.

- The impact of degradation rate, maximum charging and discharging power, and battery capacity on influencing the economic inconsistency issue is discussed.

- To mediate the economic inconsistency issue, the rebate factor is proposed in the second-stage scheduling, which stands for the economic interaction between the aggregator and EV owners. The results show the effectiveness of this strategy: the EV owner charging cost under aggregator scheduling is less than that under self-scheduling.

- An MPC-based real-time scheduling strategy is adopted in the third stage. The stochastic driving behaviours of EV owners are considered in the model, which makes the scheduling results more practical in real-world scenarios.

Chapter 5

EV Energy Management in Uncertain Electricity Markets

5.1 Introduction

In this chapter, the EV aggregator interest in EV (and ESS) participation in electricity markets is analysed. It has been shown that the EV aggregator could get higher profit from providing ancillary services or attending different DR programmes compared with charging EVs during low-electricity-price hours [49, 68]. This chapter focuses on the aggregator profit maximisation in the electricity market.

The aggregator profit maximisation problem in the electricity market is threatened by uncertainties. The information gap between the predicted and the actual prices is considered in [105] and the uncertainty of the RTP is addressed by using the RO method [75]. Apart from the deviation of electricity prices, some studies have focused on the cooperation between the aggregator or BESS with RESs and the uncertainty of the renewable sources is represented by scenarios in the model [57]. In addition, EV owners' driving behaviours are naturally random. The stochastic programming method was utilised to consider the uncertainty of EV driving characteristics [56, 106]. Furthermore, the uncertainty from the electricity market includes ancillary services such as RDR.

To address the uncertainty of ancillary services, RO method is used in [76] to deal with the uncertain amount of RDR. It is claimed that the probability density function of the amount of RDR is difficult to build, owing to the characteristic of regulation and reserve markets. A probability-based model is applied in [73] to assess the aggregator's capability of providing ancillary services to power grids. Two probabilities, i.e. the probability that the DA bidding is accepted in the DAM and the probability that the reserve is required to deploy in RTM are utilised in the model to represent the market environment by taking battery degradation into consideration. A scenario-based model is built in [107] to deal with the uncertain prices, and the probability of each price scenario is calculated based on a Monte Carlo simulation. Nevertheless, the common issue in the probability-based and scenario-based models is that the relationship between the proposed reserve in the DAM and the deployed reserve in the RTM is not presented and also different RDR are not taken into account. The impact of the uncertainty of RDR is addressed by using stochastic programming in [69, 108] and the uncertainty of EV owners' behaviours and market prices are additionally considered. The risk of the deviation between the DA bidding and the RT operation is considered in [72] and it is assumed that the aggregator will be penalised if there is any difference between the RT base load and the DA bidding base load plan.

To summarise, some researchers investigated the aggregator profit maximisation in the electricity market by considering the uncertainty of prices, EV owners' driving behaviours, RESs, and RDR. However, there four issues in the EV scheduling problem are ignored in the existing research:

- First, fewer studies considered the uncertainty of RDR in terms of the time and amount aspects. In [76], a RT method is used to take the uncertainty of the reserve deployment times in one day into account. However, it only considered the worst-case scenario, which makes the results too conservative and the uncertainty of the amount is not considered.

- Second, fewer studies investigated the relationship between the DA bidding and

different RDR in the RTM. That is, the impact of the reserve deployment in RTM on the DA bidding is neglected. The authors in [69, 108] discussed the EV bidding strategy in the DAM and reserve market using stochastic programming method; however the relationship between the DAM and the reserve market is not considered.

- The risk of reserve deployment shortage due to the uncertain RTM is not appropriately evaluated in most of the existing studies. Moreover, the impact of the reserve deployment on EV charging/discharging is less discussed, such as [69, 72, 76].

- Finally, most existing studies focused on the EV charging/discharging from a single stakeholder's viewpoint but neglect the economic relationship between different stakeholders, such as [73, 95]. The aggregator profit is maximised while the EV owners' economic benefits are sacrificed (charging fee increase). The economic inconsistency issue between the aggregator and EV owners is not fully addressed, which make the aggregator scheduling results unrealistic, as the EV owners are unwilling to attend the aggregator schedule.

5.2 Electricity Markets

5.2.1 Reserve Market Participation

The EV aggregator could participate in regulation and reserve markets in the power grid to obtain profit. The primary role of the aggregator is to satisfy EV owners' driving requirements; after that, it could provide ancillary services to maximise its profit [73]. The model of the aggregator providing reserve service to the power grid in the DAM and RTM is common to the U.S. electricity markets, such as the performance-based regulation mechanism in Pennsylvania, New Jersey and Maryland (PJM) and ERCOT [109].

Figure 5.1 illustrates the framework of the aggregator participation in the reserve market. In DAM, the aggregator must submit reserve up/down capacities and base

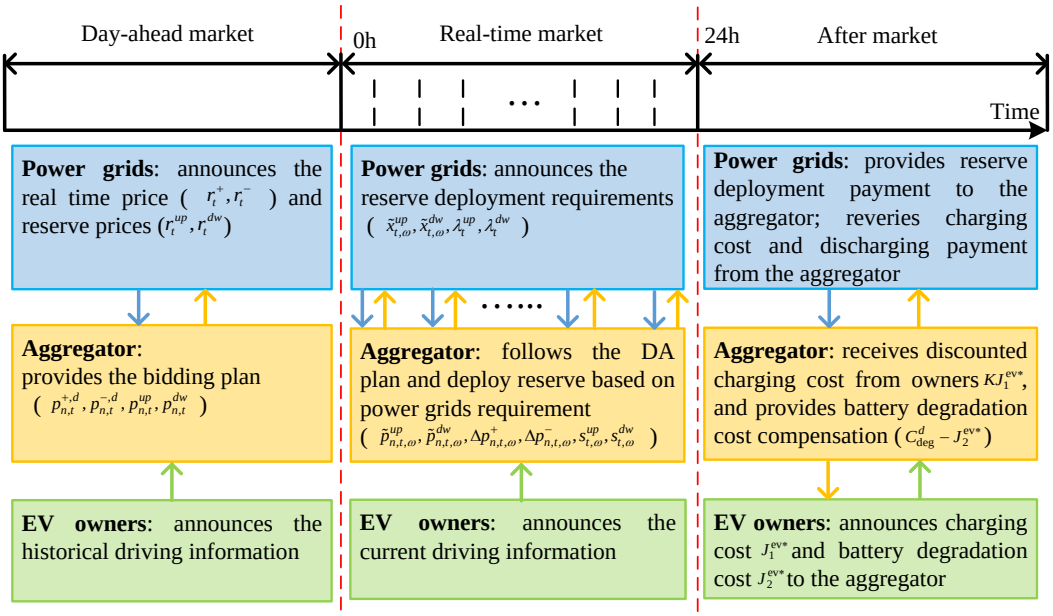

Figure 5.1: Framework of the EV aggregator participation in the reserve market

load plans to the power grid. If the plan is accepted, the aggregator receives income for stand-by reserve capacity. In RT operation of power grids, when the generation cannot meet the demand, the reserve up capacity proposed by the aggregator could be required to be deployed to offset such imbalances. If the demand is less than the generation, then the reserve down capacity will be deployed, that is to increase aggregator charging power or decrease discharging power and thus accommodate the imbalances. The aggregator operating in the RTM should deploy enough reserve according to the power grid requirements. The aggregator can receive additional payments for reserve deployment [73].

This study is based on the reserve market model proposed in [106, 110] and additionally considers the impact of uncertain reserve deployment requirements in the RTM on the DA aggregator bidding. Moreover, the risk of the aggregator not being able to deploy enough reserve (shortage) is considered in the model. Thus, a reserve deployment shortage penalty factor is introduced in the model, which means that the aggregator receives a penalty according to the difference between the deployed reserve

and the power grid requirements.

For the primary role of the aggregator, not only should the EV owners' driving requirements be met but the economic benefits of each owner should also be guaranteed [111]. To mitigate the economic inconsistency issue between EV owners and the aggregator, an owner-aggregator contract is implemented after DAM and RTM. The aggregator receives a discounted charging/discharging cost to each EV owner and also offer additional battery degradation compensation to each owner. Moreover, the aggregator provides a rebate to each EV owner for attending reserve market.

5.2.2 Uncertainty of Reserve Deployment Requirements

Reserve service is essential to ensure the security and reliability of the grid [112] by requiring deploy reserve. That is, the aggregator should change the EVs operation temporally based on the grid's RDR. In this case, the EV energy management problem is complicated by the uncertain RDR. In this section, the modelling of the uncertainty of RDR is presented.

The uncertainty of the RDR in twenty-four hours can be represented by a series of scenarios and the probability of each scenario. Figure 5.2 depicts a branch tree structure, where binary numbers are used to represent whether the reserve is required

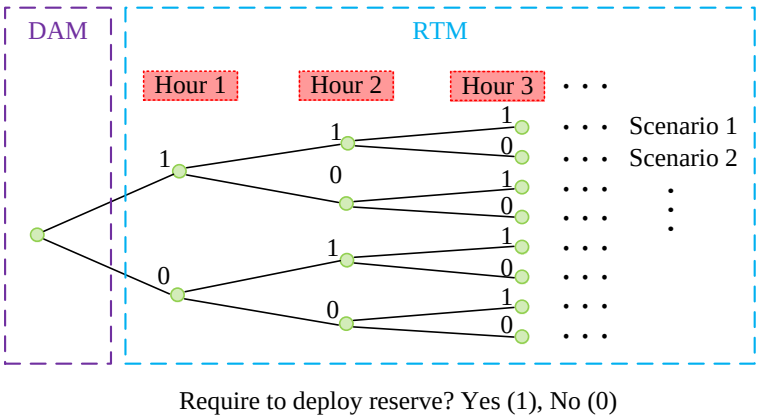

Figure 5.2: Branch tree structure of the reserve deployment requirements scenarios

to be deployed or not at each hour (1 or 0, respectively). Under this circumstance,

there are $2^{24} = 16,777,216$ scenarios in total, which lead to a large computational burden for the stochastic programming method. It is not necessary to consider all scenarios, because most scenarios have low probability and they have a low impact on the optimisation results.

It is assumed that only reserve up is deployed in the model, and different RDR scenarios can be generated based on the Monte Carol simulation method. Figure 5.3 illustrates the procedure to generate the RDR data for Q days.

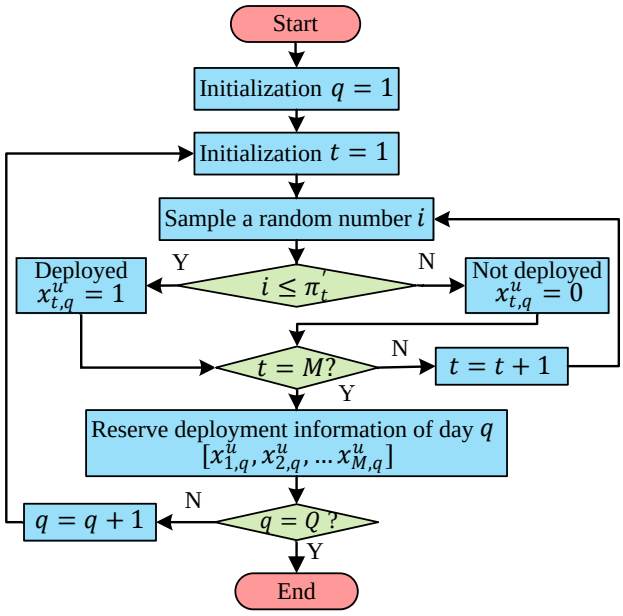

Figure 5.3: Flowchart of RDR scenarios generation approach based on Monte Carlo simulation

For the scenario generation process, the uniform distribution is utilised. That is, at each time, a random number i is generated between 0 to 1 and compared with the hourly reserve deployment probability π'_t [69]. If the hourly probability is equal to or greater than the random number, the reserve up capacity is deployed ($x^{up}_{t,q} = 1$). Otherwise, the reserve is not deployed ($x^{up}_{t,q} = 0$).

After that, all the scenarios in Q days are summarised in (5.1),

$$\begin{bmatrix} \widetilde{x}^{up}_{1,1} & \widetilde{x}^{up}_{2,1} & \cdots & \widetilde{x}^{up}_{M,1} \\ \widetilde{x}^{up}_{1,2} & \widetilde{x}^{up}_{2,2} & \cdots & \widetilde{x}^{up}_{M,2} \\ \vdots & \vdots & \ddots & \vdots \\ \widetilde{x}^{up}_{1,\Omega} & \widetilde{x}^{up}_{2,\Omega} & \cdots & \widetilde{x}^{up}_{M,\Omega} \end{bmatrix} \tag{5.1}$$

where there are Ω scenarios among Q days and V_ω days for each scenario ($\sum_{\omega=1}^{\Omega} V_\omega = Q$).

Finally, the probability of each scenario can be calculated based on (5.2):

$$\pi_\omega = \frac{V_\omega}{Q} \qquad \forall \omega \tag{5.2}$$

and the probability π_ω with the RDR $\left[\widetilde{x}^{up}_{1,\omega}, \cdots, \widetilde{x}^{up}_{M,\omega}\right]$ of each scenario will be involved in the stochastic programming of the DA aggregator bidding model. The model is discussed in detail in Section 5.3.1.

5.3 Aggregator Bidding Strategy in Electricity Markets

The EV owners' (self) scheduling strategy is discussed in Section 4.2.1, and the EV aggregator bidding strategy is discussed in this section.

5.3.1 Stochastic DA Aggregator Bidding Strategy

This section shows the stochastic DA aggregator bidding strategy based on different scenarios.

The objective function of the aggregator is to maximise the expected profit in the

energy and reserve markets by taking all scenarios into account (5.3a):

$$\begin{aligned}\text{Maximisation} \quad & \underbrace{I^{d}_{res} - C^{d}_{gri}}_{DAM} + \underbrace{\sum_{\omega=1}^{\Omega} \pi_{\omega} \left(I^{r}_{dep,\omega} - C^{r}_{pen,\omega} - C^{r}_{dev,\omega} \right)}_{RTM} \\ & + \underbrace{\left(1-\beta\right) J_1^{\mathrm{ev}*} - \left(C^{d}_{deg} - J_2^{\mathrm{ev}*} \right)}_{contract}\end{aligned} \tag{5.3a}$$

where the aggregator profit comes from three aspects: the DAM, RTM, and owner-aggregator contract.

In the DAM, I^{d}_{res} represents the income of the proposed reserve up/down capacity plan, which has been formulated in (4.10b), and the second term C^{d}_{gri} stands for the purchasing cost and selling income, which is given in (4.10c). C^{d}_{deg} in (5.3b) is the battery degradation cost due to the proposed charging and discharging of EVs,

$$C^{d}_{deg} = D^{\mathrm{ev}} \sum_{t=1}^{M} \sum_{n=1}^{N} \left(p^{+,d}_{n,t} + p^{-,d}_{n,t} \right) \Delta T \tag{5.3b}$$

In the RTM, $I^{r}_{dep,\omega}$ in (5.3c) represents the reserve deployment profit under scenario ω: the aggregator receives additional payments by deploying reserve based on power grid requirements,

$$I^{r}_{dep,\omega} = \sum_{t=1}^{M} \sum_{n=1}^{N} \left(\widetilde{r}^{up}_{t} \widetilde{p}^{up}_{n,t,\omega} + \widetilde{r}^{dw}_{t} \widetilde{p}^{dw}_{n,t,\omega} \right) \Delta T \tag{5.3c}$$

where $\widetilde{r}^{up}_{t}$ and $\widetilde{r}^{dw}_{t}$ stand for the deployed up/down reserve prices at time t.

$C^{r}_{pen,\omega}$ in (5.3d) represents the penalty for reserve deployment shortage under scenario ω,

$$C^{r}_{pen,\omega} = \sum_{t=1}^{M} \left(\gamma^{up} s^{up}_{t,\omega} + \gamma^{dw} s^{dw}_{t,\omega} \right) \Delta T \tag{5.3d}$$

where $s^{up}_{t,\omega}$ and $s^{dw}_{t,\omega}$ stand for the reserve up/down shortage at time t.

The last term in $C^{r}_{dev,\omega}$ (5.3e) represents the cost of charging and discharging

deviations in the RTM due to the uncertain RDR. It is assumed that the EV aggregator could adjust the proposed DA base load plan in RT operation only after the reserve is deployed,

$$C^{r}_{dev,\omega} = \sum_{t=1}^{M}\sum_{n=1}^{N}\left(r^{+}_{t}\,\Delta p^{+}_{n,t,\omega} - r^{-}_{t}\,\Delta p^{-}_{n,t,\omega}\right)\Delta T \tag{5.3e}$$

where $\Delta p^{+}_{n,t,\omega}$ and $\Delta p^{+}_{n,t,\omega}$ are charging and discharging deviations of EV n at time t in the RTM.

In the owner–aggregator contract, $J_1^{\text{ev}*}$ and $J_2^{\text{ev}*}$ represent the optimal charging/discharging cost and battery degradation cost from self-scheduling respectively. $(1-\beta)\,J_1^{\text{ev}*}$ stand for the discounted charging/discharging cost received from EV owners. Moreover, the aggregator provides additional battery degradation payments to EV owners $\left(C^{d}_{deg} - J_2^{\text{ev}*}\right)$.

The maximum range of EV charging/discharging operations and the relationship between charging/discharging power and the reserve capacity in the DAM were formulated in (4.11)–(4.14).

Constraints (5.4) and (5.5) are used to ensure that the summation of the deployed reserve and the charging/discharging deviations are less than the reserve capacity when the reserve is deployed for each scenario,

$$0 \le \widetilde{p}^{up}_{n,t,\omega} + \Delta p^{-}_{n,t,\omega} \le \widetilde{x}^{up}_{t,\omega} p^{up}_{n,t} \quad \forall t, n, \omega \tag{5.4}$$

$$0 \le \widetilde{p}^{dw}_{n,t,\omega} + \Delta p^{+}_{n,t,\omega} \le \widetilde{x}^{dw}_{t,\omega} p^{dw}_{n,t} \quad \forall t, n, \omega \tag{5.5}$$

Constraints (5.6), (5.7), (5.6), and (5.9) suggest that the DA reserve up/down capacities of each EV, the deployed reserve, and the power deviation at each time should not be less than zero,

$$\widetilde{p}^{up}_{n,t,\omega} \ge 0 \quad \forall n, t, \omega \tag{5.6}$$

$$\widetilde{p}^{dw}_{n,t,\omega} \ge 0 \quad \forall n, t, \omega \tag{5.7}$$

$$\Delta p^{+}_{n,t,\omega} \geq 0 \quad \forall n,t,\omega \tag{5.8}$$

$$\Delta p^{-}_{n,t,\omega} \geq 0 \quad \forall n,t,\omega \tag{5.9}$$

The relationships between the EV battery SOC limits and the DA charging/discharging power, DA reserve capacities, RT deployed reserve, and RT charging/discharging deviations are formulated in constraints (5.10) and (5.11):

$$\begin{aligned} SOC^{a}_{n} + \frac{\sum_{t=1}^{m-1}\left(p^{+,d}_{n,t} - p^{-,d}_{n,t} - \widetilde{p}^{up}_{n,t,\omega} + \widetilde{p}^{dw}_{n,t,\omega} + \Delta p^{+}_{n,t,\omega} - \Delta p^{-}_{n,t,\omega}\right)\Delta T}{E^{\mathrm{ev}}_{n}} \\ + \frac{\left(p^{+,d}_{n,m} - p^{-,d}_{n,m} + p^{dw}_{n,m}\right)\Delta T}{E^{\mathrm{ev}}_{n}} \leq \overline{\mathrm{SOC}} \quad \forall n,m,\omega \end{aligned} \tag{5.10}$$

$$\begin{aligned} SOC^{a}_{n} + \frac{\sum_{t=1}^{m-1}\left(p^{+,d}_{n,t} - p^{-,d}_{n,t} - \widetilde{p}^{up}_{n,t,\omega} + \widetilde{p}^{dw}_{n,t,\omega} + \Delta p^{+}_{n,t,\omega} - \Delta p^{-}_{n,t,\omega}\right)\Delta T}{E^{\mathrm{ev}}_{n}} \\ + \frac{\left(p^{+,d}_{n,m} - p^{-,d}_{n,m} - p^{up}_{n,m}\right)\Delta T}{E^{\mathrm{ev}}_{n}} \geq \underline{SOC}_{n,m} \quad \forall n,m,\omega \end{aligned} \tag{5.11}$$

Moreover, to guarantee that EVs are charged to the desired value at the departure time, the minimum SOC of EV n at each time is calculated based on (5.12):

$$\underline{SOC}_{n,m} = \max\{\underline{\mathrm{SOC}}, \mathrm{SOC}^{\mathrm{d}} - \frac{\overline{P}^{\mathrm{ev}}_{n}\,(M-m)\,\Delta T}{E^{\mathrm{ev}}_{n}}\} \quad \forall m,n \tag{5.12}$$

The relationships between the deployed reserve, charging and discharging deviations, reserve shortages, and power grid RDR at time t under scenario ω are shown in (5.13) and (5.14):

$$s^{up}_{t,\omega} + \sum_{n=1}^{N}\widetilde{p}^{up}_{n,t,\omega} = \sum_{n=1}^{N}\Delta p^{-}_{n,t,\omega} + \lambda^{up}\widetilde{x}^{up}_{t,\omega}\sum_{n=1}^{N}p^{up}_{n,t} \quad \forall t,\omega \tag{5.13}$$

$$s^{dw}_{t,\omega} + \sum_{n=1}^{N}\widetilde{p}^{dw}_{n,t,\omega} = \sum_{n=1}^{N}\Delta p^{+}_{n,t,\omega} + \lambda^{dw}\widetilde{x}^{dw}_{t,\omega}\sum_{n=1}^{N}p^{dw}_{n,t} \quad \forall t,\omega \tag{5.14}$$

The reserve down deployment is not considered in this model, and thus the values of

the reserve down deployment amount and the reserve down deployment requirements are both set to zero, that is, $\lambda^{dw} = \widetilde{x}^{dw}_{t,\omega} = 0, \forall t, \omega$.

The reserve deployment shortage variables at each time and scenario are defined in (5.15) and (5.16)

$$s^{up}_{t,\omega} \geq 0 \quad \forall t, \omega \tag{5.15}$$

$$s^{dw}_{t,\omega} \geq 0 \quad \forall t, \omega \tag{5.16}$$

5.3.2 Deterministic DA Aggregator Bidding Strategy

The objective function of the DA bidding strategy under deterministic RDR is shown in (5.17):

$$\begin{aligned} \sum_{\omega=1}^{\Omega} \pi_\omega \left(I^d_{res,\omega} - C^d_{gri,\omega} - C^d_{deg,\omega} + I^r_{dep,\omega} - C^r_{pen,\omega} - C^r_{dev,\omega} \right) \\ + (1-\beta)\, J_1^{\text{ev}*} + J_2^{\text{ev}*} \end{aligned} \tag{5.17}$$

where $I^d_{res,\omega}$, $C^d_{gri,\omega}$, and $C^d_{deg,\omega}$ represent the reserve capacity income, base load cost, and battery degradation cost in the DAM under scenario ω.

This is subject to constraints (4.11)–(4.14) and (5.4)–(5.16). Because this section shows the deterministic strategy, the DA bidding plan is unique for each scenario. In this case, the variables in $p^{+,d}_{n,t}$, $p^{-,d}_{n,t}$, $p^{up}_{n,t}$, and $p^{dw}_{n,t}$ in the stochastic strategy are substituted by $p^{+,d}_{n,t,\omega}$, $p^{-,d}_{n,t,\omega}$, $p^{up}_{n,t,\omega}$, and $p^{dw}_{n,t,\omega}$ in the deterministic strategy.

5.3.3 No-Deployment-Considered Bidding Strategy

The objective function of the no-deployment-considered strategy is the same as that of the stochastic strategy, that is the objective function (5.3a–5.3e) subject to constraints (4.11)–(4.14) and (5.4)–(5.16). Because no reserve deployment is considered in this strategy, the variables representing reserve deployment in the model are set to zero, that is, $\widetilde{p}^{up}_{n,t,\omega} = \widetilde{p}^{dw}_{n,t,\omega} = 0, \forall n, t, \omega$. Algorithm 1 shows the calculation process of the aggregator expected profit under the no-reserve-deployment-considered strategy.

Algorithm 1: Expected profit under no-deployment-considered bidding Strategy

Input: Price information, EV information;
Output: Expected profit;
Initialise price and EV information in DAM;
Submit the DA bidding plan based on $p_{n,t}^{up}, p_{n,t}^{dw}, p_{n,t}^{+,d}, p_{n,t}^{-,d}, \forall n, t$;
Receive profit for reserve capacity I_{res}^{d};
for $q = 1; q \leq Q; q++$ **do**
  for $t = 1; t \leq T; t++$ **do**
    if $x_{t,q}^{up} = 1$ **then**
      Penalty: $C_{pen,q,t}^{r} \leftarrow \lambda^{up} \sum_{n=1}^{N} p_{n,t}^{up}$
    else
      No penalty: $C_{pen,q,t}^{r} \leftarrow 0$
    end
  end
  Penalty in q day $C_{pen,q}^{r} \leftarrow \sum_{t=1}^{M} C_{pen,q,t}^{r}$;
end
Total penalty $C_{pen}^{r} \leftarrow \sum_{q=1}^{Q} C_{pen,q}^{r}$;
Expected profit: $I_{res}^{d} - C_{gri}^{d} - C_{deg}^{d} - C_{pen}^{r}/Q + (1-\beta)\, J_1^{\text{ev}*} + J_2^{\text{ev}*}$;

5.3.4 Aggregator Bidding with the Utilisation of ESS

Compared with EV, ESS are always ready and potentially help reduce the penalty arising from the reserve shortage. This section discusses the EV aggregator bidding strategy with the utilisation of ESS. The objective function of EV aggregator with ESS has the same format as (5.3a), which is defined in (5.18a):

$$\text{Maximise} \quad Exp^{\text{ev}} + Exp^{\text{ess}} + \sum_{\omega=1}^{\Omega} \pi_{\omega} \left(I_{\omega}^{\text{ev,ess}} - C_{\omega}^{\text{ev,ess}}\right) + \left[(1-\beta)\, J_1^{\text{ev}*} + J_2^{\text{ev}*}\right] \quad (5.18a)$$

The expected profit from EV and ESS are defined in (5.18b) and (5.18c):

$$\begin{aligned} Exp^{\mathrm{ev}} = &-\sum_{t=1}^{M}\sum_{n=1}^{N}\left(r_t^{+}p_{n,t}^{+,d} - r_t^{-}p_{n,t}^{-,d}\right)\Delta T + \sum_{t=1}^{M}\sum_{n=1}^{N}\left(r_t^{up}p_{n,t}^{up} - r_t^{dw}p_{n,t}^{dw}\right)\Delta T \\ &- \sum_{t=1}^{M}\sum_{n=1}^{N} D^{\mathrm{ev}}\left(p_{n,t}^{+,d} + p_{n,t}^{-,d}\right)\Delta T \end{aligned} \tag{5.18b}$$

$$\begin{aligned} Exp^{\mathrm{ess}} = &-\sum_{t=1}^{M}\left(r_t^{+}p_t^{+,d} - r_t^{-}p_t^{-,d}\right)\Delta T + \sum_{t=1}^{M}\left(r_t^{up}p_t^{up} - r_t^{dw}p_t^{dw}\right)\Delta T \\ &- \sum_{t=1}^{M} D^{\mathrm{ess}}\left(p_t^{+,d} + p_t^{-,d}\right)\Delta T \end{aligned} \tag{5.18c}$$

where $p_t^{+,d}$, $p_t^{-,d}$ are the charging and discharging powers of the ESS in the DAM; p_t^{up} and p_t^{dw} are the reserve up and down capacities of the ESS in the DAM.

In the RTM, the grid declares RDR to call for the reserve based on the DA proposed reserve capacity. $I_{\omega}^{ev,ess}$ represents the income by deploying the reserve under scenario ω. $R_{Pe,\omega}$ in the objective function was defined in (5.3d).

$$I_{\omega}^{\mathrm{ev,ess}} = \sum_{t=1}^{M}\sum_{n=1}^{N}\left[\widetilde{r}_t^{up}\left(\widetilde{p}_{n,t,\omega}^{up} + \widetilde{p}_{t,\omega}^{up}\right) + \widetilde{r}_t^{dw}\left(\widetilde{p}_{n,t,\omega}^{dw} + \widetilde{p}_{t,\omega}^{dw}\right)\right]\Delta T \tag{5.19}$$

where $\widetilde{p}_{t,\omega}^{up}$ and $\widetilde{p}_{t,\omega}^{dw}$ stand for the deployed reserve up and down of the ESS in the RTM.

$$C_{\omega}^{\mathrm{ev,ess}} = \sum_{t=1}^{M}\left(\gamma^{up}s_{t,\omega}^{up} + \gamma^{dw}s_{t,\omega}^{dw}\right)\Delta T \tag{5.20}$$

The scheduling constraints of the ESS are similar to those of the EVs, except that the ESS are available all the time and the ESS have no target SOC other than the final SOC. The scheduling constraints of the ESS are formulated as follows:

$$0 \le p_t^{+,d} \le \overline{P}^{\mathrm{ess}} i_t^{+} \quad \forall t \tag{5.21}$$

$$0 \le p_t^{-,d} \le \overline{P}^{\mathrm{ess}} i_t^{-} \quad \forall t \tag{5.22}$$

$$i_t^+ + i_t^- \leq 1 \quad \forall t \tag{5.23}$$

$$p_t^{+,d} - p_t^{-,d} - p_t^{up} \geq -\overline{P}^{\text{ess}} \quad \forall t \tag{5.24}$$

$$p_t^{+,d} - p_t^{-,d} + p_t^{dw} \leq \overline{P}^{\text{ess}} \quad \forall t \tag{5.25}$$

$$0 \leq \widetilde{p}_{t,\omega}^{up} \leq p_{t,\omega}^{up} \quad \forall t, \omega \tag{5.26}$$

$$0 \leq \widetilde{p}_{t,\omega}^{dw} \leq p_{t,\omega}^{dw} \quad \forall t, \omega \tag{5.27}$$

$$\text{SOC}^{\text{b}} + \frac{\sum_{t=1}^{m} \left(p_t^{+,d} - p_t^{-,d}\right) \Delta T + \sum_{t=1}^{m-1} \left(-\widetilde{p}_{t,\omega}^{up} + \widetilde{p}_{t,\omega}^{dw}\right) \Delta T - p_m^{up} \Delta T}{E^{\text{ess}}} \leq \underline{\text{SOC}} \quad \forall m, m \neq 1, \omega \tag{5.28}$$

$$\text{SOC}^{\text{b}} + \frac{\left(p_1^{+,d} - p_1^{-,d}\right) \Delta T - p_1^{up} \Delta T}{E^{\text{ess}}} \leq \underline{\text{SOC}} \tag{5.29}$$

$$\text{SOC}^{\text{b}} + \frac{\sum_{t=1}^{m} \left(p_t^{+,d} - p_t^{-,d}\right) \Delta T + \sum_{t=1}^{m-1} \left(-\widetilde{p}_{t,\omega}^{up} + \widetilde{p}_{t,\omega}^{dw}\right) \Delta T + p_m^{dw} \Delta T}{E^{\text{ess}}} \leq \overline{\text{SOC}} \quad \forall m, m \neq 1, \omega \tag{5.30}$$

$$\text{SOC}^{\text{b}} + \frac{\left(p_1^{+,d} - p_1^{-,d}\right) \Delta T + p_1^{dw} \Delta T}{E^{\text{ess}}} \leq \overline{\text{SOC}} \tag{5.31}$$

$$\text{SOC}^{\text{b}} + \frac{\sum_{t=1}^{M} \left(p_t^{+,d} - p_t^{-,d} - \widetilde{p}_{t,\omega}^{up} + \widetilde{p}_{t,\omega}^{dw}\right) \Delta T}{E^{\text{ess}}} \geq \text{SOC}^{\text{e}} \quad \forall \omega \tag{5.32}$$

With the utilisation of ESS, the constraints (5.13) and (5.14) are modified as follows:

$$s_{t,\omega}^{up} + \widetilde{p}_{t,\omega}^{up} + \sum_{n=1}^{N} \widetilde{p}_{n,t,\omega}^{up} = \lambda^{up} \widetilde{x}_{t,\omega}^{up} \left(p_{t,\omega}^{up} + \sum_{n=1}^{N} p_{n,t,\omega}^{up}\right) \quad \forall t, \omega \tag{5.33}$$

$$s_{t,\omega}^{dw} + \widetilde{p}_{t,\omega}^{dw} + \sum_{n=1}^{N} \widetilde{p}_{n,t,\omega}^{dw} = \lambda^{dw} \widetilde{x}_{t,\omega}^{dw} \left(p_{t,\omega}^{dw} + \sum_{n=1}^{N} p_{n,t,\omega}^{dw}\right) \quad \forall t, \omega \tag{5.34}$$

5.4 Numerical Examples

The results of the EV aggregator bidding strategy are discussed in this section. The results of the EV aggregator bidding without ESS are discussed in Sections 5.4.2–5.4.5; and the results of the EV aggregator bidding with ESS are presented in Sections 5.4.6–5.4.8.

The maximum charging/discharging power and capacity of EV and the ESS are given in Table B.1 and B.2 in Appendix B. One hundred ($N = 100$) EVs are used in this case study, and the EV information are generated based on TGD, where the relevant data of TGD are available in Table B.4 in Appendix B.

5.4.1 Probabilities and Scenarios of Reserve Deployment Requirements

In the RTM, one year ($Q = 365$) of RDR data are generated and the hourly probabilities are available in Table 5.1. It can be seen that the highest probability appears from

Table 5.1: Hourly probability of RDR

Time	**13:00**	**14:00**	**15:00**	**16:00**	**17:00**	**18:00**
Probability	0.089	0.091	0.099	0.121	0.122	0.156
Time	**19:00**	**20:00**	**21:00**	**22:00**	**23:00**	**0:00**
Probability	0.155	0.151	0.154	0.156	0.122	0.094
Time	**1:00**	**2:00**	**3:00**	**4:00**	**5:00**	**6:00**
Probability	0.015	0.015	0.015	0.015	0.015	0.015
Time	**7:00**	**8:00**	**9:00**	**10:00**	**11:00**	**12:00**
Probability	0.029	0.055	0.078	0.081	0.083	0.084

18:00 to 22:00. The reason is that these are peak hours in one day, and there is a higher probability that the generation side cannot meet the energy consumption from the demand side. Therefore, the power grid has a high probability of reserve up capacity deployment requirements during these times to meet the generation and demand balance. Figure 5.4 shows the 100 days data of the generated RDR data (365 days in total). The figure suggests that the reserve up capacity is usually required to deploy between 18:00–22:00, which reflects the hourly probability in Table 5.1. From 7:00 until the end,

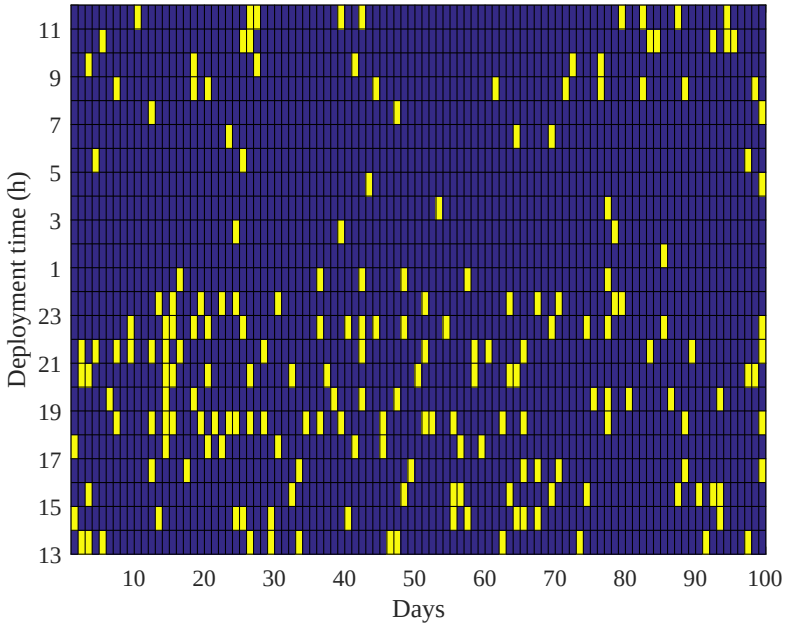

Figure 5.4: Generated reserve deployment requirements for 100 days

it is assumed that no reserve is deployed. The reason for this is that aggregator has less reserve capacity can be deployed, because most EVs are off the grid (departed from the community) after 7:00.

A summary of the number of reserve deployment requirements in one day among 365 days is shown in Figure 5.5. The figure suggests that within 365 days, there are 70 days on which no reserve is required. There are 128 and 112 days on which the reserve is required once and twice, respectively. In total, there are 310 days with no more than two requirements. There are 35 days when reserve is required three times and 16 days with four times. Finally, there are only two days when reserve is required five and six times in one day.

According to the statistical information, the probability of each scenario π_ω is illustrated in Figure 5.6. In total, there are 125 scenarios in 365 days, i.e. $\Omega = 125$. Scenario 1 represents that no reserve is required, which has the highest probability $\pi_1 = 0.19$.

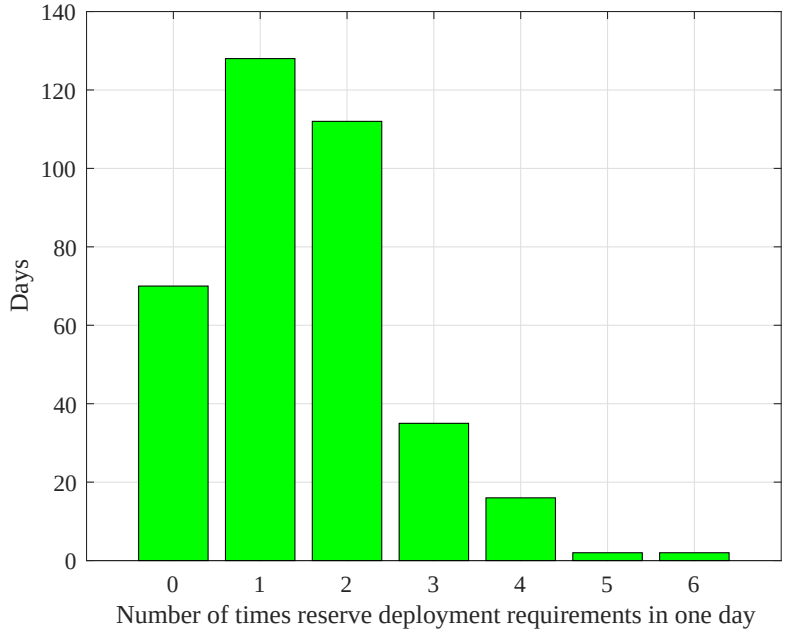

Figure 5.5: A summary of the number of times RDR in one day among 365 days

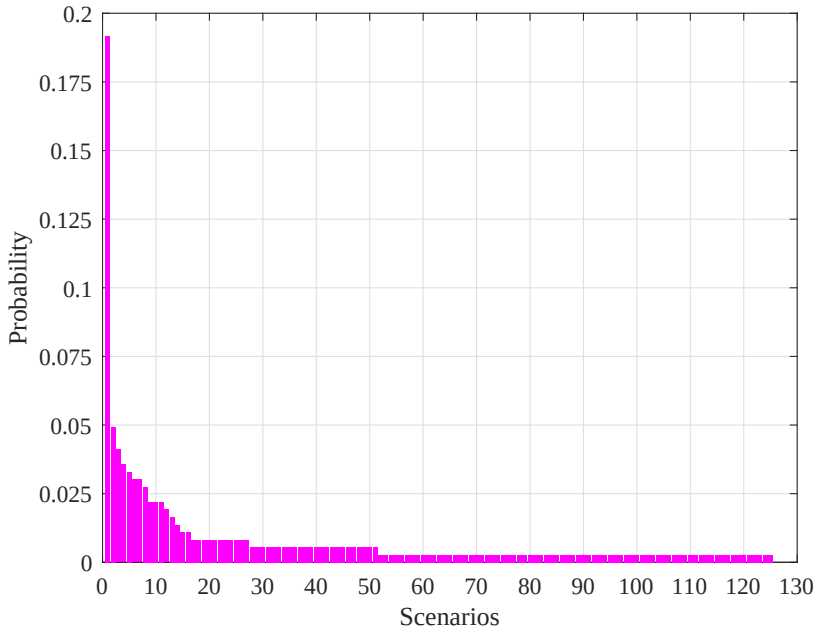

Figure 5.6: Probability of each RDR scenario

5.4.2 Aggregator Profit under Deterministic Strategy

The scheduling results of the aggregator profit under deterministic RDR are presented in Figure 5.7. The results show that the minimum profit of the aggregator within 365

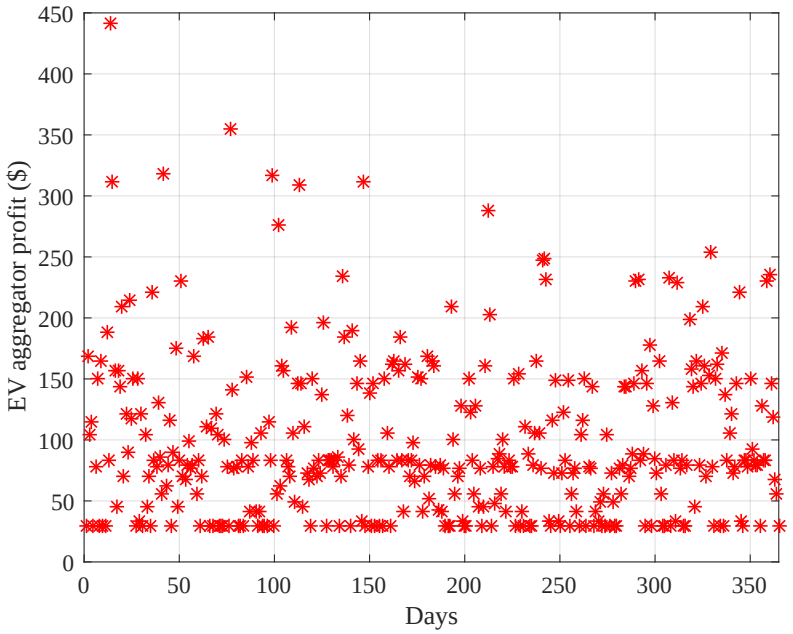

Figure 5.7: Aggregator profit with different amount of RDR under deterministic DA bidding strategy

days is $ 29.45, under the condition that no reserve is required in twenty-four hours. The reason is that for no reserve deployment, the aggregator cannot get additional payments from the RTM, even though there is no charging/discharging deviation or deployed reserve shortage penalties in RT operation.

For reserve deployment with $\lambda^{up} = 100\%$ (λ^{up} stands for the percentage of the required reserve up to be deployed to the proposed reserve up capacity), it can be seen from the figure that the highest profit could reach $ 441.94, the reserve is required six times in that day (Day 14 in Figure 5.5), which is significantly higher than that without reserve deployed ($ 29.45). The reason for this is that the aggregator could receive additional reserve deployment payments from the RTM. Moreover, the aggregator

will not receive any penalties for reserve deployment shortage because the RDR are deterministic, and there are already taken into account in the aggregator DA bidding plan.

5.4.3 Aggregator Profit under Stochastic Strategy

Figure 5.8 presents the DA base load plan with different amounts of RDR in twenty-four hours. It suggests that EVs are mainly in discharging status during peak hours (17:00–21:00) and charging status during off-peak hours (22:00–6:00). For the different amount of RDR, it has less impact on the DA base load plan. The DA base load plan is similar to the charging/discharging plan under the self-scheduling strategy in Figure 4.7, except that the maximum discharging power of the stochastic programming method (353 kW) is less than that of the self-scheduling (686 kW). This is because, in order to deploy reserve capacity during peak hours, the proposed (DA plan) discharging power during this time is reduced.

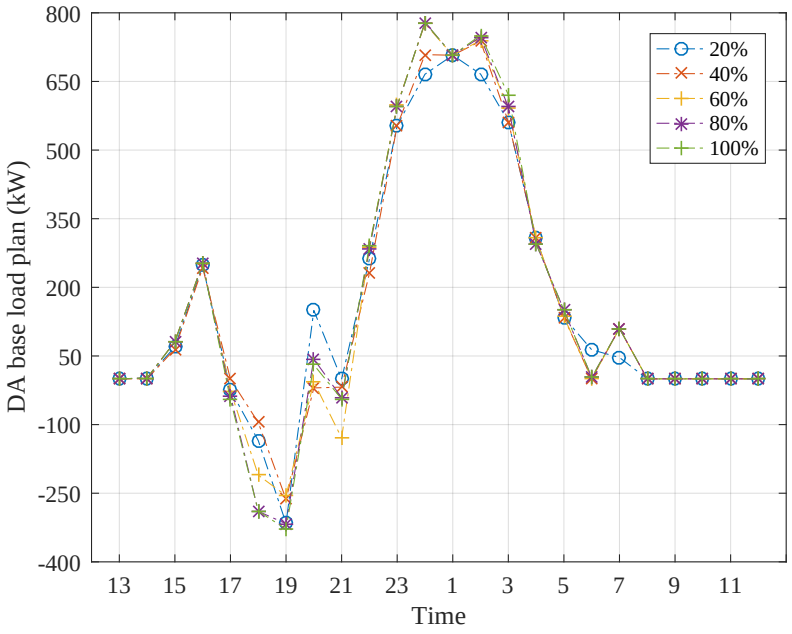

Figure 5.8: DA base load plan with different amount of RDR under stochastic programming strategy

The DA reserve up capacity plan is shown in Figure 5.9. It can be seen that the higher reserve deployment amount, the less reserve up capacity is proposed in the DA plan. The reason for this is that the aggregator proposes less reserve capacity in order to reduce the risk of reserve deployment shortage in the RTM.

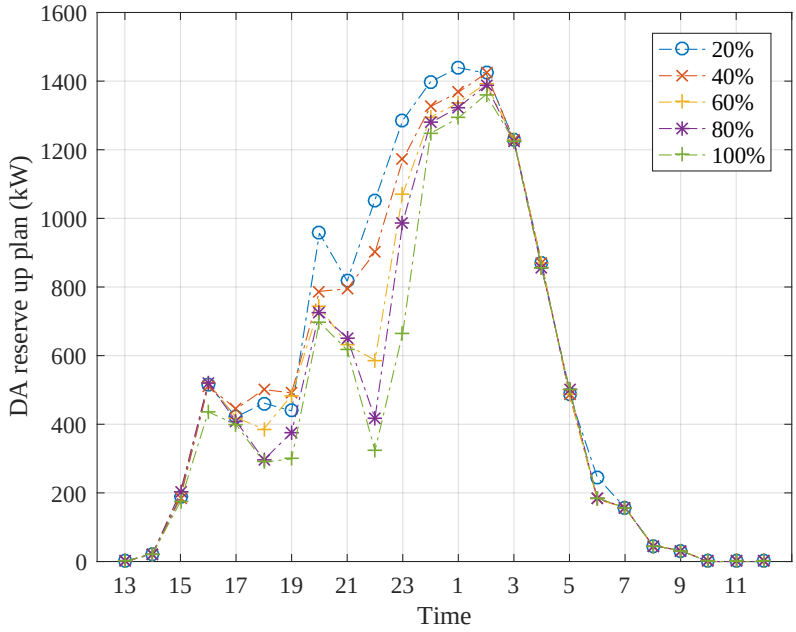

Figure 5.9: DA reserve up capacity plan with different amount of RDR under stochastic programming method

Figure 5.10 illustrates the aggregator profit over 365 days under RDR with $\lambda^{up} = 100\%$. In DA scheduling, the DA bidding plan is made based on 125 scenarios. In this case, once the DA bids plan is determined, it is suitable for all scenarios in RT operation. The results in Figure 5.10 show that the highest profit the aggregator could obtain is \$ 435.26, which is slightly less than that of the deterministic strategy (\$ 441.94). In addition, the lowest profit is $\$ -7.08$ (70 days for no reserve is required), which is much less than that of the deterministic strategy (\$ 29.45).

Figure 5.11 shows the relationship between the expected profit and 95% confidence interval (red) under different amount of RDR. For example, for 50% RDR, the expected profit of these one-year data is \$ 85.25, with the 95% confidence interval ranging from \$

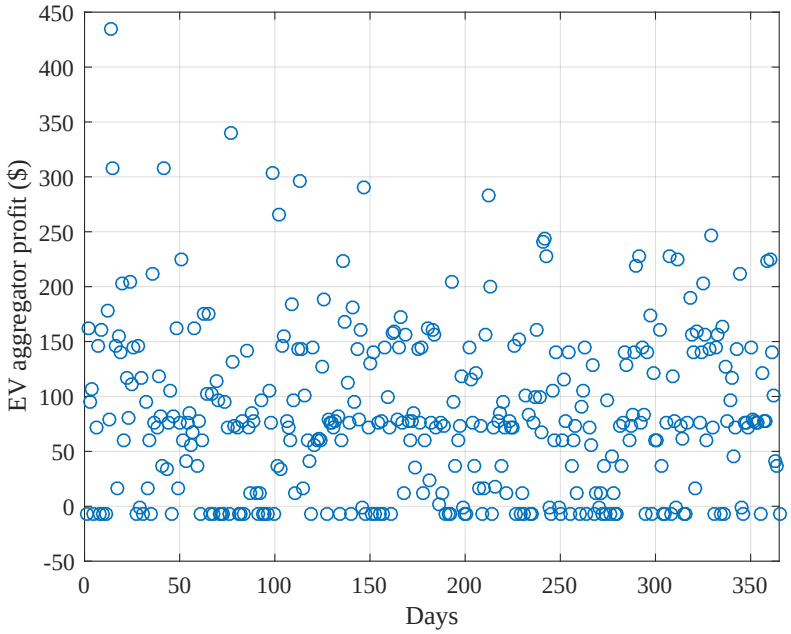

Figure 5.10: Aggregator profit with different amount of RDR under stochastic DA bidding strategy

77.47 to $ 93.03. It suggests that, with 95% probability, the expected profit for infinite days which could not be determined, will be in the range of $ 77.47 to $ 93.03.

5.4.4 Aggregator Profit under No-Reserve-Deployment Considered Strategy

In order to compare with the deterministic and stochastic strategies, the scheduling results of aggregator profit without considering reserve deployment in DA scheduling are presented in Figure 5.12. It can be seen from the figure that the highest profit the aggregator could obtain is $ 29.45, which is mulch less than those of the stochastic ($ 435.26) and deterministic strategies ($ 441.94). The lowest profit is $ − 357.71, which is much lower than those of the deterministic and stochastic strategies. The reason for this is that the aggregator will not deploy reserve in the RTM and thus lead to penalty. Therefore the profit is much lower than those of the deterministic and stochastic strategies.

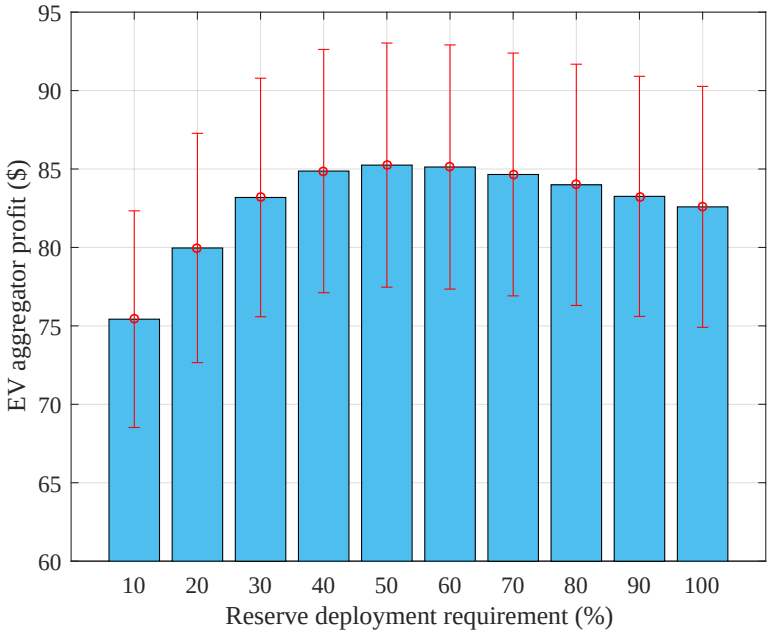

Figure 5.11: Average aggregator profit and 95% confidence interval with different amount of RDR under stochastic strategy

5.4.5 Effectiveness of the Stochastic Strategy

According to the results in the previous sections, the aggregator could obtain the highest profit under the deterministic strategy. However, this is not practical in the real world, because the aggregator cannot accurately estimate the RDR twenty-four hours ahead. It is more practical to apply the stochastic strategy. In this case, this section makes a comparison between the stochastic and deterministic strategies.

Figure 5.13 illustrates the expected aggregator profit in 365 days under different amount of RDR. For 10% requirements ($\lambda^{up} = 10\%$), the aggregator profit of stochastic strategy is $ 75.42 and deterministic strategy is $ 88.52. The aggregator gets the highest profit with 50% requirements with $ 85.24 and $ 98.96 for two strategies, respectively. For the no- reserve-deployment considered strategy, the higher amount reserve is required to deploy, the lower profit aggregator will receive. Since there is no-reserve-deployment in this strategy, the aggregator will receive penalty based on the amount of RDR.

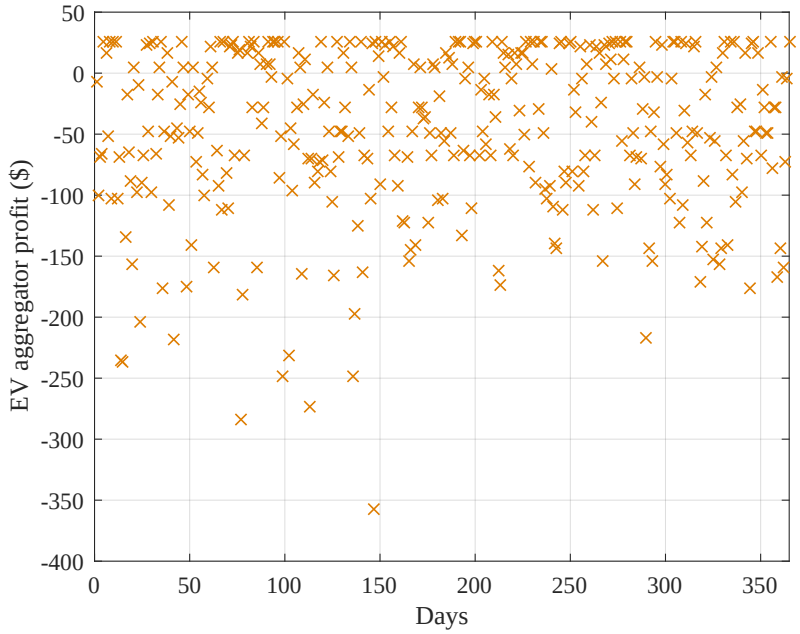

Figure 5.12: Aggregator profit with different amount of RDR under DA bidding strategy without considering reserve deployment

5.4.6 DA Bidding Plans of EVs and ESS

In this section, the DA bidding plan of the EV aggregator with the utilisation ESS is presented, which includes the DA based load plan and the reserve up/down capacities plan. It can be seen from Figure 5.14 that the blue curve represents the proposed charging/discharging power of all EVs in the DAM; at the beginning (13:00–16:00), the EVs have less charging power because most EVs are not connected to the grid. The RTP is relatively lower during these time periods, and thus EVs operate in the charging status. After that, the peak hours are from 18:00 to 21:00, when the total discharging power increases to inject energy back to the grid and the EV aggregator could obtain profit. Then, the maximum charging power appears at 0:00 and the EV aggregator could charge all the EVs at the lowest price. After 2:00, the total charging power decreases gradually; this indicates that some EVs have stored enough energy to meet the next day's driving requirements. The corresponding reserve up/down boundaries at each

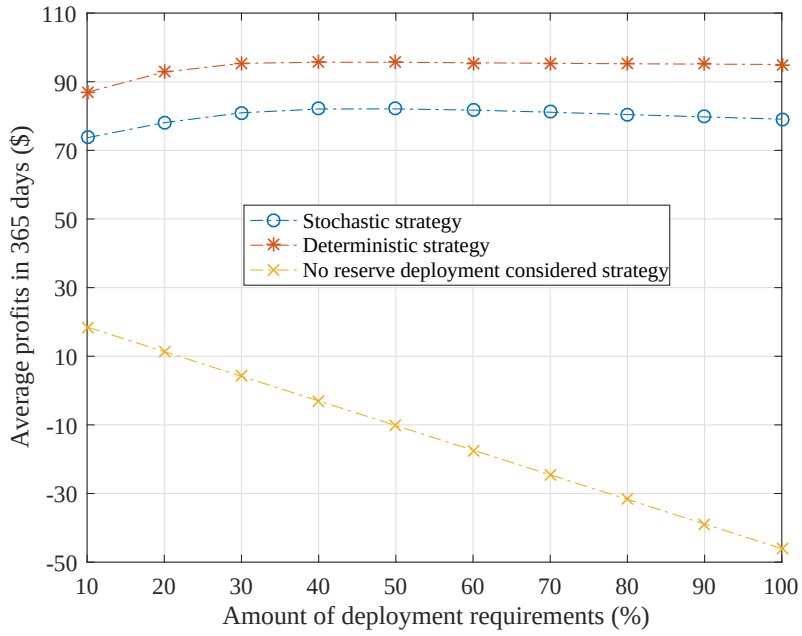

Figure 5.13: Expected aggregator profit of the stochastic, deterministic and no-reserve-deployment considered strategies under different amount of RDR

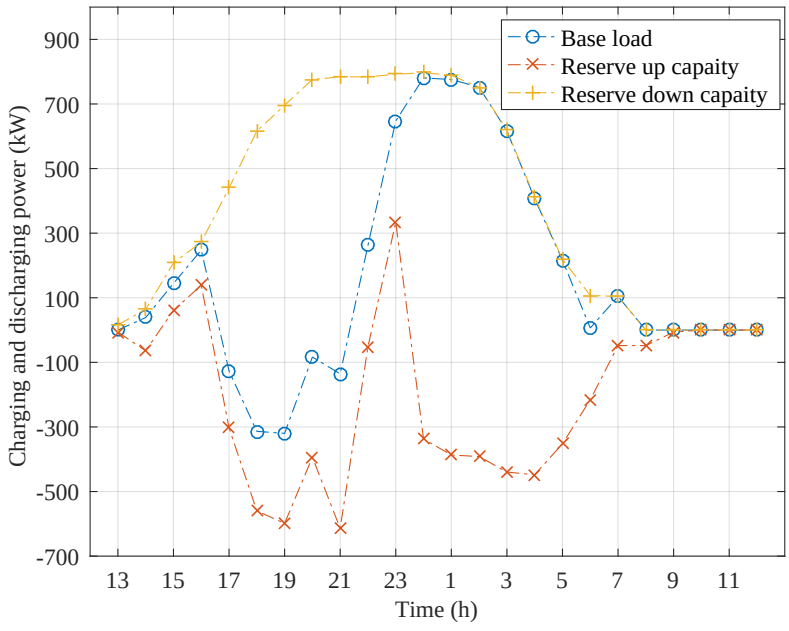

Figure 5.14: DA plan (base load and reserve up/down capacities) of the EVs

hour are also indicated in the figure. The results suggest that the EVs propose more reserve down capacity during 17:00–21:00 (most EVs operate in discharging status) and more reserve up capacity during 22:00–3:00 (most EVs operate in charging status). Because most EVs are not connected to the grid, EVs proposed less reserve up/down capacities before 17:00 or after 7:00.

Compared with the EVs' DA bidding plan, the ESS bidding plan is presented in Figure 5.15. The figure shows the proposed charging/discharging power at each hour

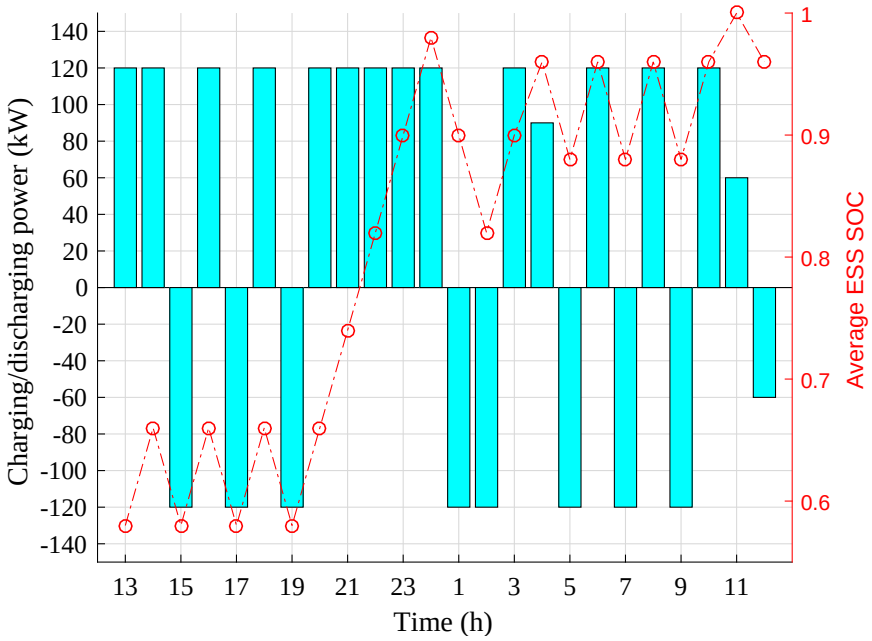

Figure 5.15: DA base-load plan and SOC of the ESS

and the corresponding SOC of the ESS. Unlike the EVs that charged during the off-peak hours and discharged during peak hours, the base-load plan of the ESS do not follow the RTP. The reason for this is that the ESS have more flexibility in providing reserve service to the grid; also, ESS have no target SOC at the end of the time. In addition, considering the dynamic change of the ESS battery SOC, at each time the SOC is bounded between 0.1 and 1; the results indicate that the proposed strategy could effectively manage the charging/discharging of the ESS and prevent it from overcharging

or discharging.

5.4.7 Expected Deployed Reserve and Penalty of EVs and the ESS

In this section, the performance of EVs and the ESS in the RT reserve market are discussed. According to the EV aggregator operation mechanism in the RTM, the average deployed reserve results of EVs at each time are shown in Figure 5.16. The

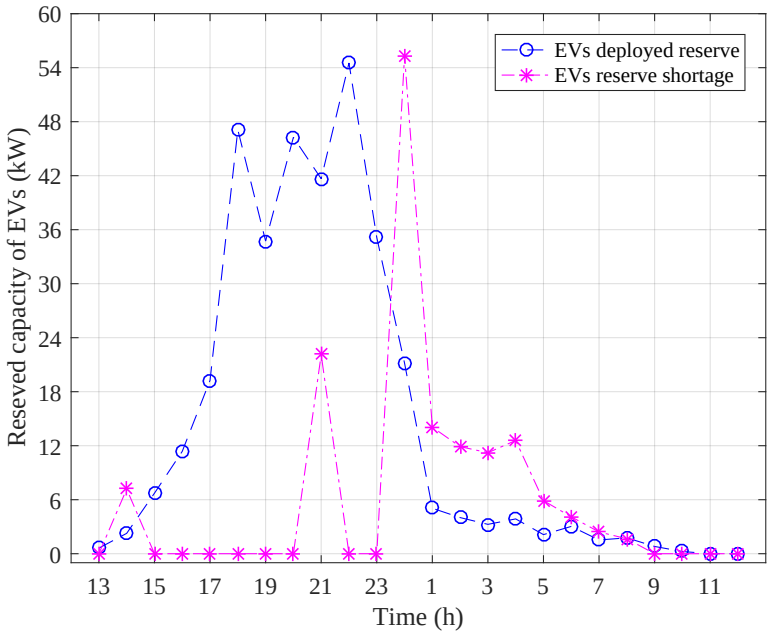

Figure 5.16: Average deployed reserve and reserve shortage of EVs

average deployed reserve is calculated based on one year of RDR data. It can be seen from the figure that, at the beginning (13:00–15:00), the reserve is less deployed; the reason for this is that most EVs are not available, i.e. EVs are not connected to the grid. As the EV information model data given in Table B.4 in Appendix B, the mean value of arrival time is 18:00 with 2 hours variance, thus most EVs are not available during 13:00–15:00. From 17:00–22:00, the deployed reserve of the EVs is greater than at other times, because these time periods are peak hours, i.e. the grid has a higher probability (referring to Table 5.1) to call for the reserve to balance the generation and

consumption. After 1:00, the deployed reserve decreases, because EVs cannot operate in discharging status as the EV aggregator must guarantee that each EV could be charged to the target SOC by departure time. Finally, after 9:00, no reserve is deployed because most EVs have disconnected from the grid (the mean departure time is 7:00 and 2 hours variance) and the proposed reserve is close to zero. The average penalty of EVs for reserve deployment shortage at each time is also represented in the figure. It can be seen that EVs receive higher penalty between 23:00–5:00, which means EVs have a higher risk of not being able to provide enough reserve as proposed. According to the EVs charging/discharging results from Figure 5.14, most EVs operate in charging status during these time periods (off-peak hours), EVs could not deploy all reserve up capacity (operate in discharging status), because they must store enough energy to meet the next day's driving requirements.

The performance of the ESS in RT reserve market is shown in Figure 5.17. Compared

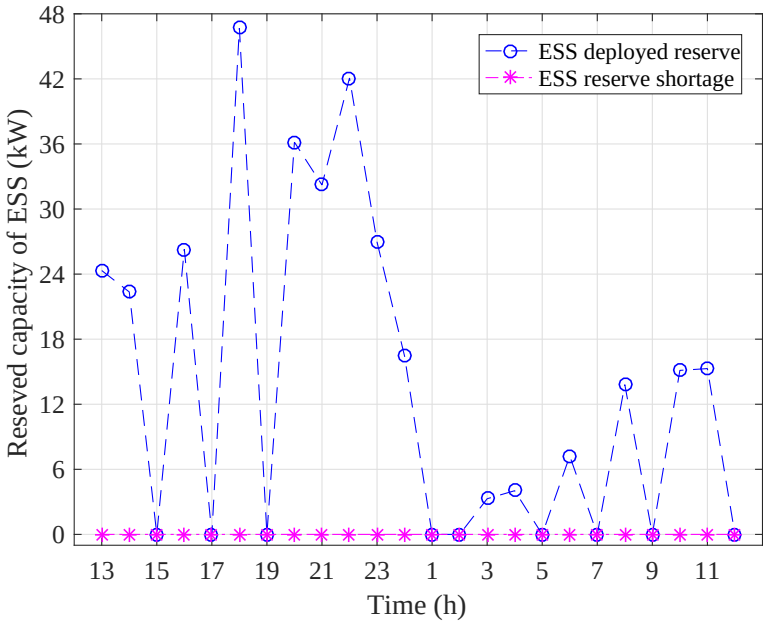

Figure 5.17: Average deployed reserve and reserve shortage of ESS

with the peak deployed reserve of 100 EVs with 54.6 kWh, the peak deployed reserve of the ESS is 47.1 kWh at 18:00, which is in the peak period. In addition, the ESS reserve

is mainly deployed in the periods 13:00–1:00 and 7:00–12:00, which has more flexibility than EVs. This is one of the advantages of the ESS, which is that it is available all the time, but EVs are only available when connected to the grid. Moreover, the ESS is much reliable than EVs in providing reserve service; the results in the figure indicate that the penalty of the ESS is zero, which means that the ESS could deploy enough reserve as proposed in the DAM.

In order to compare the performance of the EVs and ESS in providing reserve service (assume $\lambda^{up} = 100\%$) in the RTM, a summary is shown in Table 5.2. The total proposed

Table 5.2: Proposed, required and deployed reserve of EVs and the ESS in one-year

	EVs	ESS	EVs with ESS
Proposed reserve up capacity (MWh)	3193.55	1138.80	4332.35
Required reserve up capacity (MWh)	181.45	119.04	300.49
Required percentage	5.68%	10.45%	6.93%
Actual deployed up reserve (MWh)	126.48	119.04	245.52
Deployed percentage	69.71%	100%	81.71%

reserve up capacity of the EVs in one year is 3193.55 MWh, which is 2.8 times the ESS reserve up capacity (1138.80 MWh), because the total capacity of all EVs is much greater than that of the single ESS. In this table, the required percentage is defined as the required reserve according to the RDR over the proposed reserve capacity. It can be seen that the required percentage of the EVs and the ESS are 5.68% and 10.45%, respectively. This suggests that the proposed reserve of the ESS has a higher probability to be required by the grid. According to the DA bidding plan shown in Figure 5.14 and the hourly RDR probability in Table 5.1, the most reserve capacity of EVs is proposed between 0:00–5:00; however, the grid has lower probability to call for the reserve up capacity during these time periods, and thus the EVs have less required percentage compared with the ESS.

The deployed percentage is defined as the actual deployed reserve of the EV aggregator over the required reserve of the grid. In order to meet EV owners' driving requirements, the EVs' should be charged to the target SOC by the departure time. In this case, the EVs could not respond to the RDR all the time, and the deployed

percentage of EVs is 67.91%. The deployed percentage of the ESS is 100%, which means that the ESS could deploy enough reserve according to the grid requirements without shortage. Based on these results, it can be concluded that the ESS is much more flexible than the EVs in providing reserve services to the grid. With the utilisation of the ESS, the required percentage increases from 5.68% to 6.93% and the deployed percentage increases from 69.71% to 81.71%.

5.4.8 Profit Compositions under Stochastic Strategy

In this section, the expected daily profit of the EV aggregator is analysed. The expected daily profit of EV aggregator is calculated based on the generated RDR one-year data. Essentially, the EV aggregator profit comes from two sides: EVs and the ESS. To be specific, EVs and the ESS can either obtain income or incur cost from the DAM and the RTM, such as reserve capacity income, charging/discharging income, and deployed reserve income. Furthermore, to take the social aspects into account, not only does the EV aggregator guarantee owners' driving requirements, but the economic benefits of each owner are also considered.

Table 5.3 shows the income, cost, and penalty of EVs and the ESS from the DAM, RTM, and aggregator–owner contract. The DA reserve capacity income of EVs is $

Table 5.3: EVs and the ESS income, cost and penalty

	Daily expected cost/income	EVs only	EVs with ESS	
		EVs	EVs	ESS
DAM	DA reserve up/down capacity income	$ 53.38	$ 53.38	$ 16.52
	DA charging/discharging cost/income	$ 144.38	$ 144.38	$ 203.68
	Battery degradation cost	N/A	N/A	$ -144.00
	Total	$ 197.76	$ 197.76	$ 76.20
RTM	Deployed reserve income	$ 93.48	$ 93.48	$ 87.31
	Reserve shortage penalty cost	$ − 2.97	$ − 2.97	$ 0
	Total	$ 90.51	$ 90.51	$ 87.31
Contract	Charging income/cost from owners	$ − 350.57	$ − 350.57	N/A
	Degradation compensation	$ 143.42	$ 143.42	N/A
	Total	$ − 207.15	$ − 207.15	N/A
Daily profit of the EV aggregator		$ 81.12	$ 81.12	$ 163.51
			$ 244.63	

53.38, which is significantly greater than that of the ESS ($ 16.52). However, compared with the deployed reserve, the EVs and the ESS incomes are much closer, at $ 93.48 and $ 87.31 for EVs and the ESS, respectively. The reason is that the total capacity of all EVs is 6.4 MWh (100 EVs with 64 kWh for each vehicle), which is much greater than the ESS capacity (1500 kWh). Although EVs propose more reserve capacity than the ESS, the deployed reserve income is slightly greater than the ESS. This is because the operation of the ESS is much more flexible than that of the EVs, i.e. the ESS is available for twenty-four hours, and could therefore respond to the grid's requirements at any time. Regarding the penalty of reserve shortage in the RTM, the penalties for the EVs and the ESS are only $ 2.97 and $ 0, respectively, which are significantly less than the income of the EV aggregator in participating in the DAM and RTM. Thus, these results prove that the strategy proposed in this chapter could reduce the risk of the EV aggregator not being able to deploy enough reserve as proposed in the DAM. The proposed stochastic programming method effectively accounts for the uncertainty of the reserve market in the DA bidding, and the expected profit of the EV aggregator is maximised.

Another point that must be mentioned is that the battery degradation of the ESS is $ 144.00 for both charging and discharging. However, the EV aggregator will not be responsible for the battery degradation for all EVs, because EVs do not belong to the EV aggregator. From the social aspect, the EV aggregator gets the full right in scheduling charging/discharging operation of EVs under the condition that it must reimburse the additional battery degradation cost to each owner compared with the degradation cost obtained from the EV owners' scheduling results. In addition, the EV aggregator could receive the income from each EV owner for parking and charging EVs to the target SOC at departure time. Finally, the average daily profit of the EV aggregator is $ 244.63, including $ 81.12 from the EVs and $ 163.51 from the ESS.

Moreover, Table 5.3 shows the profit of the EV aggregator with and without ESS utilisation. It can be seen from the table that the EV scheduling results are not affected by the ESS, which means that the ESS do not cooperate with the EVs in providing

reserve service to the grid, i.e. the ESS cannot reduce the EVs' reserve shortage penalty, even though the ESS have more flexibility in responding to the RDR. The reason for this is that the ESS bidding strategy changes if the ESS are used to reduce the EVs' reserve shortage, and the EVs' reserve shortage penalty is less than the ESS profit reduction.

5.5 Summary

In this chapter, considering aggregator's interest, a DA aggregator bidding strategy in an uncertain reserve market is proposed. The uncertainty of the reserve market is addressed in terms of the amount and time of RDR based on a stochastic programming method. The risk of the aggregator not being able to deploy enough reserve is considered by introducing a penalty factor in the model. Moreover, an owner–aggregator contract is designed to mitigate the economic inconsistency issue between EV owners and the aggregator.

The main outcomes of this chapter are summarised as follow:

- The scheduling results verify that the proposed stochastic programming strategy effectively managed the uncertainty of the RDR, such that the expected aggregator profit is 13–16% less than the optimal profit under the deterministic strategy based on data from one year.

- The proposed strategy could effectively reduce the risk of the reserve shortage, the reserve shortage penalty of the EV aggregator is $ 2.97 ($ 2.79 for EVs and $ 0 for the ESS).

- A comparison is made between EVs and the ESS in providing reserve services to the grid. Results show that the ESS have more flexibility in making response to the grid's requirements, that is in average 10.45% is required to be deployed and it could deploy enough reserve as proposed.

- With the utilisation of the ESS, the ability of the EV aggregator in providing reserve services in improved, where the required percentage increases from 5.68%

to 6.93% and the deployed percentage increases from 69.71% to 81.71%. However the EVs' reserve shortage cannot be reduced by the ESS, because the bidding plan of the ESS will be affected and the total profit will be reduced.

Chapter 6

EV Energy Management in a Transmission Power Network

6.1 Introduction

In this chapter, the impact of EV integration in transmission systems is evaluated and the grid interest, that is the TSO interest, in EV energy management problem is considered. As EVs are connected directly to the distribution network, several studies have been carried out to examine the impact of EV charging behaviours on the distribution network [113–115]. A multi-stage optimal EV scheduling approach is applied in [89] to examine the impact of EV charging behaviours on the grid. The performance of the proposed strategy is evaluated based on three aspects: controllability, manageability, and economics of the distribution network. The results show that the fluctuations caused by the intermittent sources are smoothed and the network topology can be reconfigured for better performance. Considering the uncertainty of the distribution network, a distributed MPC method is proposed in [95] to minimise the total system energy cost based on short-term predicted information. In [91], the authors investigated the coordination between EVs with DGs and stochastic power flow is proposed to solve the uncertainties of EVs and RESs. In [116], the authors developed a hierarchical

coordination model to manage the active and reactive power in the distribution network. The authors in [82] and [117] built spatio-temporal models to analyse the effects of the charging behaviours of PHEVs on the transmission network. A bi-layer strategy is proposed in [82], where the upper level stands for the unit commitment in the transmission network and the lower level represents the OPF in a distribution network. However, the power flow in the transmission network is not taken into account.

A number of studies have addressed the impact of EV charging behaviours on the transmission network. In [118], the role of ESS in ensuring the adequacy and security of the transmission systems is studied. The authors in [88] optimise the charging load of PHEVs to reduce the transmission congestion and load curtailment. The authors in [119] presented a network-based model to evaluate the PHEVs charging behaviours on the GHG emissions for the California electricity transmission grid. A security-constrained DC-OPF problem is studied in [120], where BESS are utilised to maintain the supply–demand balance. In [121], the authors proposed a network-constrained unit commitment problem in a transmission network and jointly considered the transportation information of EVs in the model. Benders cut method is used to enable the model to handle large-scale EV optimisation.

Recent studies aimed at investigating EV integration in transmission/distribution networks have focused on single objectives [91, 117, 120, 121] and the TSO could dispatch both generators and all EVs. Actually, a single EV cannot directly participate in OPF or unit commitment owing to the limited capacity and charging power. Thus, the aggregator acts as a third party between the TSO and EVs, which could participate in DC-OPF and respond based on TSO requirements. Therefore, the cooperative strategy between the TSO and the aggregator must be investigated. To clearly define the responsibilities of the TSO and the aggregator, a bi-level strategy is proposed in this study. Figure 6.1 illustrates the concept of the proposed bi-level strategy. In the upper level, the TSO is responsible for the generator output power at each bus and the power flow at each branch of the transmission network based on DC-OPF. In the lower level, the aggregator manages the actual charging/discharging operation of each EV to

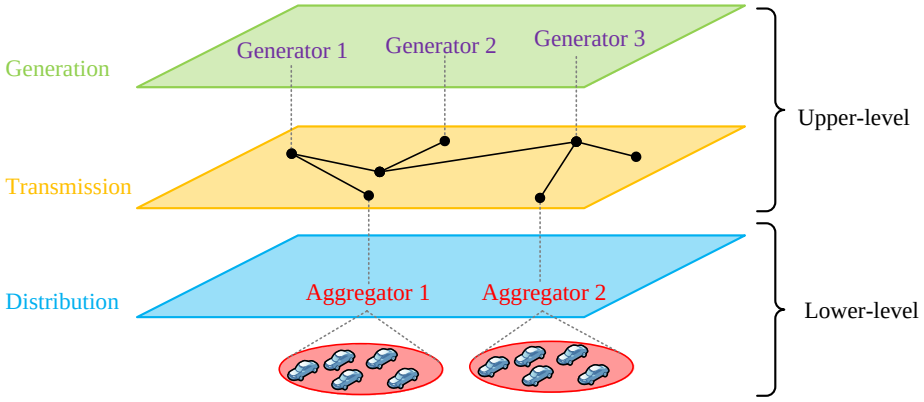

Figure 6.1: Bi-level structure of the EV integration in the transmission network

satisfy EV owners' driving requirements.

In this chapter, a bi-level EV energy management strategy in the transmission network is studied. Two main contributions of this study are summarised as follows:

- First, the proposed bi-level strategy clearly defines the responsibility of the TSO and EV aggregator in the power grid operation. This is the first work to jointly consider the cooperation mechanism between the aggregator and TSO in DC-OPF and the EV charging/discharging operation management problem.
- Second, an EV information grouping method is proposed in this study. The proposed method could effectively reduce the optimisation complexity, which could achieve large-scale EV integration into the power network.

6.2 Bi-Level Strategy

In the upper level, the TSO coordinates the output power of each generator on the generation side and the grouped EVs on the load side to minimise the total cost of the system, while taking power flow constraints into account. The optimisation results determine the charging/discharging power of the EV groups at each bus i, where $i \in \boldsymbol{L}$, which are utilised as a reference for the real EV scheduling in the lower level.

In the lower level, the aggregator determines the actual charging/discharging power

of each EV, while satisfying the TSO requirements.

6.2.1 EV Information Grouping Method

In the bi-level scheduling strategy, on one hand, the aggregator is responsible for the charging/discharging operation of each EV directly; on the other hand, it needs to follow the TSO requirements. Therefore, the aggregator must collect the EV information and submit the grouped EV information to the TSO. Because the TSO is responsible for the power flow to determine the output power of the generators (in MW) and it is not realistic to manage the operation of each vehicle (in kW). Thus, the aggregator should process the EV information before submitting it to the TSO. The grouped EV information will be considered by the TSO in determining the power flow in the upper level. Figure 6.2 shows the EV information grouping method, i.e. all EVs are aggregated and categorised into several groups.

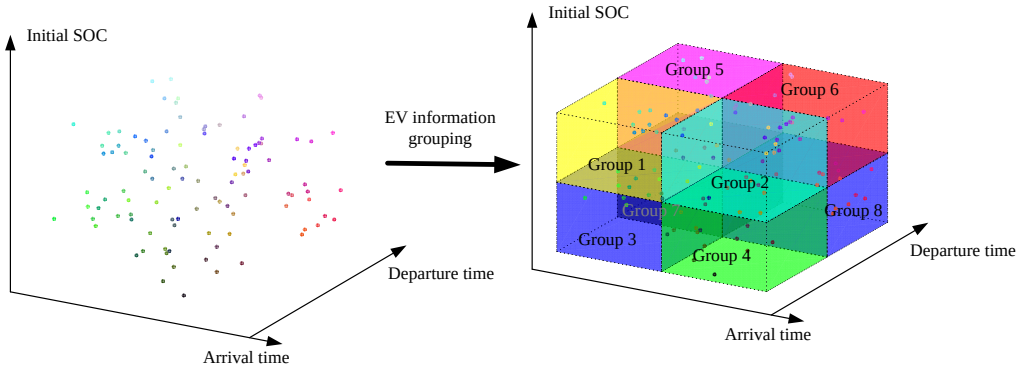

Figure 6.2: Concept illustration of the EV information aggregation and grouping method

The EV information is categorised into several groups based on EVs' three characteristics: the arrival time ($t^a_{n,t,i}$), departure time ($t^d_{n,t,i}$), and initial SOC at arrival time ($SOC^a_{n,i}$). The aggregator should define the feasible region of the group, e.g. arrival time between 18:00–19:00, departure time between 7:00–8:00 am and initial SOC 0.3, and determine the number of EVs in each group. The average charging/discharging power and the average battery capacity of the EV group v at bus i are defined in (6.1)

and (6.2):

$$P_{i,v} = \frac{\sum_{n \in \boldsymbol{K_{i,v}}} \overline{P}^{\text{ev}}_{i,n}}{k_{i,v}} \quad \forall i, v \tag{6.1}$$

$$E_{i,v} = \frac{\sum_{n \in \boldsymbol{K_{i,v}}} E_{i,n}}{k_{i,v}} \quad \forall i, v \tag{6.2}$$

Algorithm 2 shows the method to calculate the number of EVs in each group.

Algorithm 2: EV information grouping method

Input: EV information $\{t^a_{i,n}, t^d_{i,n}, SOC^a_{i,n}\}, k_{i,v} = 0, \forall i, n, v$;
Output: EV groups information;
for $i \in \boldsymbol{I}$ **do**
  for $n = 1; n \leq N; n++$ **do**
    for $v = 1; v \leq V_i; v++$ **do**
      if $|t^a_{i,n} - t^a_{i,v}| \leq 0.5\Delta T, |t^d_{i,n} - t^d_{i,v}| \leq 0.5\Delta T, |SOC^a_{i,n} - SOC^a_{i,v}| \leq 0.2$ **then**
        $k_{i,v} \leftarrow k_{i,v} + 1$;
      else
        $k_{i,v} \leftarrow k_{i,v}$;
      end
    end
  end
end
Obtain the EV groups information: $k_{i,v}$ and $\{t^a_{i,v}, t^d_{i,v}, SOC^a_{i,v}\}$;
Calculate the EV groups information based on Equations (6.1) and (6.2);
EV groups information: $\{t^a_{i,v}, t^d_{i,v}, SOC^a_{i,v}, k_{i,v}, P_{i,v}, E_{i,v}\}, \forall i, v$;

6.2.2 Upper Level: DC-OPF with Grouped EV information

From the TSO viewpoint, the DC-OPF aims to meet all load requirements and minimise the total cost at the same time. The total cost of the system includes the generator output cost and the EV cost. Specifically, the EV cost consists of two parts, the charging/discharging cost or income and the corresponding battery degradation cost.

The objective function can be written as (6.3a):

$$\text{Minimise} \quad \sum_{i\in\boldsymbol{G}} C_i^{\mathrm{G}} + \sum_{i\in\boldsymbol{L}} \left(C_{1,i}^{\mathrm{ev}} + C_{2,i}^{\mathrm{ev}}\right) \tag{6.3a}$$

$$C_i^{\mathrm{G}} = \sum_{t=1}^{M} \left(a_i \cdot {p_{i,t}^{\mathrm{G}}}^2 + b_i \cdot p_{i,t}^{\mathrm{G}} + c_i\right) \Delta T \quad \forall i \in \boldsymbol{G} \tag{6.3b}$$

where C_i^{G} in (6.3b) stands for the generation cost of the generator at the bus i during the whole scheduling time.

In Equations (6.3c) and (6.3d), $C_{1,i}^{\mathrm{ev}}$ and $C_{2,i}^{\mathrm{ev}}$ represents the EV charging and discharging cost or income and the battery degradation cost of the EV fleets at bus i during the scheduling time, respectively.

$$C_{1,i}^{\mathrm{ev}} = \sum_{t=1}^{M}\sum_{v=1}^{V_i} k_{i,v} P_{i,v} \left(r_t^{+} x_{i,v,t}^{+} - r_t^{-} x_{i,v,t}^{-}\right) \Delta T \quad \forall i \in \boldsymbol{L}, \tag{6.3c}$$

$$C_{2,i}^{\mathrm{ev}} = \sum_{t=1}^{M}\sum_{v=1}^{V_i} D^{\mathrm{ev}} k_{i,v} P_{i,v} \left(x_{i,v,t}^{+} + x_{i,v,t}^{-}\right) \Delta T \quad \forall i \in \boldsymbol{L}. \tag{6.3d}$$

Equation (6.4) represents the power balance of the system, for each bus i:

$$p_{i,t}^{\mathrm{G}} - \sum_{i,j,i\neq j}^{\boldsymbol{N_i},\boldsymbol{N_j}} \frac{\theta_{i,t} - \theta_{j,t}}{X_{i,j}} = P_{i,t}^{\mathrm{L}} + p_{i,t}^{\mathrm{EV}} \quad \forall t, i = 1:B, \tag{6.4}$$

where $p_{i,t}^{\mathrm{EV}}$ stands for the total charging/discharging power of all EVs in bus i. The generator output variable, the EV charging/discharging load are forced to zero when there is no generator or load in bus i, i.e, $p_{i,t}^{\mathrm{G}} = 0, \forall i \notin \boldsymbol{G}$ and $p_{i,t}^{\mathrm{EV}} = 0, \forall i \notin \boldsymbol{L}$.

$$-F_{ij} \leq \sum_{i,j}^{\boldsymbol{N_i},\boldsymbol{N_j}} \frac{\theta_{i,t} - \theta_{j,t}}{X_{ij}} \leq F_{ij} \quad \forall t. \tag{6.5}$$

Constraint (6.6) represents the generation output limits of the generator i at time t:

$$-\underline{P}_i^{\mathrm{G}} \leq p_{i,t}^{\mathrm{G}} \leq \overline{P}_i^{\mathrm{G}} \quad \forall t, i \in \boldsymbol{G} \tag{6.6}$$

The ramp rate limit constraint of the generator is shown in constraint (6.7):

$$-\overline{R}_i \leq p_{i,t}^{\mathrm{G}} - p_{i,t-1}^{\mathrm{G}} \leq \overline{R}_i \quad \forall t, i \in \boldsymbol{G} \tag{6.7}$$

Constraint (6.8) stands for range of the voltage angle of bus i at time t:

$$-\pi \leq \theta_{i,t} \leq \pi \quad \forall t, i = 1 : B \tag{6.8}$$

In Equations (6.9) and (6.10), binary variables used in the DC-OFP model represent the charging and discharging of the EV group:

$$x_{i,v,t}^{+} = \begin{cases} 0 & 1 \leq t < t_{i,v}^{a} \\ \{0,1\} & t_{i,v}^{a} \leq t < t_{i,v}^{d} \\ 0 & t_{i,v}^{d} \leq t \leq M \end{cases} \quad \forall v, t, i \in \boldsymbol{L} \tag{6.9}$$

$$x_{i,v,t}^{-} = \begin{cases} 0 & 1 \leq t < t_{i,v}^{a} \\ \{0,1\} & t_{i,v}^{a} \leq t < t_{i,v}^{d} \\ 0 & t_{i,v}^{d} \leq t \leq M \end{cases} \quad \forall v, t, i \in \boldsymbol{L}. \tag{6.10}$$

When EVs are off the grid, i.e., $t < t_{i,v}^{a}$ or $t > t_{i,v}^{d}$, binary variables $x_{i,v,t}^{+}$ and $x_{i,v,t}^{-}$ are forced to zero, which means the EVs cannot be scheduled during these time intervals.

Constraint (6.11) is used to ensure that EV cannot be charged and discharged simultaneously:

$$x_{i,v,t}^{+} + x_{i,v,t}^{-} \leq 1 \quad \forall i \in \boldsymbol{L}, v, t. \tag{6.11}$$

By taking the EV batteries into consideration, constraints (6.12) and (6.13) are used to guarantee that at each time m, the battery should not greater than the upper SOC limit or less than the lower SOC limit.

$$SOC_{i,v}^{a} + \frac{\sum_{t=1}^{m} P_{i,v} \left(x_{i,v,t}^{+} - x_{i,v,t}^{-} \right) \Delta T}{E_{i,v}} \leq \overline{\mathrm{SOC}}, \quad \forall i \in \boldsymbol{L}, v, m, \tag{6.12}$$

$$SOC_{i,v}^{a} + \frac{\sum_{t=1}^{m} P_{i,v} \left(x_{v,t,i}^{+} - x_{v,t,i}^{-} \right) \Delta T}{E_{i,v}} \geq \underline{\mathrm{SOC}}, \quad \forall i \in \boldsymbol{L}, v, m. \tag{6.13}$$

Considering the EV owners' driving requirements, constraint (6.14) means that at the departure time of EV $t_{i,v}^{d}$, the battery SOC should not be less than the target value $\mathrm{SOC}^{\mathrm{d}}$. The target value is manually set by the owner according to their own willingness at the arrival time.

$$SOC_{i,v}^{a} + \frac{\sum_{t=1}^{t_{i,v}^{d}} P_{i,v} \left(x_{i,v,t}^{+} - x_{i,v,t}^{-} \right) \Delta T}{E_{i,v}} \geq \mathrm{SOC}^{\mathrm{d}}, \quad \forall i \in \boldsymbol{L}, v. \tag{6.14}$$

The upper level scheduling results yield the output of the generators $\boldsymbol{G}$ and the charging/discharging operations of EV groups v at each time t. The upper level results are involved as a reference in the lower level aggregator scheduling strategy. The optimal solution of EV groups are written as $x_{i,v,t}^{+*}$ and $x_{i,v,t}^{-*}$. Thus, the scheduled EV fleets operation results of bus i at time t is obtained:

$$P_{i,t}^{\mathrm{EV}*} = \sum_{v=1}^{V_i} k_{i,v} P_{i,v} \left(x_{i,v,t}^{+*} - x_{i,v,t}^{-*} \right) \quad \forall t, i \in \boldsymbol{L}. \tag{6.15}$$

6.2.3 Lower Level: Aggregator Scheduling Strategy

In the lower level, the aggregator is responsible for the actual charging and discharging operations of each EV. The objective function of the aggregator i is to minimise the total cost of all EVs including charging/discharging cost and income and the corresponding

battery degradation cost. The objective function of the aggregator i is formulated in (6.16a)–(6.16c):

$$\text{Minimise} \quad J_{1,i}^{\text{ev}} + J_{2,i}^{\text{ev}} \quad \forall i \in \boldsymbol{L} \tag{6.16a}$$

$$J_{1,i}^{\text{ev}} = \sum_{t=1}^{M} \sum_{n=1}^{N} \left(r_t^+ p_{i,n,t}^+ - r_t^- p_{i,n,t}^- \right) \Delta T, \quad \forall i \in \boldsymbol{L} \tag{6.16b}$$

$$J_{2,i}^{\text{ev}} = \sum_{t=1}^{M} \sum_{n=1}^{N} D^{\text{ev}} \left(p_{i,n,t}^+ + p_{i,n,t}^- \right) \Delta T. \quad \forall i \in \boldsymbol{L} \tag{6.16c}$$

Equations (6.17) and (6.18) are used to guarantee that the charging and discharging of the EV is bounded between zero to the maximum power during available time:

$$z_{i,n,t}^+ = \begin{cases} 0 & 1 \leq t < t_{i,n}^a \\ \{0,1\} & t_{i,n}^a \leq t < t_{i,n}^d \\ 0 & t_{i,n}^d \leq t \leq M \end{cases} \quad \forall i \in \boldsymbol{L}, n, t, \tag{6.17}$$

$$z_{i,n,t}^- = \begin{cases} 0 & 1 \leq t < t_{i,n}^a \\ \{0,1\} & t_{i,n}^a \leq t < t_{i,n}^d \\ 0 & t_{i,n}^d \leq t \leq M \end{cases} \quad \forall i \in \boldsymbol{L}, n, t, \tag{6.18}$$

where $z_{i,n,t}^+$ and $z_{i,n,t}^-$ are both binary variables.

Constraint (6.19) indicates the EV cannot be charged and discharged simultaneously:

$$z_{i,n,t}^+ + z_{i,n,t}^- \leq 1 \quad \forall i \in \boldsymbol{L}, n, t. \tag{6.19}$$

The linearised dynamic maximum charging power limits are considered in the lower level scheduling in constraints (6.20)-(6.23):

$$0 \leq p_{i,n,t}^+ \leq \frac{F_{s+1} - F_s}{R_{s+1} - R_s} SOC_{i,n,t-1} + \frac{R_{s+1} F_s}{R_{s+1} - R_s}, \qquad \forall s, i \in \boldsymbol{L}, t, t \neq t_{i,n}^a, \tag{6.20}$$

$$0 \leq p^{+}_{i,n,t} \leq \frac{F_{s+1}-F_s}{R_{s+1}-R_s} SOC^{a}_{i,n} + \frac{R_{s+1}F_s}{R_{s+1}-R_s}, \qquad \forall s, n, t = t^{a}_{i,n}, \tag{6.21}$$

$$0 \leq p^{+}_{i,n,t} \leq \mathrm{M_{big}} z^{+}_{i,n,t} \qquad \forall n, t, i \in \boldsymbol{L}, \tag{6.22}$$

$$0 \leq p^{-}_{i,n,t} \leq \overline{P}^{\mathrm{ev}}_{i,n} z^{-}_{i,n,t}, \qquad \forall n, t, i \in \boldsymbol{L}. \tag{6.23}$$

where $SOC_{i,n,t-1}$ represents the SOC of EV n in bus i at time $t-1$. The linearisation of the maximum charging versus SOC is discussed in 3.3.3

Constraints (6.24)–(6.26) represent the battery SOC upper and lower limits, and the EV owners' driving requirements, respectively, which have the same format with (6.12)–(6.14) in the upper level TSO scheduling.

$$SOC^{a}_{i,n} + \frac{\sum_{t=1}^{m}(p^{+}_{i,n,t} - p^{-}_{i,n,t})\Delta T}{E_{i,n}} \leq \overline{\mathrm{SOC}} \quad \forall i \in \boldsymbol{L}, n, m \tag{6.24}$$

$$SOC^{a}_{i,n} + \frac{\sum_{t=1}^{m}(p^{+}_{i,n,t} - p^{-}_{i,n,t})\Delta T}{E_{i,n}} \geq \underline{\mathrm{SOC}} \quad \forall i \in \boldsymbol{L}, n, m \tag{6.25}$$

$$SOC^{a}_{i,n} + \frac{\sum_{t=1}^{M}(p^{+}_{i,n,t} - p^{-}_{i,n,t})\Delta T}{E_{i,n}} \geq \mathrm{SOC^{d}} \quad \forall i \in \boldsymbol{L}, n. \tag{6.26}$$

To guarantee that the aggregator scheduling results meet the TSO requirements, constraint (6.27) means that at each time t, the total charging/discharging power of the aggregator i is not greater or less than the upper-level results $P^{\mathrm{EV}*}_{i,t}$ with a deviation range:

$$-\sigma \sum_{n=1}^{N} \overline{P}^{\mathrm{ev}}_{i,n} + P^{\mathrm{EV}*}_{i,t} \leq \sum_{n=1}^{N}(p^{+}_{i,n,t} - p^{-}_{i,n,t}) \leq \sigma \sum_{n=1}^{N} \overline{P}^{\mathrm{ev}}_{i,n} + P^{\mathrm{EV}*}_{i,t} \quad \forall i, t. \tag{6.27}$$

where $\sigma \sum_{n=1}^{N} \overline{P}^{\mathrm{ev}}_{i,n}$ represents the deviation range of the aggregator i, which is the production of the deviation parameter σ with the total rated power of all EVs of the aggregator i.

6.3 Numerical Examples

A IEEE 14-bus system is used in this case study to test the proposed strategy, and the detailed 14-bus systems data can be obtained in [122], the relevant data including generator characteristics, branch characteristics and locations of generators and load is summarised in Table B.5–B.7 in Appendix B. Figure 6.3 shows the topology of the modified 14-bus systems, where EVs are integrated into the transmission network at different busses. It can be seen from the figure that EVs are distributed in load busses

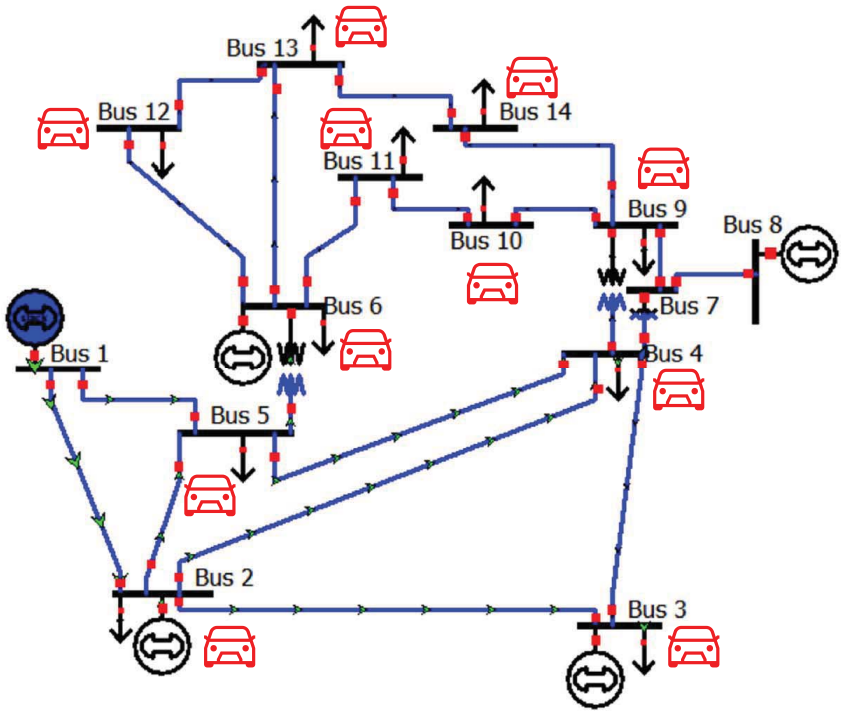

Figure 6.3: IEEE 14-bus systems with EV integration

$\boldsymbol{L}$, where $\boldsymbol{L} = \{2, 3, 4, 5, 6, 9, 10, 11, 12, 13, 14\}$. Five generators are distributed in the generator busses $\boldsymbol{G}$, where $\boldsymbol{G} = \{1, 2, 3, 6, 8\}$.

6.3.1 Accuracy of the EV Information Grouping Method

To verify the accuracy of the proposed bi-level strategy, a comparison study of EVs charging/discharging results is conducted between with and without EV information grouping method. Considering the complexity of the optimisation problem by involving EVs in the DC-OPF model, it is assumed that it has the same EV number at each bus, i.e., $N = 100$. The number of groups at each bus V_i equals to the number of EVs without the EV information grouping method and EV information is the same with the EV grouping information, i.e, $V_i = N, t^a_{i,v,t} = t^a_{i,n,t}, t^d_{i,v,t} = t^d_{i,n,t}, SOC^a_{i,v} = SOC^a_{i,n}, \forall i, v, n$. Figure 6.4 shows that the total EV charging/discharging power at bus 2 with and without the EV information grouping method.

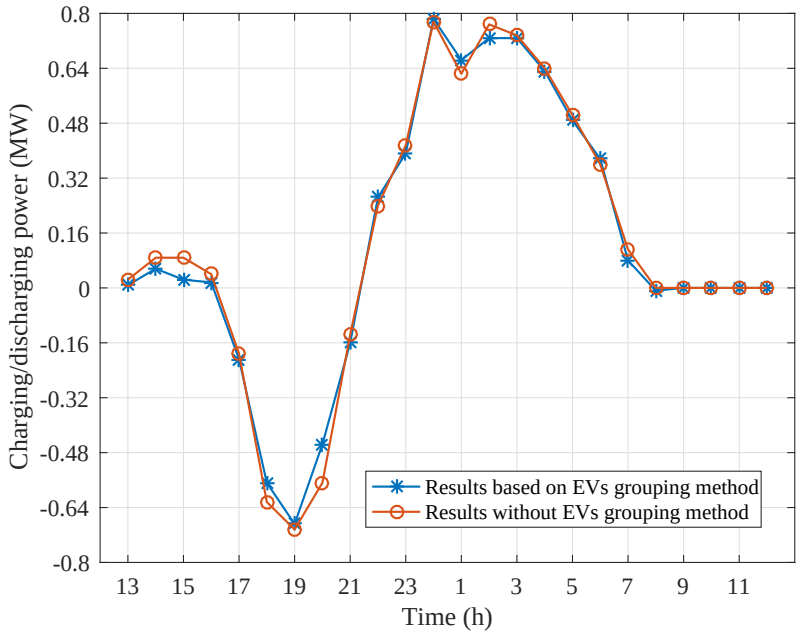

Figure 6.4: Comparison of EV charging/discharging power with and without EV information grouping method

The results in Figure 6.4 show that the two curves are very close. This indicates that for the EVs with the same information (same arrival/departure time and initial SOC), the charging/discharging powers are almost the same. The results demonstrate the

rationality of the proposed EV information grouping method. That is, the aggregator could categorise EV into several groups based on their information and the TSO could determine the DC-OPF based on the grouped EV information.

6.3.2 Upper Level: TSO Scheduling Results

The TSO obtains the grouped EV information from the aggregator and determines the output power of all generators and the charging/discharging power of all EV groups in the transmission network. It is assumed that there are 1000 EVs at each bus, $N = 1000$. Figures 6.5 and 6.6 show the output power of all generators and the charging/discharging power of all EV groups at each load bus, respectively.

It can be seen from Figure 6.5 that the red curve represents the total generation without EVs, where the peak hours appear in 17:00–20:00 and the total output power is around 700 MW. The off-peak hours appear in 22:00–6:00 and the total output power is around 600 MW. With EV participation, the load during peak hours is reduced (significant reduction from 18:00 to 20:00), and most EVs operate in charging status during off-peak hours.

Compared with the results in Figure 6.6, the EV groups perform as ESS, that is EV groups operate in charging status during peak hours (17:00–20:00) and discharging status during off-peak hours (22:00–6:00). These results suggest that the TSO achieves the coordination between generators on the generation side and EVs on the load side, where the peak output is shaved under such coordination.

The power flow at each branch and the voltage angle at each bus of the transmission network are given in Figure 6.7 and 6.8 (detailed numeral results are given in Table C.2–C.5 in Appendix C). It can be seen from Figure 6.7 that branch 1 (from bus 1 to bus 2) has the maximum power flow with 204.47 MW on average for one day. This is because generator 1 has the maximum average output power, the generated power is mainly transmitted from bus 1 to bus 2, and less power is transmitted from bus 1 to bus 5 (where the average power flow is 89.08 MW). See Table B.6 in Appendix B; the impedance of branch 1 $X_{1,2} = 0.059$ is less than that of branch 2 $X_{1,5} = 0.223$; and the

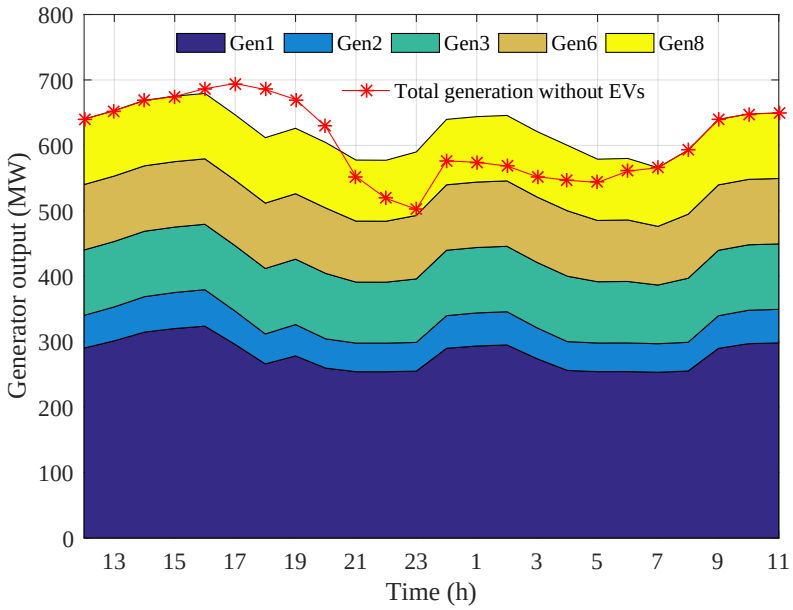

Figure 6.5: Output power of each generator in one day

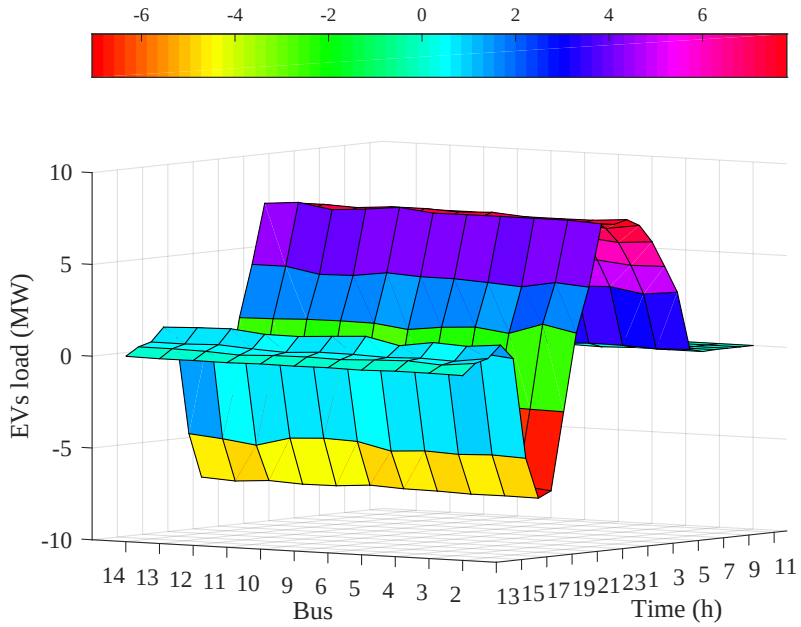

Figure 6.6: Total charging/discharging power of EVs in each bus in one day

average absolute value of the voltage angle at bus 2 and bus 5 are 0.12 rad (6.68°) and 0.19 rad (10.83°). In this case, according the Equation (3.42), the generated power from bus 1 is mainly transmitted through branch 1.

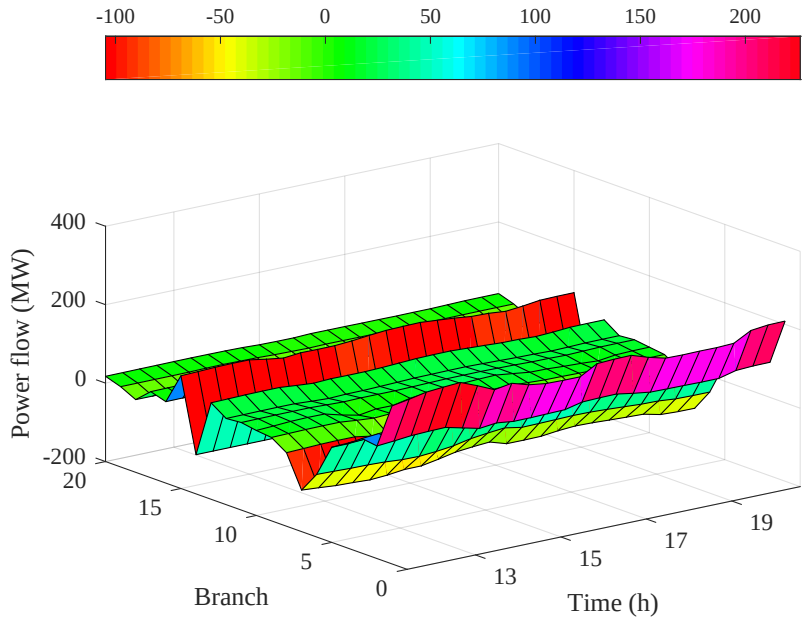

Figure 6.7: Power flow in each branch of the transmission network in one day

Figure 6.8 shows the voltage angle in each bus at each time. The maximum absolute value of the voltage angle is 0.39 rad (22.34°), which is small enough that follows the approximation made in Equation (3.42).

6.3.3 Lower Level: Aggregator Scheduling Results

The EV aggregator determines the actual charging/discharging operation of each EV in the lower level. Figure 6.9 shows the total charging/discharging power of 1000 EVs in bus 2 and the average SOC over one day. It implies that EVs are discharged during peak hours and charged during off-peak hours. The corresponding SOC reaches 0.95 at 8:00, which guarantees the EV owners' driving requirements.

Figure 6.10 shows the total load of the transmission systems with and without EV

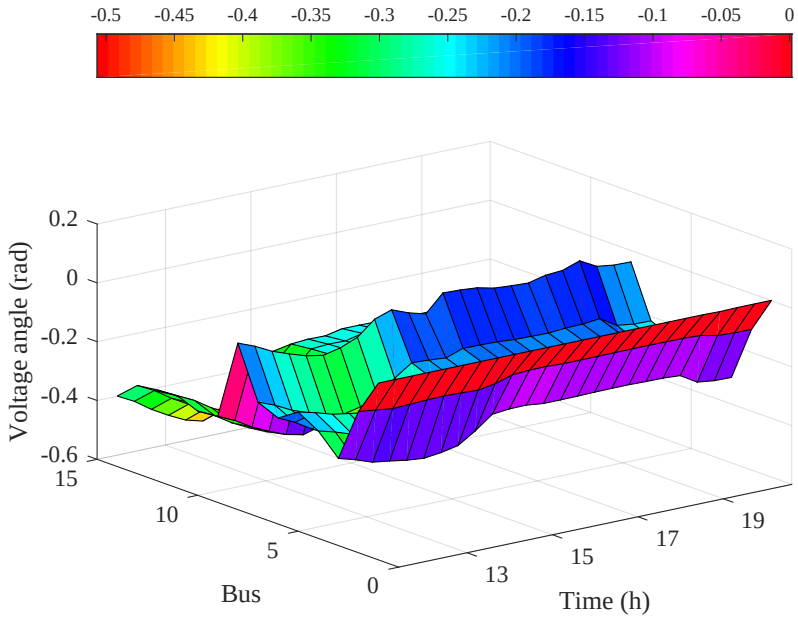

Figure 6.8: Voltage angle of each bus in one day

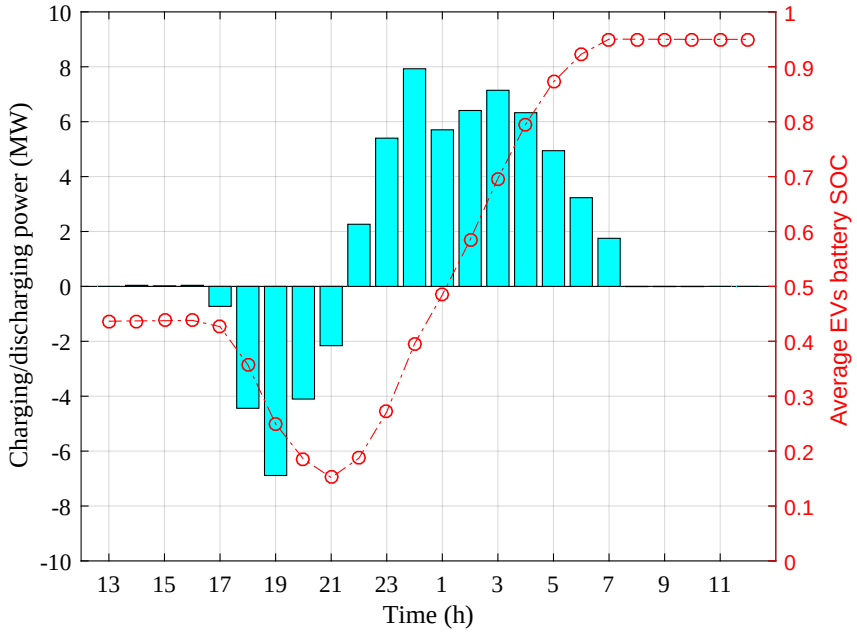

Figure 6.9: EVs charging/discharging power and average SOC under aggregator scheduling

integration. It can be seen from the figure that the peak load is reduced (peak shaving) and the off-peak load increases (valley filling) with EV integration.

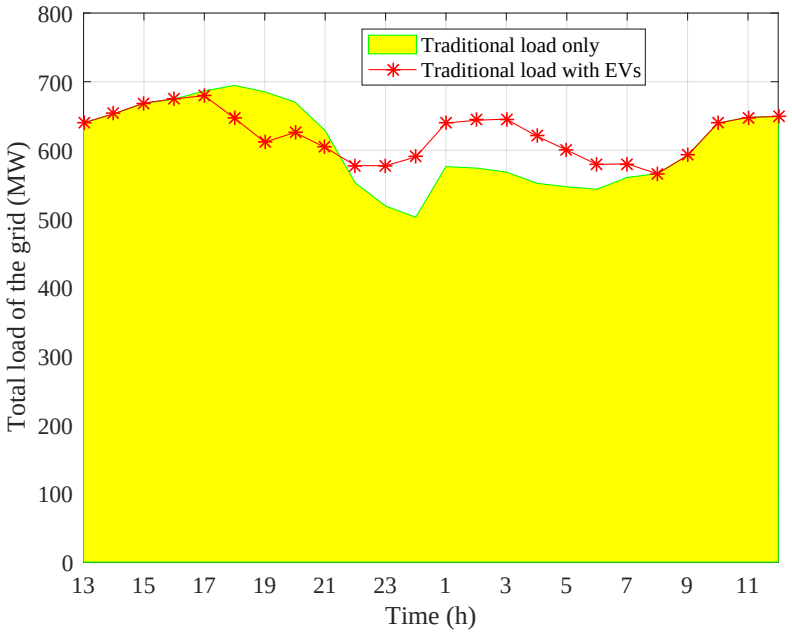

Figure 6.10: Total load of the transmission network with and without EV integration

6.3.4 Aggregator Scheduling with Deviations

In this proposed bi-level strategy, a deviation range σ defined in constraints (6.27) is used to ensure the aggregator can meet the TSO requirements. Figure 6.11 gives the grouped EVs charging/discharging power (TSO results) and the actual EVs charging/discharging power under different deviation range values, $\sigma = 3\%, \sigma = 80\%$ and infinite. It can be seen from Figure 6.11 that, when $\sigma = 3\%$, the aggregator scheduling results nearly follow the TSO results with smaller deviations. When the deviation is infinite, the differences exist between 15:00–17:00 and the charging power is greater than that of $\sigma = 3\%$. The reason is that, in order to reduce the total load between 15:00–17:00, less EVs operate in charging status under $\sigma = 3\%$. However, with infinite deviations, in order to inject more energy back to the grid during off-peak hours, EVs need to operate

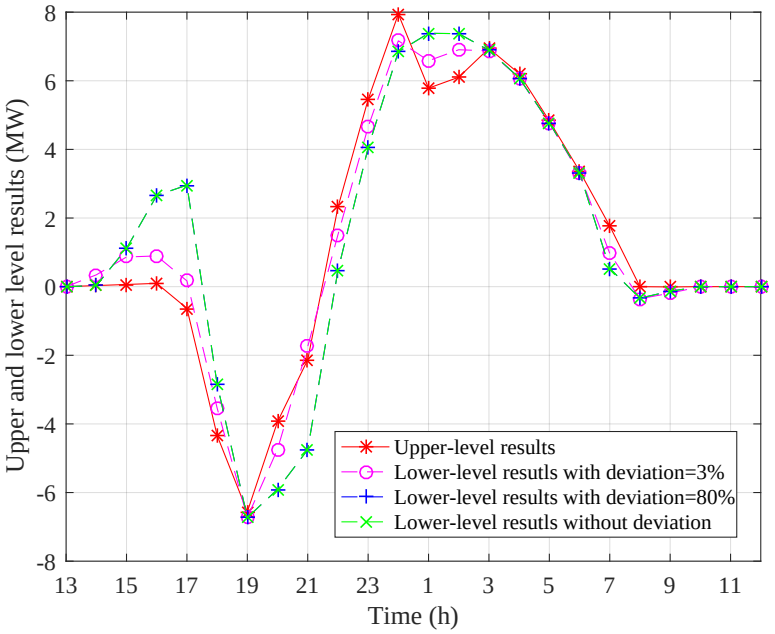

Figure 6.11: TSO results and aggregator results under different deviation ranges

in charging status to store more energy before off-peak hours.

6.3.5 Effectiveness of the Bi-Level Strategy

The performance of the proposed strategy and the EV information grouping method are evaluated in this section. Table 6.1 shows the generator cost with/without the proposed bi-level strategy. In order to make a comparison, the uncoordinated charging scenario is used, that is all EVs follow the 'first come first served' rule and it is assumed that no discharging in this scenario. The coordinated charging represents the scenario that the charging and discharging of all EVs are determined by the TSO and EV aggregator according to the bi-level strategy. It can be seen from Table 6.1 that, the generation cost of all generators in the transmission systems in twenty-four hours are $ 538,591 and $ 543,178 under coordinated charging, which is less than the uncoordinated charging scenario ($ 542,486 and $ 549,631) under 700 and 1000 EVs in each load bus respectively. The reason is that, the charging load of EVs are scheduled from peak hours to off-peak

Table 6.1: A comparison of generator cost with/without the proposed strategy (bi-level strategy)

	700 EVs in each load bus	1000 EVs in each load bus
Uncoordinated charging ($)	542,486	549,631
Coordinated charging ($)	538,591	543,178
Total cost reduction ($)	3895	6453

hours under coordinated charging scenario, moreover EVs operate in discharging status and the peak load is shaved. These results can be found in Figure 6.10. Based on the objective function given in (6.3b), it can be noticed that during peak hours the marginal generation cost is much greater than that in off-peak hours. Thus, by coordinating the charging and discharging of the EV groups, the generation cost could be minimised.

The proposed EV information grouping method could effectively handle the optimisation complexity. As shown in Table 6.2, the optimisation time consumption with the EV information grouping method is 3.48 seconds (there are 766 groups in all busses), while it takes 7.21 s without the EV information grouping method when there are 100 EVs in each load bus. There is a significant difference when 1000 EVs in each load bus.

Table 6.2: A comparison of model complexity and solutions times with/without the EV information grouping method

	Number of groups	Number of variables	Number of constraints	Time
100 EVs in each load bus (no grouping)	N/A	29,548	74,622	7.21 s
100 EVs in each load bus (grouping)	766	20,016	50,428	3.48 s
1000 EVs in each load bus (no grouping)	N/A	286,182	726,107	$>$ 1 h
1000 EVs in each load bus (grouping)	2246	56,346	142,688	21.53 s

It can be seen from the table that by using the EV information grouping method, the complexity of the model is much reduced, where there are 2,246 EV groups in all busses, and the number of variables and constraints are reduced from 286,182 and 726,107 to

56,346 and 142,688, respectively. Therefore, the optimal solution is found in 21.53 s under the EV information grouping method. On the contrary, the optimal solution could not be found in 1 hour without the EV information grouping method, since there are too many variables and constraints.

6.4 Summary

In this chapter, a bi-level EV energy management strategy in a transmission network is presented considering the grid (TSO) interest. The TSO is responsible for the generator output and power flow of the transmission network in the upper level. The aggregator determines the actual charging/discharging operations of each EV at the lower level.

Some conclusions in this chapter are drawn as follows:

- The proposed bi-level strategy could minimise the total cost of the system and the EV charging/discharging could shave the peak and fill the valley loads. Under the proposed strategy, the generation cost is reduced by $ 6453 and $ 3895 with 1000 and 700 EVs in each load bus.
- The proposed EV information grouping method could effectively reduce the optimisation complexity with a negligible difference in the optimal solution, where the optimisation time consumption reduces from $>$ 1h to 21.53 s with 1000 EVs in each load bus.
- It is found that, for the EVs with the same information, the scheduling results of EVs' charging/discharging power are almost the same. Thus the EV information grouping method is accurate in the TSO scheduling.

Chapter 7

Conclusions and Future Work

7.1 Summary of Contents

Faced with the fast development of EVs, the charging behaviours of EVs will bring a series problems for the power grids operation. On the other hand, EV energy management strategies enable EVs to perform as ESS and thus provide benefits for stakeholders. Under certain background, a series of strategies are proposed in this thesis for EV energy management in smart grids. Special consideration has been given to the three stakeholders' interest (EV owners, aggregator, and grid), which has imposed significant impact on EV energy management. Three case studies are presented in this thesis based on stakeholders' interest. Considering EV owners' and aggregator's interest, the economic inconsistency issue raised between two stakeholders is discussed and mitigated based on a three-stage scheduling strategy. Considering aggregator's interest, an aggregator bidding strategy in uncertain electricity markets is proposed and the aggregator profit is maximised. Considering the grid's interest, a bi-level strategy is proposed and the total generation cost of the system is minimised.

The contents of each chapter are summarised as follows. Chapter 1 introduces the background information of smart grids, and the state of the art of EVs. The motivations, objectives and the structure of this thesis are presented. Chapter 2 is a review of ESS and EVs. A categorisation of ESS and a general working principle of

certain types of ESS are discussed. The EV energy management strategies are reviewed from different stakeholders' viewpoints. Chapter 3 presents the mathematical models of ESS, a single EV charging/discharging model, and a DC-OPF model. The MOO, RHO, and stochastic programming methods used in this thesis are introduced. Chapter 4 investigates the economic relationship between EV owners and the aggregator, MOO methods are applied to balance the trade-off between the EV owners' charging fee minimisation and the aggregator profit maximisation. Chapter 5 focuses on the EV aggregator profit maximisation problem in uncertain electricity markets. Stochastic programming method is applied to address the uncertainty of the RTM. Chapter 6 develops a bi-level strategy, the responsibilities of the TSO and aggregator are clearly defined. An EV information grouping method is designed, which could effectively reduce the optimisation complexity.

7.2 Main Conclusions and Findings

The main conclusions and findings of the three case studies in this thesis are summarised as follows:

- **Economic Inconsistency Issue:** Considering EV owners' and aggregator's interest, the economic inconsistency issue between the two stakeholders is addressed and the issue is mitigated by introducing a rebate factor in the model.
  - The economic relationship between EV owners and the aggregator is evaluated and the Pareto optimal of the optimisation problem has been achieved. It is found that, on the right hand side of the marginal point, the EV owners' charging fee significantly increases when w_1 or ε increase, and on the left hand side of the marginal point, the aggregator profit significantly reduces when w_1 or ε decrease. This can provide a reference to design a reasonable settlement mechanism between the two stakeholders.
  - To mitigate the economic inconsistency issue between the stakeholders, a rebate factor is introduced, which can be regarded as an update of the ε-

constraint method. The proposed three-stage strategy could guarantee EV owners benefits while the aggregator profit is maximised.

  - An RHO method is proposed in the aggregator scheduling strategy. By using the proposed online optimisation method, the EV information is updated and corrected hourly, which effectively handles the problem of the uncertainty of EV owners' driving behaviours.

- **Bidding Strategy in Electricity Markets:** Considering the aggregator's interest, an EV aggregator bidding strategy in uncertain electricity markets is proposed based on a scenario-based stochastic programming method. The impact of the uncertainty of the RTM on the bidding in the DAM is taken into consideration.

  - The proposed strategy could maximise the expected profit of the aggregator, and thus the uncertainty of the electricity market is well managed. The uncertainty of the reserve market is represented as several scenarios and these scenarios are generated based on a Monte Carlo simulation.

  - The risk of the aggregator in reserve deployment shortage is taken into consideration, where a penalty is involved in the model. The proposed strategy could effectively balance the reserve deployment benefits and penalty, and thus the optimal bidding strategy could be determined.

  - A comparison is made between the performance of EVs and ESS in providing reserve service; it is found that the required and deployed percentage of EVs are much less than those of ESS, because of EVs' transportation characteristics and driving requirements compared with ESS.

- **EVs in Transmission Systems:** Considering the grid's interest, the impact of EVs' charging and discharging behaviours on the operation of transmission systems is investigated and the proposed bi-level strategy could achieve the cooperation between EVs on the load side and generators on the generation side.

  - The proposed strategy achieves a significant cost reduction of the generators,

i.e., the generation cost reduces by $ 6453 in one day with 1000 EVs at each load bus under bi-level strategy compared with uncoordinated charging.

- The responsibilities of the TSO and the aggregator in the power grid operation are defined. The proposed EV information grouping method could reduce the number of variables and constraints of the optimisation problem, and thus the optimisation complexity is significantly reduced.
- For EVs with the same information, the charging/discharging scheduling results are almost the same. It is reasonable to use the EV groups in the upper level.

7.3 Future Work

The theoretical analysis presented in thesis evaluates the performance of EVs charging and discharging to power grids. This research could be further developed in the following aspects:

- **EVs in Distribution Systems:** EVs are directly connected with distributions systems. Therefore, the cooperation mechanisms of the EV aggregator with the DSO and the DSO with the TSO, which can guarantee each stakeholder's benefits, should be developed. It is worth examining the impact of EVs' charging behaviours on the AC-OPF to distribution systems and the relationships between DSO with the EV aggregator need to be investigated.

  It is worth considering the cooperation of DGs and smart buildings with EVs in distribution systems. As the penetration level of renewable energy increases and due to its uncertainty, EVs are expected to take responsibility for smoothing the output of renewable energy, and thus the whole power grid will benefit.

- **Coupling Between the Power Network and Transportation Network:** In this thesis, a temporal model is built to examine the operation of power grids, which involves spatial constraints in the optimisation. For real planning of power

grids, both temporal and spatial information should be considered, where the optimal sitting and sizing of charging stations need to be optimised.

Distribution systems could be mainly classified into commercial, residential, and industrial areas, where these areas are geographically connected based on the transportation network. Thus, it is worth jointly consider the power network and the transportation network in the charging stations' siting and sizing problem.

- **An Accurate EV Battery Model:** In this study, considering the characteristics of the Li-ion battery, the relationship between maximum charging power with SOC is formulated as linear constraints in the optimisation model. However, for simplification, the battery degradation rate is assumed as a constant. It is practical to consider the relationships of battery degradation rate with charging power and SOC, especially during fast-charging mode.

- **Advanced EV Information Grouping Methods:** In this thesis, only one type of EV is considered in numerical examples, it is worth building more realistic EV model, with varies types of EVs and different driving patterns.

  Therefore, it is worth exploring advanced EV information grouping method based on artificial intelligence and machine learning techniques, such as K-means method. The trade-off between the computational complexity with the scheduling accuracy should be examined.

Appendix A

Publications

Journal Papers

1. B. Han, S. Lu, F. Xue and L. Jiang, "Day-Ahead Electric Vehicle Aggregator Bidding Strategy using Stochastic Programming in an Uncertain Reserve Market," in *IET Generation, Transmission & Distribution*, 2019.

2. B. Han, S. Lu, F. Xue, L. Jiang and X. Xu, "A Three-Stage Electric Vehicle Scheduling Considering Stakeholders Economic Inconsistency and Battery Degradation," in *IET Cyber-Physical Systems: Theory & Applications*, vol. 2, no. 3, pp. 102-110, 10 2017.

3. Y. Zhang, Y. Zhang, X. Han, B. Han, S. Lu, F. Xue, "Research on Electric Vehicle Smart Charging Strategy on Carbon Emission Minimization," in *Electric Power*, 2019. (in Chinese)

Conference Papers

1. B. Han, S. Lu, F. Xue and L. Jiang, "Electric Vehicle Charging and Discharging Scheduling Considering Reserve Call-Up Services," *2017 IEEE International Smart Cities Conference (ISC2)*, Wuxi, 2017, pp. 1-6.

2. B. Han, S. Lu, F. Xue, L. Jiang and H. Zhu, "A Two-Stage Electric Vehicles Scheduling Strategy to Address Economic Inconsistency Issues of Stakeholders," *2017 IEEE Intelligent Vehicles Symposium (IV)*, Los Angeles, CA, 2017, pp. 1904-1909.

3. B. Han, S. Lu, L. Jiang and Y. Du, "A Review of Energy Storage Systems Applied in Power Grids," *Proceedings of the 8th Asia-Pacific Power and Energy Engineering Conference*, Suzhou, 2016, pp. 91-96.

Appendix B

Parameters and Data

A typical residential community is considered in numerical examples in Chapter 4–6, and the EV energy management strategies are applied from 13:00 to 13:00 next day. Private EVs with normal charging in residential area (fast charging is common in commercial area) are considered in this thesis. It is assumed that EV owners are all residential customers, that is most EVs arrive in the evening and leave in the morning next day (detailed information is given in Table B.4).

B.1 EV Battery Information

The total time period is twenty-four hours (13:00–13:00 next day) and the scheduling interval is set to $\Delta T = 1$ h. Thus, the total number of time intervals is $M = 24$. The upper and lower bounds on the SOC are $\overline{\text{SOC}} = 1$ and $\underline{\text{SOC}} = 0.1$ (these parameters are generic and can be easily changed according to the requirements) for all EVs and the depth of discharge is set as DoD = 1.

It is assumed that EVs in these models are all with BYD e6 type; the EVs charging/discharging parameters are summarised in Table B.1.

Table B.1: EV battery parameters

$\overline{P}_n^{\text{ev}}$	E_n^{ev}	D^{ev}	$\underline{\text{SOC}}$	$\overline{\text{SOC}}$	SOC^{d}
8 kW	64 kWh	0.083 \$/kWh	0.1	1	0.95

The relevant parameters of ESS are summarised in Table B.2.

Table B.2: ESS battery parameters

$\overline{P}^{\text{ess}}$	E^{ess}	D^{ess}	SOC^{b}	SOC^{e}
120 kW	1500 kWh	0.08 \$/kWh	0.5	0.5

B.2 Piecewise Linear Approximation of Maximum Charging Power

In the dynamic EV charging/discharging model, the dynamic maximum charging power limits are approximated by four linear curves in Figure 3.2. The value parameters R_{1-5} and F_{1-5} are summarised in Table B.3

Table B.3: Piecewise linear approximation of maximum charging power

R_1	R_2	R_3	R_4	R_5
0	0.74	0.82	0.926	1
F_1	F_2	F_3	F_4	F_5
7.34	8.00	6.35	3.09	0

B.3 Real-Time Pricing

The hourly RTP (charging price) and the hourly reserve capacity prices are shown in Figure B.1 [73]. The aggregator could receive an additional reward (feed-in-tariff) at the time for injecting energy back to the grids and the reward is set as $\hat{r} = 0.16$\$/kWh. The reserve shortage penalty values are set as $\gamma^{up} = \gamma^{dw} = 0.13$\$/kWh.

B.4 EV Driving Information

The EV owners' driving patterns are assumed to follow the TGD, i.e. the arrival time, departure time and the battery SOC at arrival time follow the TGD. Table B.4 illustrates the EV driving information parameters [68].

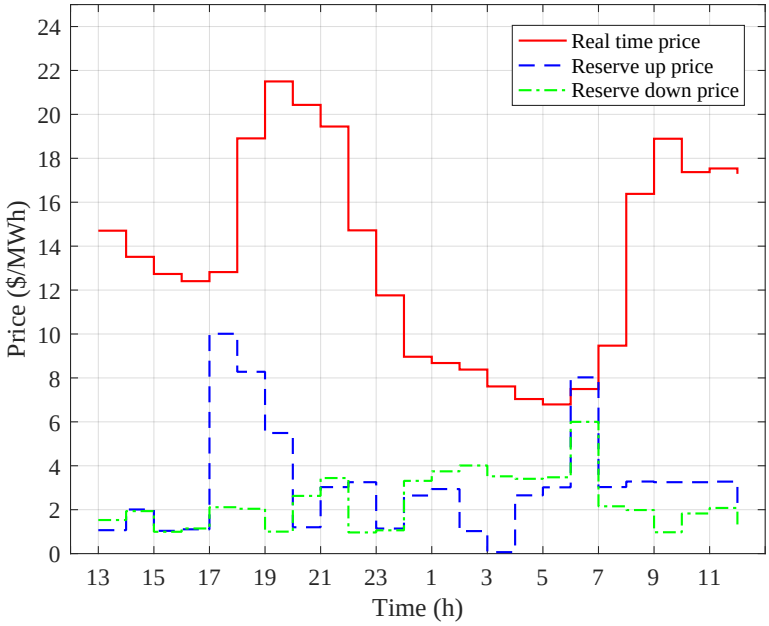

Figure B.1: RTP (charging price) and reserve up/down capacities prices

Table B.4: EV Information Model Data

	Mean	Variance	Min	Max
Initial SOC	0.3	0.1	0.1	1
Arrival time	18:00	2h	13:00	13:00 next day
Departure time	7:00	2h	13:00	13:00 next day

B.5 Power Grids Information

Table B.5 summarises the characteristics of five generators including cost coefficients and the maximum/minimum output power limits.

Table B.5: Generator characteristics

Generator ID	a_i (\$/MW^{2}h)	b_i (\$/MWh)	c_i (\$/h)	$\underline{P}_i^G$(MW)	$\overline{P}_i^G$ (MW)
Gen 1	0.04	20	0	0	332.4
Gen 2	0.25	20	0	0	140
Gen 3	0.01	40	0	0	100
Gen 6	0.01	40	0	0	100
Gen 8	0.01	40	0	0	100

The impedance (in p.u.) and the transmission capacity of each branch of the transmission network are shown in Table B.6. It can be seen that there are 20 branches of the systems.

Table B.6: Branch characteristics

Branch	From bus i	To bus j	Impedance $X_{i,j}$ (p.u.)	Capacity $F_{i,j}$ (MW)
1	1	2	0.059	300
2	1	5	0.223	300
3	2	3	0.197	300
4	2	4	0.176	300
5	2	5	0.173	300
6	3	4	0.171	300
7	4	5	0.042	300
8	4	7	0.209	300
9	4	9	0.556	300
10	5	6	0.252	300
11	6	11	0.199	300
12	6	12	0.256	300
13	6	13	0.130	300
14	7	8	0.176	300
15	7	9	0.110	300
16	9	10	0.084	300
17	9	14	0.270	300
18	10	11	0.192	300
19	12	13	0.200	300
20	13	14	0.348	300

Table B.7 illustrates total bus number of the transmission network $B = 14$ and the distribution of the load and generators at each bus.

Table B.7: Load and generator units locations

Bus ID	1	2	3	4	5	6	7
Load (MW)	N/A	21.7	94.2	47.8	7.6	11.2	N/A
Generator ID	Gen 1	Gen 2	Gen 3	N/A	N/A	Gen 6	N/A
Bus ID	8	9	10	11	12	13	14
Load (MW)	N/A	29.5	9	3.5	6.1	13.5	14.9
Generator ID	Gen 8	N/A	N/A	N/A	N/A	N/A	N/A

Appendix C

Numerical Results

The relationship between aggregatgor profit and EV owners charging fee with different value of weights is shown in Table C.1.

Table C.1: Aggregator profit and EV owners' charging fee versus weights in WSM

Aggregator Profit ($)	EV owners charging fee ($)	Weight w_1	Weight w_2
29.86	324.38	0	1.00
33.94	324.63	0.10	0.90
40.48	325.71	0.20	0.80
49.25	328.45	0.30	0.70
51.80	329.60	0.33	0.67
53.68	330.64	0.40	0.60
58.64	334.65	0.50	0.50
60.56	336.98	0.60	0.40
62.34	340.11	0.70	0.30
63.08	342.27	0.80	0.20
63.34	343.80	0.90	0.10
63.80	353.03	1.00	0

Table C.2 and C.3 summarise the detailed power flow of each branch of the transmission network at each hour. Table C.4 and C.5 show the voltage angle of each bus at each hour.

Table C.2: Power flow in branch 1–10 of the transmission network in one day (MW)

Time	Branch 1	Branch 2	Branch 3	Branch 4	Branch 5	Branch 6	Branch 7	Branch 8	Branch 9	Branch 10
13:00	205.16	88.24	92.95	65.36	43.37	-40.21	-94.60	-11.76	13.03	17.88
14:00	217.06	94.32	97.69	70.03	47.13	-40.89	-98.61	-8.66	14.81	22.59
15:00	229.93	102.47	104.38	77.22	53.20	-41.22	-103.63	-3.81	17.59	29.95
16:00	226.02	106.38	109.38	83.91	59.54	-40.10	-105.47	0.56	20.10	36.55
17:00	222.17	110.23	115.18	90.70	65.79	-39.82	-108.09	4.57	22.40	42.50
18:00	219.58	112.82	119.07	95.27	70.00	-39.62	-109.85	7.27	23.95	46.52
19:00	221.97	110.43	115.19	90.98	66.11	-39.54	-107.96	4.87	22.57	42.98
20:00	227.01	105.39	107.7	82.13	57.94	-40.00	-104.62	-0.40	19.55	35.14
21:00	210.56	92.11	93.46	68.39	46.50	-37.67	-94.37	-8.37	14.98	23.36
22:00	179.98	77.70	80.17	57.38	38.42	-33.64	-81.62	-9.74	11.89	17.01
23:00	174.37	75.90	79.02	56.46	38.02	-33.26	-79.42	-5.60	11.99	18.80
0:00	173.13	75.74	78.94	56.51	38.24	-33.12	-78.73	-3.05	12.27	20.34
1:00	178.14	75.86	80.85	56.02	36.69	-35.84	-83.06	-13.68	10.54	12.55
2:00	177.98	75.85	80.82	56.03	36.72	-35.79	-82.95	-13.35	10.58	12.77
3:00	177.59	75.83	80.68	56.06	36.84	-35.59	-82.63	-12.52	10.71	13.37
4:00	176.47	75.79	80.29	56.17	37.17	-35.04	-81.69	-10.14	11.08	15.07
5:00	176.11	75.78	80.17	56.20	37.28	-34.85	-81.39	-9.38	11.20	15.62
6:00	175.86	75.77	80.08	56.22	37.35	-34.73	-81.19	-8.87	11.28	15.99
7:00	177.05	75.81	80.49	56.11	37.00	-35.32	-82.18	-11.37	10.89	14.19
8:00	177.42	75.83	80.62	56.08	36.89	-35.51	-82.48	-12.16	10.77	13.63
9:00	179.26	75.89	81.26	55.91	36.34	-36.43	-84.02	-16.06	10.15	10.82
10:00	202.82	86.94	92.24	64.37	42.50	-40.40	-94.06	-12.58	12.56	16.60
11:00	207.68	89.26	94.51	66.16	43.82	-41.19	-96.09	-11.64	13.10	17.97
12:00	208.45	89.63	94.87	66.45	44.03	-41.31	-96.41	-11.49	13.19	18.19

Table C.3: Power flow in branch 10–20 of the transmission network in one day (MW)

Time	Branch 1	Branch 2	Branch 3	Branch 4	Branch 5	Branch 6	Branch 7	Branch 8	Branch 9	Branch 10
13:00	23.39	20.04	46.43	-100.00	88.24	8.19	19.82	-14.39	4.62	17.34
14:00	24.08	21.00	48.18	-100.00	91.34	9.62	21.07	-14.16	4.53	17.58
15:00	25.15	22.54	50.87	-100.00	96.19	12.08	23.08	-13.63	4.31	17.86
16:00	26.07	23.98	53.21	-100.00	100.56	14.71	25.00	-12.84	3.98	17.92
17:00	26.90	25.24	55.38	-100.00	104.57	16.81	26.68	-12.34	3.79	18.10
18:00	27.46	26.09	56.85	-100.00	107.27	18.22	27.82	-11.99	3.66	18.22
19:00	26.97	25.36	55.54	-100.00	104.87	17.07	26.83	-12.22	3.74	18.07
20:00	25.88	23.70	52.68	-100.00	99.60	14.28	24.61	-12.91	4.01	17.85
21:00	24.17	21.35	48.21	-100.00	91.63	11.04	21.51	-13.24	4.10	17.10
22:00	20.84	18.08	41.32	-88.37	78.63	8.36	17.98	-12.10	3.80	15.06
23:00	18.74	16.35	37.71	-76.89	71.29	7.24	16.47	-11.26	3.66	13.85
0:00	17.73	15.56	36.03	-70.88	67.83	6.86	15.84	-10.77	3.56	13.23
1:00	21.13	17.85	41.57	-92.95	79.27	6.73	17.41	-13.32	4.25	15.76
2:00	21.01	17.76	41.37	-92.20	78.86	6.70	17.34	-13.25	4.24	15.68
3:00	20.74	17.57	40.93	-90.45	77.94	6.69	17.21	-13.06	4.19	15.49
4:00	19.96	17.04	39.66	-85.46	75.32	6.68	16.84	-12.50	4.04	14.92
5:00	19.71	16.87	39.25	-83.85	74.47	6.68	16.72	-12.32	3.99	14.74
6:00	19.54	16.75	38.98	-82.78	73.91	6.68	16.64	-12.20	3.96	14.62
7:00	20.36	17.32	40.32	-88.05	76.67	6.69	17.03	-12.79	4.11	15.21
8:00	20.62	17.49	40.74	-89.69	77.54	6.69	17.16	-12.97	4.16	15.4
9:00	21.90	18.37	42.82	-97.91	81.85	6.71	17.77	-13.89	4.4	16.33
10:00	23.20	19.75	45.99	-100.00	87.42	7.67	19.46	-14.56	4.69	17.34
11:00	23.41	20.00	46.54	-100.00	88.36	7.87	19.78	-14.65	4.74	17.50
12:00	23.44	20.04	46.63	-100.00	88.51	7.90	19.83	-14.66	4.74	17.53

Table C.4: Voltage angle of bus 1–7 in one day (rad)

Time	Bus 1	Bus 2	Bus 3	Bus 4	Bus 5	Bus 6	Bus 7
13:00	0	-0.12	-0.31	-0.24	-0.20	-0.24	-0.21
14:00	0	-0.13	-0.32	-0.25	-0.21	-0.27	-0.23
15:00	0	-0.14	-0.34	-0.27	-0.23	-0.30	-0.26
16:00	0	-0.13	-0.35	-0.28	-0.24	-0.33	-0.28
17:00	0	-0.13	-0.36	-0.29	-0.25	-0.35	-0.30
18:00	0	-0.13	-0.37	-0.30	-0.25	-0.37	-0.31
19:00	0	-0.13	-0.36	-0.29	-0.25	-0.35	-0.30
20:00	0	-0.13	-0.35	-0.28	-0.24	-0.32	-0.28
21:00	0	-0.12	-0.31	-0.25	-0.21	-0.26	-0.23
22:00	0	-0.11	-0.27	-0.21	-0.17	-0.22	-0.19
23:00	0	-0.10	-0.26	-0.20	-0.17	-0.22	-0.19
0:00	0	-0.10	-0.26	-0.20	-0.17	-0.22	-0.20
1:00	0	-0.11	-0.27	-0.20	-0.17	-0.20	-0.18
2:00	0	-0.11	-0.27	-0.20	-0.17	-0.20	-0.18
3:00	0	-0.11	-0.26	-0.20	-0.17	-0.20	-0.18
4:00	0	-0.10	-0.26	-0.20	-0.17	-0.21	-0.18
5:00	0	-0.10	-0.26	-0.20	-0.17	-0.21	-0.18
6:00	0	-0.10	-0.26	-0.20	-0.17	-0.21	-0.18
7:00	0	-0.10	-0.26	-0.20	-0.17	-0.20	-0.18
8:00	0	-0.10	-0.26	-0.20	-0.17	-0.20	-0.18
9:00	0	-0.11	-0.27	-0.21	-0.17	-0.20	-0.17
10:00	0	-0.12	-0.30	-0.23	-0.19	-0.24	-0.21
11:00	0	-0.12	-0.31	-0.24	-0.20	-0.24	-0.22
12:00	0	-0.12	-0.31	-0.24	-0.20	-0.25	-0.22

Table C.5: Voltage angle of bus 8–14 in one day (rad)

Time	Bus 8	Bus 9	Bus 10	Bus 11	Bus 12	Bus 13	Bus 14
13:00	-0.04	-0.31	-0.32	-0.29	-0.29	-0.30	-0.36
14:00	-0.06	-0.33	-0.34	-0.32	-0.32	-0.33	-0.39
15:00	-0.09	-0.37	-0.38	-0.35	-0.36	-0.37	-0.43
16:00	-0.11	-0.39	-0.41	-0.38	-0.39	-0.40	-0.46
17:00	-0.12	-0.42	-0.43	-0.41	-0.42	-0.43	-0.49
18:00	-0.14	-0.43	-0.45	-0.42	-0.44	-0.44	-0.51
19:00	-0.13	-0.42	-0.43	-0.41	-0.42	-0.43	-0.49
20:00	-0.10	-0.39	-0.40	-0.38	-0.38	-0.39	-0.45
21:00	-0.05	-0.33	-0.34	-0.31	-0.32	-0.33	-0.39
22:00	-0.03	-0.27	-0.28	-0.26	-0.26	-0.27	-0.32
23:00	-0.06	-0.27	-0.28	-0.25	-0.26	-0.27	-0.31
0:00	-0.07	-0.27	-0.28	-0.26	-0.26	-0.27	-0.31
1:00	-0.01	-0.26	-0.27	-0.24	-0.25	-0.25	-0.31
2:00	-0.01	-0.26	-0.27	-0.24	-0.25	-0.26	-0.31
3:00	-0.02	-0.26	-0.27	-0.24	-0.25	-0.26	-0.31
4:00	-0.03	-0.27	-0.27	-0.25	-0.25	-0.26	-0.31
5:00	-0.04	-0.27	-0.27	-0.25	-0.25	-0.26	-0.31
6:00	-0.04	-0.27	-0.27	-0.25	-0.25	-0.26	-0.31
7:00	-0.02	-0.26	-0.27	-0.25	-0.25	-0.26	-0.31
8:00	-0.02	-0.26	-0.27	-0.24	-0.25	-0.26	-0.31
9:00	0	-0.26	-0.27	-0.24	-0.24	-0.25	-0.31
10:00	-0.03	-0.30	-0.31	-0.28	-0.29	-0.30	-0.36
11:00	-0.04	-0.31	-0.32	-0.29	-0.30	-0.30	-0.37
12:00	-0.04	-0.31	-0.32	-0.29	-0.30	-0.31	-0.37

Bibliography

[1] European Commission. A clean planet for all a european strategic long-term vision for a prosperous, modern, competitive and climate neutral economy. [Online]. Available: https://eur-lex.europa.eu/legal-content/EN/TXT/?uri=CELEX:52018DC0773

[2] White House, "Fact sheet: U.S. reports its 2025 emissions target to the UNFCCC," 2015.

[3] State Council of the People's Republic of China. "Thirteenth Five-Year Plan" greenhouse gas emissions control plan. [Online]. Available: http://www.gov.cn/zhengce/content/2016-11/04/content_5128619.htm

[4] Statistics IEA, "Key world energy statistics. paris. international energy agency," p. 82, 2014.

[5] A. Ipakchi and F. Albuyeh, "Grid of the future," *IEEE power and energy magazine*, vol. 7, no. 2, pp. 52–62, 2009.

[6] Facts Fast, "U.S. transportation sector greenhouse gas emissions 1990-2017," *United States Environmental Protection Agency*, 2019.

[7] J. McLaren, J. Miller, E. O'Shaughnessy, E. Wood, and E. Shapiro, "Emissions associated with electric vehicle charging: Impact of electricity generation mix, charging infrastructure availability, and vehicle type," National Renewable Energy Lab.(NREL), Golden, CO (United States), Tech. Rep., 2016.

[8] T. Bunsen, P. Cazzola, M. Gorner, L. Paoli, S. Scheffer, R. Schuitmaker, J. Tattini, and J. Teter, "Global EV outlook 2018: Towards cross-modal electrification," *International Energy Agency*, 2018.

[9] T. Bunsen, P. Cazzola, M. Gorner, L. Paoli, S. Scheffer, R. Schuitmaker, J. Tattini, and Teter, "Global EV outlook 2019: Scaling-up the transition to electric mobility," *International Energy Agency*, 2019.

[10] A. Tavakoli, M. Negnevitsky, D. T. Nguyen, and K. M. Muttaqi, "Energy exchange between electric vehicle load and wind generating utilities," *IEEE Transactions on Power Systems*, vol. 31, no. 2, pp. 1248–1258, March 2016.

[11] Y. Cao, S. Tang, C. Li, P. Zhang, Y. Tan, Z. Zhang, and J. Li, "An optimized EV charging model considering TOU price and SOC curve," *IEEE Transactions on Smart Grid*, vol. 3, no. 1, pp. 388–393, March 2012.

[12] U.S. Department of Energy. Fact 841: October 6, 2014 vehicles per thousand people: U.S. vs. other world regions. [Online]. Available: https://www.energy.gov/eere/vehicles/fact-841-october-6-2014-vehicles-thousand-people-us-vs-other-world-regions

[13] Z. Ji and X. Huang, "Plug-in electric vehicle charging infrastructure deployment of China towards 2020: Policies, methodologies, and challenges," *Renewable and Sustainable Energy Reviews*, vol. 90, pp. 710–727, 2018.

[14] Qdr QJUDE, "Benefits of demand response in electricity markets and recommendations for achieving them," *US Dept. Energy, Washington, DC, USA, Tech. Rep*, 2006.

[15] U.S. Department of Energy. Smart grid system report. [Online]. Available: https://www.smartgrid.gov/files/systems_report.pdf

[16] M. S. ElNozahy and M. M. Salama, "A comprehensive study of the impacts of

phevs on residential distribution networks," *IEEE Transactions on Sustainable Energy*, vol. 5, no. 1, pp. 332–342, 2013.

[17] J. Meng, Y. Mu, H. Jia, J. Wu, X. Yu, and B. Qu, "Dynamic frequency response from electric vehicles considering travelling behavior in the great britain power system," *Applied energy*, vol. 162, pp. 966–979, 2016.

[18] H. Chen, T. N. Cong, W. Yang, C. Tan, Y. Li, and Y. Ding, "Progress in electrical energy storage system: A critical review," *Progress in natural science*, vol. 19, no. 3, pp. 291–312, 2009.

[19] N. Miller, D. Manz, J. Roedel, P. Marken, and E. Kronbeck, "Utility scale battery energy storage systems," in *IEEE PES General Meeting*. IEEE, 2010, pp. 1–7.

[20] A. A. Akhil, G. Huff, A. B. Currier, B. C. Kaun, D. M. Rastler, S. B. Chen, A. L. Cotter, D. T. Bradshaw, and W. D. Gauntlett, "Electricity storage handbook in collaboration with nreca," *Sandia National Laboratories*, 2013.

[21] M. Hannan, M. Hoque, A. Mohamed, and A. Ayob, "Review of energy storage systems for electric vehicle applications: Issues and challenges," *Renewable and Sustainable Energy Reviews*, vol. 69, pp. 771–789, 2017.

[22] A. Chatzivasileiadi, "Electrical energy storage technologies and the built environment," *International renewable energy storage conference*, 2012.

[23] J. Kondoh, I. Ishii, H. Yamaguchi, A. Murata, K. Otani, K. Sakuta, N. Higuchi, S. Sekine, and M. Kamimoto, "Electrical energy storage systems for energy networks," *Energy Conversion and Management*, vol. 41, no. 17, pp. 1863–1874, 2000.

[24] T. M. Masaud, K. Lee, and P. Sen, "An overview of energy storage technologies in electric power systems: What is the future?" in *North American Power Symposium 2010*. IEEE, 2010, pp. 1–6.

[25] R. Sebastián and R. P. Alzola, "Flywheel energy storage systems: Review and simulation for an isolated wind power system," *Renewable and Sustainable Energy Reviews*, vol. 16, no. 9, pp. 6803–6813, 2012.

[26] S. Chen, T. Zhang, H. B. Gooi, R. D. Masiello, and W. Katzenstein, "Penetration rate and effectiveness studies of aggregated bess for frequency regulation," *IEEE Transactions on Smart Grid*, vol. 7, no. 1, pp. 167–177, 2016.

[27] X. Feng, H. Gooi, and S. Chen, "Hybrid energy storage with multimode fuzzy power allocator for PV systems," *IEEE Transactions on Sustainable Energy*, vol. 5, no. 2, pp. 389–397, 2014.

[28] D. Pavlov, *Lead-acid batteries: science and technology*. Elsevier, 2011.

[29] J. Baker, "New technology and possible advances in energy storage," *Energy Policy*, vol. 36, no. 12, pp. 4368–4373, 2008.

[30] X. Luo, J. Wang, M. Dooner, and J. Clarke, "Overview of current development in electrical energy storage technologies and the application potential in power system operation," *Applied energy*, vol. 137, pp. 511–536, 2015.

[31] F. Nadeem, S. S. Hussain, P. K. Tiwari, A. K. Goswami, and T. S. Ustun, "Comparative review of energy storage systems, their roles, and impacts on future power systems," *IEEE Access*, vol. 7, pp. 4555–4585, 2019.

[32] S. Faddel, A. Al-Awami, and O. Mohammed, "Charge control and operation of electric vehicles in power grids: A review," *Energies*, vol. 11, no. 4, p. 701, 2018.

[33] SAE, "Electric vehicle and plug in hybrid electric vehicle conductive charge coupler," 2010.

[34] S. Mehar, S. Zeadally, G. Remy, and S. M. Senouci, "Sustainable transportation management system for a fleet of electric vehicles," *IEEE transactions on intelligent transportation systems*, vol. 16, no. 3, pp. 1401–1414, 2015.

[35] A. Briones, J. Francfort, P. Heitmann, M. Schey, S. Schey, and J. Smart, "Vehicle-to-grid (V2G) power flow regulations and building codes review by the AVTA," *Idaho National Lab., Idaho Falls, ID, USA*, 2012.

[36] J. J. Escudero-Garzás, A. García-Armada, and G. Seco-Granados, "Fair design of plug-in electric vehicles aggregator for V2G regulation," *IEEE Transactions on Vehicular Technology*, vol. 61, no. 8, pp. 3406–3419, 2012.

[37] K. S. Ko, S. Han, and D. K. Sung, "Performance-based settlement of frequency regulation for electric vehicle aggregators," *IEEE Transactions on Smart Grid*, vol. 9, no. 2, pp. 866–875, 2016.

[38] E. Yao, V. W. Wong, and R. Schober, "Optimization of aggregate capacity of PEVs for frequency regulation service in day-ahead market," *IEEE Transactions on Smart Grid*, vol. 9, no. 4, pp. 3519–3529, 2016.

[39] M. Datta and T. Senjyu, "Fuzzy control of distributed PV inverters/energy storage systems/electric vehicles for frequency regulation in a large power system," *IEEE Transactions on Smart Grid*, vol. 4, no. 1, pp. 479–488, 2013.

[40] M. D. Galus, M. Zima, and G. Andersson, "On integration of plug-in hybrid electric vehicles into existing power system structures," *Energy Policy*, vol. 38, no. 11, pp. 6736–6745, 2010.

[41] W. Kempton and J. Tomić, "Vehicle-to-grid power fundamentals: Calculating capacity and net revenue," *Journal of power sources*, vol. 144, no. 1, pp. 268–279, 2005.

[42] E. Hirst and B. Kirby, "Ancillary-service details: operating reserves," Oak Ridge National Lab., TN (United States), Tech. Rep., 1997.

[43] J. C. Mukherjee and A. Gupta, "A review of charge scheduling of electric vehicles in smart grid," *IEEE Systems Journal*, vol. 9, no. 4, pp. 1541–1553, Dec 2015.

[44] A. Mohamed, V. Salehi, T. Ma, and O. Mohammed, "Real-time energy management algorithm for plug-in hybrid electric vehicle charging parks involving sustainable energy," *IEEE Transactions on Sustainable Energy*, vol. 5, no. 2, pp. 577–586, April 2014.

[45] S. Gao, K. T. Chau, C. Liu, D. Wu, and C. C. Chan, "Integrated energy management of plug-in electric vehicles in power grid with renewables," *IEEE Transactions on Vehicular Technology*, vol. 63, no. 7, pp. 3019–3027, Sept 2014.

[46] M. G. Vayá, L. B. Roselló, and G. Andersson, "Optimal bidding of plug-in electric vehicles in a market-based control setup," in *Power Systems Computation Conference (PSCC), 2014*, Aug 2014, pp. 1–8.

[47] K. Qian, C. Zhou, M. Allan, and Y. Yuan, "Modeling of load demand due to EV battery charging in distribution systems," *IEEE Transactions on Power Systems*, vol. 26, no. 2, pp. 802–810, May 2011.

[48] M. G. Vayá and G. Andersson, "Optimal bidding strategy of a plug-in electric vehicle aggregator in day-ahead electricity markets under uncertainty," *IEEE Transactions on Power Systems*, vol. 30, no. 5, pp. 2375–2385, Sept 2015.

[49] C. Jin, J. Tang, and P. Ghosh, "Optimizing electric vehicle charging with energy storage in the electricity market," *IEEE Transactions on Smart Grid*, vol. 4, no. 1, pp. 311–320, 2013.

[50] H. Wu, M. Shahidehpour, A. Alabdulwahab, and A. Abusorrah, "A game theoretic approach to risk-based optimal bidding strategies for electric vehicle aggregators in electricity markets with variable wind energy resources," *IEEE Transactions on Sustainable Energy*, vol. 7, no. 1, pp. 374–385, Jan 2016.

[51] C. S. Antúnez, J. F. Franco, M. J. Rider, and R. Romero, "A new methodology for the optimal charging coordination of electric vehicles considering vehicle-to-grid technology," *IEEE Transactions on Sustainable Energy*, vol. 7, no. 2, pp. 596–607, April 2016.

[52] L. Igualada, C. Corchero, M. Cruz-Zambrano, and F. J. Heredia, "Optimal energy management for a residential microgrid including a vehicle-to-grid system," *IEEE Transactions on Smart Grid*, vol. 5, no. 4, pp. 2163–2172, July 2014.

[53] H. Zhang, Z. Hu, Z. Xu, and Y. Song, "Evaluation of achievable vehicle-to-grid capacity using aggregate PEV model," *IEEE Transactions on Power Systems*, vol. PP, no. 99, pp. 1–1, 2016.

[54] S. Vandael, B. Claessens, M. Hommelberg, T. Holvoet, and G. Deconinck, "A scalable three-step approach for demand side management of plug-in hybrid vehicles," *IEEE Transactions on Smart Grid*, vol. 4, no. 2, pp. 720–728, June 2013.

[55] K. N. Kumar, B. Sivaneasan, P. H. Cheah, P. L. So, and D. Z. W. Wang, "V2G capacity estimation using dynamic EV scheduling," *IEEE Transactions on Smart Grid*, vol. 5, no. 2, pp. 1051–1060, March 2014.

[56] P. Sánchez-Martín, S. Lumbreras, and A. Alberdi-Alén, "Stochastic programming applied to EV charging points for energy and reserve service markets," *IEEE Transactions on Power Systems*, vol. 31, no. 1, pp. 198–205, Jan 2016.

[57] I. Momber, A. Siddiqui, T. G. S. Román, and L. Söder, "Risk averse scheduling by a PEV aggregator under uncertainty," *IEEE Transactions on Power Systems*, vol. 30, no. 2, pp. 882–891, March 2015.

[58] L. Yang, J. Zhang, and H. V. Poor, "Risk-aware day-ahead scheduling and real-time dispatch for electric vehicle charging," *IEEE Transactions on Smart Grid*, vol. 5, no. 2, pp. 693–702, March 2014.

[59] S. Lefeng, L. Tong, and W. Yandi, "Vehicle-to-grid service development logic and management formulation," *Journal of Modern Power Systems and Clean Energy*, vol. 7, no. 4, pp. 935–947, 2019.

[60] C. Jin, J. Tang, and P. Ghosh, "Optimizing electric vehicle charging: A customer's perspective," *IEEE Transactions on Vehicular Technology*, vol. 62, no. 7, pp. 2919–2927, Sept 2013.

[61] A. Ravichandran, S. Sirouspour, P. Malysz, and A. Emadi, "A chance-constraints-based control strategy for microgrids with energy storage and integrated electric vehicles," *IEEE Transactions on Smart Grid*, vol. 9, no. 1, pp. 346–359, 2016.

[62] O. Erdinc, N. G. Paterakis, T. D. Mendes, A. G. Bakirtzis, and J. P. Catalão, "Smart household operation considering bi-directional EV and ESS utilization by real-time pricing-based DR," *IEEE Transactions on Smart Grid*, vol. 6, no. 3, pp. 1281–1291, 2014.

[63] N. G. Paterakis, O. Erdinc, A. G. Bakirtzis, and J. P. Catalão, "Optimal household appliances scheduling under day-ahead pricing and load-shaping demand response strategies," *IEEE Transactions on Industrial Informatics*, vol. 11, no. 6, pp. 1509–1519, 2015.

[64] H. Pandžić and V. Bobanac, "An accurate charging model of battery energy storage," *IEEE Transactions on Power Systems*, vol. 34, no. 2, pp. 1416–1426, 2018.

[65] N. Rotering and M. Ilic, "Optimal charge control of plug-in hybrid electric vehicles in deregulated electricity markets," *IEEE Transactions on Power Systems*, vol. 26, no. 3, pp. 1021–1029, 2010.

[66] H. Farzin, M. Fotuhi-Firuzabad, and M. Moeini-Aghtaie, "A practical scheme to involve degradation cost of lithium-ion batteries in vehicle-to-grid applications," *IEEE Transactions on Sustainable Energy*, vol. 7, no. 4, pp. 1730–1738, Oct 2016.

[67] M. Tabari and A. Yazdani, "An energy management strategy for a DC distribution system for power system integration of plug-in electric vehicles," *IEEE Transactions on Smart Grid*, vol. 7, no. 2, pp. 659–668, 2015.

[68] M. Shafie-khah, E. Heydarian-Forushani, G. J. Osório, F. A. S. Gil, J. Aghaei, M. Barani, and J. P. S. Catalão, "Optimal behavior of electric vehicle parking lots as demand response aggregation agents," *IEEE Transactions on Smart Grid*, vol. PP, no. 99, pp. 1–12, 2015.

[69] M. Alipour, B. Mohammadi-Ivatloo, M. Moradi-Dalvand, and K. Zare, "Stochastic scheduling of aggregators of plug-in electric vehicles for participation in energy and ancillary service markets," *Energy*, vol. 118, pp. 1168–1179, 2017.

[70] B. Han, S. Lu, F. Xue, and L. Jiang, "Electric vehicle charging and discharging scheduling considering reserve call-up service," in *2017 International Smart Cities Conference (ISC2)*. IEEE, 2017, pp. 1–6.

[71] D. R. Melo, A. Trippe, H. B. Gooi, and T. Massier, "Robust electric vehicle aggregation for ancillary service provision considering battery aging," *IEEE Transactions on Smart Grid*, vol. PP, no. 99, pp. 1–1, 2016.

[72] G. He, Q. Chen, C. Kang, Q. Xia, and K. Poolla, "Cooperation of wind power and battery storage to provide frequency regulation in power markets," *IEEE Transactions on Power Systems*, vol. 32, no. 5, pp. 3559–3568, Sept 2017.

[73] M. R. Sarker, Y. Dvorkin, and M. A. Ortega-Vazquez, "Optimal participation of an electric vehicle aggregator in day-ahead energy and reserve markets," *IEEE Transactions on Power Systems*, vol. 31, no. 5, pp. 3506–3515, 2015.

[74] N. Korolko and Z. Sahinoglu, "Robust optimization of EV charging schedules in unregulated electricity markets," *IEEE Transactions on Smart Grid*, vol. 8, no. 1, pp. 149–157, 2015.

[75] G. Liu, Y. Xu, and K. Tomsovic, "Bidding strategy for microgrid in day-ahead market based on hybrid stochastic/robust optimization," *IEEE Transactions on Smart Grid*, vol. 7, no. 1, pp. 227–237, Jan 2016.

[76] M. Kazemi, H. Zareipour, N. Amjady, W. D. Rosehart, and M. Ehsan, "Operation scheduling of battery storage systems in joint energy and ancillary services markets," *IEEE Transactions on Sustainable Energy*, vol. 8, no. 4, pp. 1726–1735, Oct 2017.

[77] J. de Hoog, T. Alpcan, M. Brazil, D. A. Thomas, and I. Mareels, "A market mechanism for electric vehicle charging under network constraints," *IEEE Transactions on Smart Grid*, vol. 7, no. 2, pp. 827–836, March 2016.

[78] J. Zheng, X. Wang, K. Men, C. Zhu, and S. Zhu, "Aggregation model-based optimization for electric vehicle charging strategy," *IEEE Transactions on Smart Grid*, vol. 4, no. 2, pp. 1058–1066, June 2013.

[79] Z. Sun, X. Zhou, J. Du, and X. Liu, "When traffic flow meets power flow: On charging station deployment with budget constraints," *IEEE Transactions on Vehicular Technology*, vol. 66, no. 4, pp. 2915–2926, 2016.

[80] Y. Sun, Z. Chen, Z. Li, W. Tian, and M. Shahidehpour, "EV charging schedule in coupled constrained networks of transportation and power system," *IEEE Transactions on Smart Grid*, 2018.

[81] X. Wang, M. Shahidehpour, C. Jiang, and Z. Li, "Coordinated planning strategy for electric vehicle charging stations and coupled traffic-electric networks," *IEEE Transactions on Power Systems*, vol. 34, no. 1, pp. 268–279, 2018.

[82] L. He, J. Yang, J. Yan, Y. Tang, and H. He, "A bi-layer optimization based temporal and spatial scheduling for large-scale electric vehicles," *Applied energy*, vol. 168, pp. 179–192, 2016.

[83] B. Lian, A. Sims, D. Yu, C. Wang, and R. W. Dunn, "Optimizing LiFePO4 battery energy storage systems for frequency response in the UK system," *IEEE Transactions on Sustainable Energy*, vol. 8, no. 1, pp. 385–394, 2016.

[84] Z. Xu, W. Su, Z. Hu, Y. Song, and H. Zhang, "A hierarchical framework for

coordinated charging of plug-in electric vehicles in China," *IEEE Transactions on Smart Grid*, vol. 7, no. 1, pp. 428–438, Jan 2016.

[85] M. L. Crow *et al.*, "Electric vehicle scheduling considering co-optimized customer and system objectives," *IEEE Transactions on Sustainable Energy*, vol. 9, no. 1, pp. 410–419, 2017.

[86] A. Hamidi, D. Nazarpour, and S. Golshannavaz, "Multiobjective scheduling of microgrids to harvest higher photovoltaic energy," *IEEE Transactions on Industrial Informatics*, vol. 14, no. 1, pp. 47–57, 2017.

[87] Y. Guo, J. Xiong, S. Xu, and W. Su, "Two-stage economic operation of microgrid-like electric vehicle parking deck," *IEEE Transactions on Smart Grid*, vol. 7, no. 3, pp. 1703–1712, May 2016.

[88] Y. Li, K. Xie, L. Wang, and Y. Xiang, "The impact of phevs charging and network topology optimization on bulk power system reliability," *Electric Power Systems Research*, vol. 163, pp. 85–97, 2018.

[89] X. Zhu, H. Han, S. Gao, Q. Shi, H. Cui, and G. Zu, "A multi-stage optimization approach for active distribution network scheduling considering coordinated electrical vehicle charging strategy," *IEEE Access*, vol. 6, pp. 50 117–50 130, 2018.

[90] A. Tavakoli, M. Negnevistky, S. Saha, M. E. Haque, M. T. Arif, J. Contreras, and A. T. Oo, "Self-scheduling of a generating company with an EV load aggregator under an energy exchange strategy," *IEEE Transactions on Smart Grid*, 2018.

[91] S. Tabatabaee, S. S. Mortazavi, and T. Niknam, "Stochastic scheduling of local distribution systems considering high penetration of plug-in electric vehicles and renewable energy sources," *Energy*, vol. 121, pp. 480–490, 2017.

[92] G. R. C. Mouli, M. Kefayati, R. Baldick, and P. Bauer, "Integrated PV charging of EV fleet based on energy prices, V2G and offer of reserves," *IEEE Transactions on Smart Grid*, 2017.

[93] D. van der Meer, G. R. C. Mouli, G. M.-E. Mouli, L. R. Elizondo, and P. Bauer, "Energy management system with PV power forecast to optimally charge EVs at the workplace," *IEEE transactions on industrial informatics*, vol. 14, no. 1, pp. 311–320, 2016.

[94] D. Tang and P. Wang, "Nodal impact assessment and alleviation of moving electric vehicle loads: From traffic flow to power flow," *IEEE Transactions on Power Systems*, vol. 31, no. 6, pp. 4231–4242, 2016.

[95] Y. Zheng, Y. Song, D. J. Hill, and K. Meng, "Online distributed MPC-based optimal scheduling for EV charging stations in distribution systems," *IEEE Transactions on Industrial Informatics*, vol. 15, no. 2, pp. 638–649, 2019.

[96] R. D. Christie, B. F. Wollenberg, and I. Wangensteen, "Transmission management in the deregulated environment," *Proceedings of the IEEE*, vol. 88, no. 2, pp. 170–195, 2000.

[97] C. W. Tan, D. W. Cai, and X. Lou, "DC optimal power flow: Uniqueness and algorithms," in *2012 IEEE Third International Conference on Smart Grid Communications (SmartGridComm)*. IEEE, 2012, pp. 641–646.

[98] J. Carpentier, "Contribution to the economic dispatch problem," *Bulletin de la Societe Francoise des Electriciens*, vol. 3, no. 8, pp. 431–447, 1962.

[99] A. J. Conejo and J. A. Aguado, "Multi-area coordinated decentralized DC optimal power flow," *IEEE Transactions on Power Systems*, vol. 13, no. 4, pp. 1272–1278, 1998.

[100] R. S. Wibowo, A. Soeprijanto, O. Penangsang *et al.*, "Dynamic DC optimal power flow using quadratic programming," in *2013 International Conference on Information Technology and Electrical Engineering (ICITEE)*. IEEE, 2013, pp. 360–364.

[101] P. Ngatchou, A. Zarei, and A. El-Sharkawi, "Pareto multi objective optimization," in *Proceedings of the 13th International Conference on, Intelligent Systems Application to Power Systems*. IEEE, 2005, pp. 84–91.

[102] K. Chang, "Chapter 19 - multiobjective optimization and advanced topics," in *e-Design*, K. Chang, Ed. Boston: Academic Press, 2015, pp. 1105 – 1173. [Online]. Available: http://www.sciencedirect.com/science/article/pii/B9780123820389000193

[103] M. S. Kuran, A. C. Viana, L. Iannone, D. Kofman, G. Mermoud, and J. P. Vasseur, "A smart parking lot management system for scheduling the recharging of electric vehicles," *IEEE Transactions on Smart Grid*, vol. 6, no. 6, pp. 2942–2953, Nov 2015.

[104] R. Garcia-Valle and J. A. P. Lopes, *Electric vehicle integration into modern power networks*. Springer Science & Business Media, 2012.

[105] J. Zhao, C. Wan, Z. Xu, and J. Wang, "Risk-based day-ahead scheduling of electric vehicle aggregator using information gap decision theory," *IEEE Transactions on Smart Grid*, vol. 8, no. 4, pp. 1609–1618, July 2017.

[106] S. I. Vagropoulos and A. G. Bakirtzis, "Optimal bidding strategy for electric vehicle aggregators in electricity markets," *IEEE Transactions on Power Systems*, vol. 28, no. 4, pp. 4031–4041, Nov 2013.

[107] T. Zhang, S. X. Chen, H. B. Gooi, and J. M. Maciejowski, "A hierarchical EMS for aggregated besss in energy and performance-based regulation markets," *IEEE Transactions on Power Systems*, vol. 32, no. 3, pp. 1751–1760, May 2017.

[108] M. Shafie-Khah, M. Moghaddam, M. Sheikh-El-Eslami, and J. Catalão, "Optimised performance of a plug-in electric vehicle aggregator in energy and reserve markets," *Energy Conversion and Management*, vol. 97, pp. 393–408, 2015.

[109] C. Goebel and H. A. Jacobsen, "Aggregator-controlled EV charging in pay-as-bid reserve markets with strict delivery constraints," *IEEE Transactions on Power Systems*, vol. 31, no. 6, pp. 4447–4461, Nov 2016.

[110] G. He, Q. Chen, C. Kang, P. Pinson, and Q. Xia, "Optimal bidding strategy of battery storage in power markets considering performance-based regulation and battery cycle life," *IEEE Transactions on Smart Grid*, vol. 7, no. 5, pp. 2359–2367, Sept 2016.

[111] B. Han, S. Lu, F. Xue, L. Jiang, and X. Xu, "Three-stage electric vehicle scheduling considering stakeholders economic inconsistency and battery degradation," *IET Cyber-Physical Systems: Theory Applications*, vol. 2, no. 3, pp. 102–110, 2017.

[112] M. Honarmand, A. Zakariazadeh, and S. Jadid, "Integrated scheduling of renewable generation and electric vehicles parking lot in a smart microgrid," *Energy Conversion and Management*, vol. 86, pp. 745–755, 2014.

[113] K. Clement-Nyns, E. Haesen, and J. Driesen, "The impact of charging plug-in hybrid electric vehicles on a residential distribution grid," *IEEE Transactions on power systems*, vol. 25, no. 1, pp. 371–380, 2010.

[114] E. Sortomme, M. M. Hindi, S. J. MacPherson, and S. Venkata, "Coordinated charging of plug-in hybrid electric vehicles to minimize distribution system losses," *IEEE transactions on smart grid*, vol. 2, no. 1, pp. 198–205, 2011.

[115] A. D. Hilshey, P. D. Hines, P. Rezaei, and J. R. Dowds, "Estimating the impact of electric vehicle smart charging on distribution transformer aging," *IEEE Transactions on Smart Grid*, vol. 4, no. 2, pp. 905–913, 2013.

[116] J. Wang, G. R. Bharati, S. Paudyal, O. Ceylan, B. P. Bhattarai, and K. S. Myers, "Coordinated electric vehicle charging with reactive power support to distribution grids," *IEEE Transactions on Industrial Informatics*, vol. 15, no. 1, pp. 54–63, 2019.

[117] Y. Mu, J. Wu, N. Jenkins, H. Jia, and C. Wang, "A spatial–temporal model for grid impact analysis of plug-in electric vehicles," *Applied Energy*, vol. 114, pp. 456–465, 2014.

[118] Z. Luburić, H. Pandžić, T. Plavšić, L. Teklić, and V. Valentić, "Role of energy storage in ensuring transmission system adequacy and security," *Energy*, vol. 156, pp. 229–239, 2018.

[119] J. Sohnen, Y. Fan, J. Ogden, and C. Yang, "A network-based dispatch model for evaluating the spatial and temporal effects of plug-in electric vehicle charging on GHG emissions," *Transportation Research Part D: Transport and Environment*, vol. 38, pp. 80–93, 2015.

[120] Y. Xu, J. Hu, W. Gu, W. Su, and W. Liu, "Real-time distributed control of battery energy storage systems for security constrained DC-OPF," *IEEE Transactions on Smart Grid*, vol. 9, no. 3, pp. 1580–1589, 2018.

[121] M. E. Khodayar, L. Wu, and Z. Li, "Electric vehicle mobility in transmission-constrained hourly power generation scheduling," *IEEE Transactions on Smart Grid*, vol. 4, no. 2, pp. 779–788, June 2013.

[122] Illinois Center for a Smarter Electric Grid (ICSEG), "IEEE 14-bus system." [Online]. Available: https://icseg.iti.illinois.edu/ieee-14-bus-system/